MARINE PHYSICAL LABORATORY

SCRIPPS INSTITUTION OF OCEANOGRAPHY

San Diego, California 92152

Least Squares Adaptive and Bayes Optimal Array Processors for the Active Sonar Problem

David Almagor

SIO REFERENCE 89-16

MPL-U-75/89
October 1989

Approved for public release; distribution unlimited.

SECURITY CLASSIFICATION OF THIS PAGE

REPORT DOCUMENTATION PAGE

1a REPORT SECURITY CLASSIFICATION UNCLASSIFIED	1b RESTRICTIVE MARKINGS
2a SECURITY CLASSIFICATION AUTHORITY	3 DISTRIBUTION/AVAILABILITY OF REPORT Approved for public release; distribution unlimited.
2b DECLASSIFICATION/DOWNGRADING SCHEDULE	
4 PERFORMING ORGANIZATION REPORT NUMBER(S) SIO Reference 89-16 [MPL-U-75/89]	5 MONITORING ORGANIZATION REPORT NUMBER(S)
6a NAME OF PERFORMING ORGANIZATION Marine Physical Laboratory 6b OFFICE SYMBOL (If applicable) MPL	7a NAME OF MONITORING ORGANIZATION Office of Naval Research Department of the Navy
6c ADDRESS (City, State, and ZIP Code) University of California, San Diego Scripps Institution of Oceanography San Diego, CA 92152	7b ADDRESS (City, State, and ZIP Code) 800 North Quincy Street Arlington, VA 22217-5000
8a NAME OF FUNDING/SPONSORING ORGANIZATION Office of Naval Research 8b OFFICE SYMBOL (If applicable) ONR	9 PROCUREMENT INSTRUMENT IDENTIFICATION NUMBER N00014-87-K-0010
8c ADDRESS (City, State, and ZIP Code) Department of the Navy 800 North Quincy Street Arlington, VA 22217-5000	10 SOURCE OF FUNDING NUMBERS PROGRAM ELEMENT NO. / PROJECT NO. / TASK NO / WORK UNIT ACCESSION NO

11 TITLE (Include Security Classification)
Least Squares Adaptive and Bayes Optimal Array Processors for the Active Sonar Problem

12 PERSONAL AUTHOR(S)
David Almagor

13a TYPE OF REPORT	13b TIME COVERED	14 DATE OF REPORT (Year, Month, Day)	15 PAGE COUNT
sio reference	FROM _____ TO _____	September 1989	162

16 SUPPLEMENTARY NOTATION

17 COSATI CODES			18 SUBJECT TERMS (Continue on reverse if necessary and identify by block number)
FIELD	GROUP	SUB-GROUP	active sonar echoes, ocean reverberation, pole-zero adaptive filter, least squares adaptive processor

19 ABSTRACT (Continue on reverse if necessary and identify by block number)

This dissertation examines the problem of detecting active sonar echoes under ocean reverberation limiting conditions. The properties of acoustic reverberation pertinent to the design of active sonar detectors are first studied. Two detection schemes representing different approaches are then proposed and developed. One approach is an ad-hoc engineering approach, which preprocesses the received signal with an adaptive noise canceler, and then performs the detection. The second approach takes a global point of view and utilizes the known statistics of the problem to design an optimum detector in the Bayesian sense.

A new, joint process, pole-zero adaptive filter is developed, and it is shown that under certain circumstances its performance is superior to its all-zero counterpart. It is a candidate for an adaptive, ad-hoc detection scheme.

Often times, when closed expressions for system performance are hard to achieve, a Monte-Carlo simulation approach is used. In this context, the ability to synthesize an

20 DISTRIBUTION/AVAILABILITY OF ABSTRACT	21 ABSTRACT SECURITY CLASSIFICATION
☐ UNCLASSIFIED/UNLIMITED ☒ SAME AS RPT ☐ DTIC USERS	UNCLASSIFIED
22a NAME OF RESPONSIBLE INDIVIDUAL W. S. Hodgkiss	22b TELEPHONE (Include Area Code) (619) 534-1798 / 22c OFFICE SYMBOL MPL

DD FORM 1473, 84 MAR 83 APR edition may be used until exhausted
All other editions are obsolete

SECURITY CLASSIFICATION OF THIS PAGE

☆ U.S. Government Printing Office: 1986—607-044

ensemble of active sonar pings is a key to assessing detector performance. One of the major contributions of this dissertation is the development of a multi-channel element level reverberation time series generator.

Three active sonar problems of ever-increasing complexity are then examined. The first problem is one of the signal, known exactly with a boundary interference coming from a known direction. In the second problem the interference is coming from an uncertain direction, and in the third another fixed interference coming from an uncertain direction is added.

Finally, for all the above problems, comparisons are made between the ad-hoc detector and two implementations of the Bayes detector, a block processor (sub-optimum), and a time sequential processor. This is done using the reverberation time series generator, and through the comparison of Receiver Operating Characteristic (ROC) curves. It is shown that when the optimum detector is allowed to be time sequential it performs uniformly better than the ad-hoc detector. Furthermore, the optimum detector demonstrates an adaptive learning quality, through the process of updating the a-priori probability density functions of the unknown parameters, from iteration to interation..

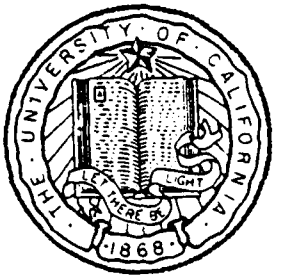

UNIVERSITY OF CALIFORNIA
SAN DIEGO

Least Squares Adaptive and Bayes Optimal

Array Processors for the Active Sonar Problem

A dissertation submitted in partial satisfaction of the

requirements for the degree Doctor of Philosophy

in Electrical Engineering

(Communication Theory and Systems)

by

Dav[illegible]magor

Committee in charge:

Professor Victor C. Anderson
Professor Lawrence B. Milstein
Professor Elias Masry
Professor Bhaskar D. Rao
Professor William S. Hodgkiss, Chairman

SIO REFERENCE 89-16

MPL-U-75/89
October 1989

To my wife

Table of Contents

List of Figures

ACKNOWLEDGEMENTS

I would like to sincerely thank Dr. Hodgkiss for his support throughout this work. His enjoyable and instructive digital signal processing class originally attracted me to this field, and his guidance, encouragement and understanding made this effort successful. Thanks go also to my committee members for reviewing this dissertation and offering their constructive criticism. This research was sponsored by the Office of Naval Research, Contract #N00014-87-K-0010.

The Marine Physical Lab enjoys an outstanding digital signal processing environment thanks to the dedicated work of a few individuals. I would like to thank Dr. Hodgkiss, John McInerney and Eric Wolin for their skillful management and unfailing support of the computing facilities.

I have enjoyed sharing ideas and learning from my research peers. Special thanks go to Lee Culver, Rick Brienzo and Amos Dotan.

Being associated with KETEMA A&E (formerly AMETEK/Straza Division), I have always enjoyed the highest level of understanding for my needs, and acceptance of my unconventional schedules. This support is well appreciated.

Captain Amnon Shefi of the Israel Navy has introduced me to the exciting underwater world, and has been my professional mentor throughout the beginning of my engineering career. I will be proud to remain his friend for years to come.

I would like to thank my parents Chava and Yizhar, who have planted in me the appreciation for education, and who have continuously encouraged me to go farther. The support I have enjoyed from my family - my mom Chava, Fredek, sister Lidia and brother Nimrod - has sustained me when being so far away from home.

Last, but certainly not least, I'd like to thank my wife, Ora. She had skillfully and lovingly been able to give me moral encouragement and support, while completing her own higher education. To her, with love, I dedicate this work.

VITA

November 11, 1956	Born, Jerusalem, Israel
1975-1979	B.S., Electrical Engineering, Technion, Israel Institute of Technology, Haifa, Israel
1980-1984	Electronics Engineering Officer, Israel Navy, Israel
1985	Teaching Assistant, Electrical and Computer Engineering Dept. University of California San Diego
1986-1989	Research Assistant, Marine Physical Laboratory, University of California, San Diego
1986	M.S., University of California, San Diego
1986	Senior Electronics Engineer, AMETEK/Straza Division, El Cajon, Ca
1988	Principal Engineer, AMETEK Aerospace and Electronics Division, El Cajon, Ca
1989	Ph.D., University of California, San Diego

PUBLICATIONS

D. Almagor and W.S. Hodgkiss, "The performance of two classes of active sonar detectors in a shallow water environment", in progress, to be submitted for publication in ICASSP - the IEEE International Conference on Acoustics, Speech, and Signal Processing (1990).

D. Almagor and J.M. Peters, "Moving target discrimination using T-statistics", in progress, to be submitted for publication in ICASSP - The IEEE International Conference on Acoustics, Speech, and Signal Processing (1990).

W. S. Hodgkiss and D. Almagor, "Oceanic Reverberation Time Series Synthesis", in progress, to be submitted for publication in the IEEE Journal of Oceanic Engineering in August 1989.

W.S. Hodgkiss and D. Almagor, "A pole-zero complex adaptive joint process least squares lattice", Proceedings of ICASSP - the IEEE International Conference on Acoustics, Speech, and Signal Processing (1988).

W. S. Hodgkiss and D. Almagor "Element level reverberation time series synthesis", Proceedings of ICASSP - the IEEE International Conference on Acoustics, Speech, and Signal Processing (1988).

W.S. Hodgkiss and D. Almagor, "An eigenvalue/eigenvector interpretation of surface reverberation rejection performance", Proceedings of ICASSP - the IEEE International Conference on Acoustics, Speech, and Signal Processing (1987).

D. Almagor and W. S. Hodgkiss, "Preliminary SNR Improvement Results, 1985 ARTUT Lake Travis Field Test Data", MPL U-34/86, Marine Physical Laboratory, Scripps Institution of Oceanography, La Jolla, CA, July 1986.

PATENTS

D. Almagor and J.M. Peters, "Sonar System with Area Moving Target Indicator". Allowed, and will be issued in Oct. 1989 (application No. 137,525).

FIELDS OF STUDY

Major Field: Electrical Engineering

Studies in Digital Signal Processing.
Professors William S. Hodgkiss

Studies in Communication Systems
Professor Lawrence B. Milstein

Studies in Detection Theory
Professor Carl W. Helstrom

ABSTRACT OF THE DISSERTATION

Least Squares Adaptive and Bayes Optimal

Array Processors for the Active Sonar Problem

by

David Almagor

Doctor of Philosophy in Electrical Engineering

(Communication Theory and Systems)

University of California, San Diego, 1989

Dr. William S. Hodgkiss, Chairman

This dissertation examines the problem of detecting active sonar echoes under ocean reverberation limiting conditions. The properties of acoustic reverberation pertinent to the design of active sonar detectors are first studied. Two detection schemes representing different approaches are then proposed and developed. One approach is an ad-hoc engineering approach, which preprocesses the received signal with an adaptive noise canceler, and then performs the detection. The second approach takes a global point of view and utilizes the known statistics of the problem to design an optimum detector in the Bayesian sense.

A new, joint process, pole-zero adaptive filter is developed, and it is shown that under certain circumstances its performance is superior to its all-zero counterpart. It is a candidate for an adaptive, ad-hoc detection scheme.

Often times, when closed expressions for system performance are hard to achieve, a Monte-Carlo simulation approach is used. In this context, the ability to synthesize an ensemble of active sonar pings is a key to assessing detector performance. One of the major contributions of this dissertation is the development

of a multi-channel element level reverberation time series generator.

Three active sonar problems of ever-increasing complexity are then examined. The first problem is one of signal known exactly with a boundary interference coming from a known direction. In the second problem the interference is coming from an uncertain direction, and in the third another fixed interference coming from an uncertain direction is added.

Finally, for all the above problems, comparisons are made between the ad-hoc detector and two implementations of the Bayes detector, a block processor (sub-optimum), and a time sequential processor. This is done using the reverberation time series generator, and through the comparison of Receiver Operating Characteristic (ROC) curves. It is shown that when the optimum detector is allowed to be time sequential it performs uniformly better than the ad-hoc detector. Furthermore, the optimum detector demonstrates an adaptive learning quality, through the process of updating the a-priori probability density functions of the unknown parameters, from iteration to iteration.

Introduction

Acoustic reverberation is a phenomenon which active sonar systems have to combat. Reverberation results when the propagating pulse's energy is scattered from inhomogeneities in the ocean and its boundaries. Reverberation data usually has a complex and highly variable range-Doppler map, which depends on the location of the sonar array in the water column, and on its beampatterns.

Ocean boundary reverberation (surface or bottom), can leak through sidelobes or even through the edges of a main lobe in a conventional forward looking beam output. The above leakage typically has a sudden onset and can contribute to the overall noise level. In conventional active sonar systems, discrimination against boundary reverberation is typically achieved through controlling the sidelobe characteristics of the main, forward looking beam.

A more sophisticated approach to the problem has suggested the use of an *adaptive beamforming structure which dynamically steers spatial nulls in the* direction of the interferent boundary patch (surface or bottom). Such a structure is called in the literature a noise canceler[66]. In addition to the conventional forward looking beam, the adaptive noise canceling structure uses one or more reference beams. The reference beams are constructed such that they receive well the boundary reverberation, but are essentially prevented from receiving signals coming in from the main look direction. The processor adaptively filters the reference beams to provide a good estimate of the boundary reverberation contaminant in the main beam. It then subtracts the adaptive filter output from the main beam output to get the desired - reverberation canceled - signal. Implementations of such adaptive beamforming structures which take advantage of the spatial separation between desired signals and boundary reverberation contaminants are presented in[23]. Additional relevant sources are[54,64].

The above solution to the problem is representative of an approach which is based on intuition, but it is not at all clear that it yields an optimal processor (under any optimization criterion).

Another approach suggests treating the problem as a whole right from the beginning without imposing intuitive components on the processor structure, and using all a-priori knowledge available. Detection theory provides us with a mathematical framework out of which optimum processors can be designed. The processor will evolve out of the mathematical solution of the problem, and will not be restricted to using familiar structures.

Although Bayes optimal processors have been derived for the case of volume reverberation[55], little work has been done which takes advantage of a-priori knowledge of the time-evolving spatial characteristics of boundary reverberation. Related Bayes optimal work concerning interference sources of certain and uncertain (but not time varying) location is contained in [1] and [26,24,25] respectively.

Here, a classical detection theoretic approach will be applied to the processing of a vector time series. That vector may be composed of the single array element outputs, or of some preformed beams. Some optimality criterion is chosen, and then the processor structure is allowed to evolve freely out of the mathematical solution of the problem. Any uncertain parameters are treated as random variables and all knowledge about them is summarized in a-priori probability density functions.

This dissertation is organized as follows: Chapter 1 reviews the current scientific knowledge about the reverberation phenomenon. It then details some of the physical and statistical properties of reverberation important for attempting to quantify spatial covariance matrix expressions of it. These matrices play a

major role in the optimum detector expressions.

In the second chapter, an important tool is developed. Often times, when likelihood ratio expressions are complex, computing the detector performance analytically is either very hard, or impossible. Then, being capable of synthesizing multi-element (or multi-beam) active sonar pings becomes a prerequisite to one's ability to test detection algorithms using a Monte-Carlo simulation approach. In lieu of sonar synthesis programs, which are time-consuming and impractical for this application, this chapter uses a spectral estimation approach, to compute the multi-channel, time evolving power spectrum of the problem, including the transmit pulse, the element (beam) transmit and receive beampatterns, the volume and boundary effects, and the dynamics of the scenario. Then, the multi-channel covariance matrices are computed, and the normal equations problem is solved, yielding a time variable, one-step forward prediction filter. The inverse filter frequency response is an estimate of the spectral character of the problem. Now, all that's left is to pass vectors of uncorrelated white noise through the filter, in order to get multiple sonar pings of the same sonar scenario, for a relatively low time investment. Lastly, the synthesis capability is demonstrated through an example.

Chapter 3 reviews the two approaches to detection of active sonar pings in a reverberating environment. As discussed above, the first is a combination ad-hoc noise canceler-matched filter. The chapter then lays the ground rules for Bayes optimum detection, and examines the array detection problem. Lastly, it develops the Bayes optimum detector (BOD) for the simple case of signal known exactly in noise known exactly, which turns out to be a matched filter.

All-zero adaptive filters exist in many variations, where the main difference is in the adaptive algorithm modifying the filter weights. In the fourth

chapter, the Joint Process Least Squares Lattice (JCLSL) all-zero filter is reviewed, and then its pole-zero (IIR) counterpart is developed using an embedding approach, which makes use of the all-zero filter recursions to create the pole-zero filter recursions. Then, through a set of simulations, it is shown that in some scenarios, it is beneficial for the adaptive filter to possess the ability to adapt poles. Another simulation shows that in the scenarios used in this dissertation, the performance advantage of the pole-zero filter is marginal.

The fifth chapter develops the Bayes optimum detectors for the three cases tested in this dissertation:

1. Signal known exactly in correlated Gaussian interference of precisely known direction.
2. Signal known exactly in correlated Gaussian interference of uncertain direction.
3. Signal known exactly in correlated Gaussian interference of uncertain direction, plus a fixed interference of uncertain direction.

The sixth chapter distinguishes between two different implementations for the Bayes optimum detector, namely block processing and time sequential. It develops the time-sequential detector design equations including the updates of the a-priori probability density function estimates which increase its knowledge about the problem as time progresses.

Chapter 7 reviews the main methods used to evaluate and compare the performance of the various detection schemes.

Chapters 8 compares the performance of both detection approaches, when the Bayes optimum detector is restricted to the block processing method. Finally, chapter 9 concludes this work by comparing the performance of both detectors when this time the BOD is allowed the time sequential method. It also

demonstrates the adaptive quality of the time sequential BOD through the updating process of the a-priori probability density function from one iteration to the next.

1. Reverberation in the Ocean:

Active underwater electronic systems propagate acoustic signals through the water column and use the information carried by these signals to detect targets, echo range, or communicate voice and data. Like every other electronic system, these systems suffer from noise effects, which mask the desired return signal, and limit their performance. Underwater systems' performance in general is limited by external noise sources and not internal (thermal) noise. In the absence of hostile jammers, this external noise is usually divided into two main categories, namely ambient ocean noise, and reverberation. Among ambient ocean noise contributors one can find rain, waves, seismic noise, various biological noise sources, ship traffic etc., and they all exist independent of the presence of the underwater system. An inherent difference between reverberation noise and ocean noise is that reverberation exists only as a result of acoustic energy being transmitted, whereas ambient ocean noise is always there.

System's performance may be limited by either type of interference (reverberation or sea noise), and in fact the same system may be reverberation limited for part of its operating range, and ambient noise limited for the rest of its operating range. The systems considered in this dissertation are assumed to operate in conditions which dictate that performance be reverberation limited. Therefore, ambient ocean noise is neglected in all derivations.

Reverberation is the result of scattering of energy originating from the propagating pulse, by inhomogeneities in the ocean and its boundaries. In some respects this problem is akin to the radar "clutter" problem. Reverberation is usually divided into three classes, namely, surface, volume and bottom reverberation. Irregularities in the ocean surface and the acoustic impedance contrast of the air/sea interface, gives rise to surface reverberation. This type of

reverberation varies with wind speed and transmission frequency[5,6,10,18]. In the ocean body, air bubbles, suspended sediment, thermal inhomogeneities, fish, plankton, and other biological sources are the main contributors to what is classified as volume reverberation[11]. Bottom reverberation is caused by energy scattered from the sea floor, and is highly dependent on the floor type. Both particle size and bottom relief are important factors[3,7,8]. In general, ocean acoustic reverberation has a very complex nature, and a highly variable power spectrum. In some situations, where the sonar is fairly close to the ocean boundaries, or when its beam's sidelobes are pointing towards those boundaries, the energy reflected off of these boundaries makes a significant contribution to the range-Doppler map. This contribution usually has a sudden onset, may appear at nonzero Doppler frequencies, and therefore may mask legitimate sonar echoes.

1.1. The statistical and spectral properties of reverberation:

1.1.1. Amplitude distribution

Common reverberation models assume that the reverberation signal is comprised of a combination of numerous individual sources which scatter the acoustic energy. These sources scatter the energy with different magnitudes and random phase. An expression for the intensity distribution of numerous sources of equal magnitude and random phase has been derived by Rayleigh[51]. The probability that the resultant intensity will exceed the value I is given by:

$$P = \exp\left(-\frac{I}{\bar{I}}\right) \tag{1.1}$$

where $\bar{I}$ is the average intensity. The actual received intensity is, of course, a combination of sources of many different magnitudes, because the individual

scatterers are of different size and strength, because the projector may be directional, and because the transmission loss in different parts of the ocean may vary. Nevertheless, it can be shown that Equation (1.1) is still valid provided that there are a large number of sources of each magnitude, and that the number of sources of each magnitude remains constant.

The applicability of the Rayleigh model has been tested in numerous studies[44,36,35] , for all reverberation classes (surface, volume and bottom). All of the studies have found that in general, the actual probability distribution of reverberation intensity fits the Rayleigh model well. Moreover, it has been found that the received envelope of the reverberation is a complex Gaussian random process (i.e. it's real and imaginary parts are jointly Gaussian distributed).

1.1.2. Coherence

Coherence includes both the autocorrelation and crosscorrelation properties of a statistical process. The observed reverberation envelope of pulsed sonar possesses a "blobby" nature, where the "blobs" are about a pulse width long. The temporal autocorrelation coefficient of reverberation envelope has been found to almost diminish in a time delay equal to one pulse duration[38]. Spatial correlation of reverberation received at two vertically separated hydrophones plays an important role when implementing reverberation rejection algorithms. This correlation has been studied, modeled[4] and measured[58,59,57] for both volume and boundary reverberation. Both the models and the experimental results show that boundary reverberation is more correlated than volume reverberation, and that the crosscorrelation coefficient of both types diminishes with increased frequency and hydrophone separation.

1.1.3. Frequency distribution

The reverberation return resulting from a single frequency sonar pulse typically occupies a spectral band which is non-congruent to the original pulse band. The reverberation band is shifted in frequency due to Doppler effects caused by the sonar platform movement, combined with any velocities possessed by the scattering media be it volume scatterers or surface waves. Furthermore, a spectral spread is observed. Naturally, the finite duration of the transmission pulse, results in a basic spread of $\frac{1}{\tau}$, where τ is the pulse duration. Further spread is a result of the fact that different Doppler shifts are caused by the reverberation returns received from various directions. The Doppler shift depends linearly on the sonar platform's velocity component in that direction, and therefore reverberation coming in from different directions suffer different Doppler shifts. A third contributor to the spectral spread is the one caused by the random motion of the scattering media.

A typical range-Doppler map of a reverberation return is shown in Figure 1.1. It was generated using a reverberation simulation package (REVSIM) developed for this research, which will be described in detail in a later chapter of this dissertation. Here, the vehicle was purposefully given a relatively high speed (30 m/s), so as to well separate boundary reverberation from volume reverberation in the frequency domain, and make each of them well defined. The range-Doppler map has also been left shifted to compensate for the vehicle's own speed. The sonar array is placed at a depth of 100m, where the ocean depth is 400m. The transmit beam illuminates a sector $\pm 75°$ in elevation, and the receive beam spans $\pm 60°$. Early in the ping, around 0.1 sec, the onset of the surface reverberation is well noticeable. It slowly creeps towards 0 Doppler joining the volume reverberation, when around 0.5 sec the onset of bottom reverberation appears. It

too, then, slowly joins the volume reverberation until around 1 sec the two spectral peaks become very close.

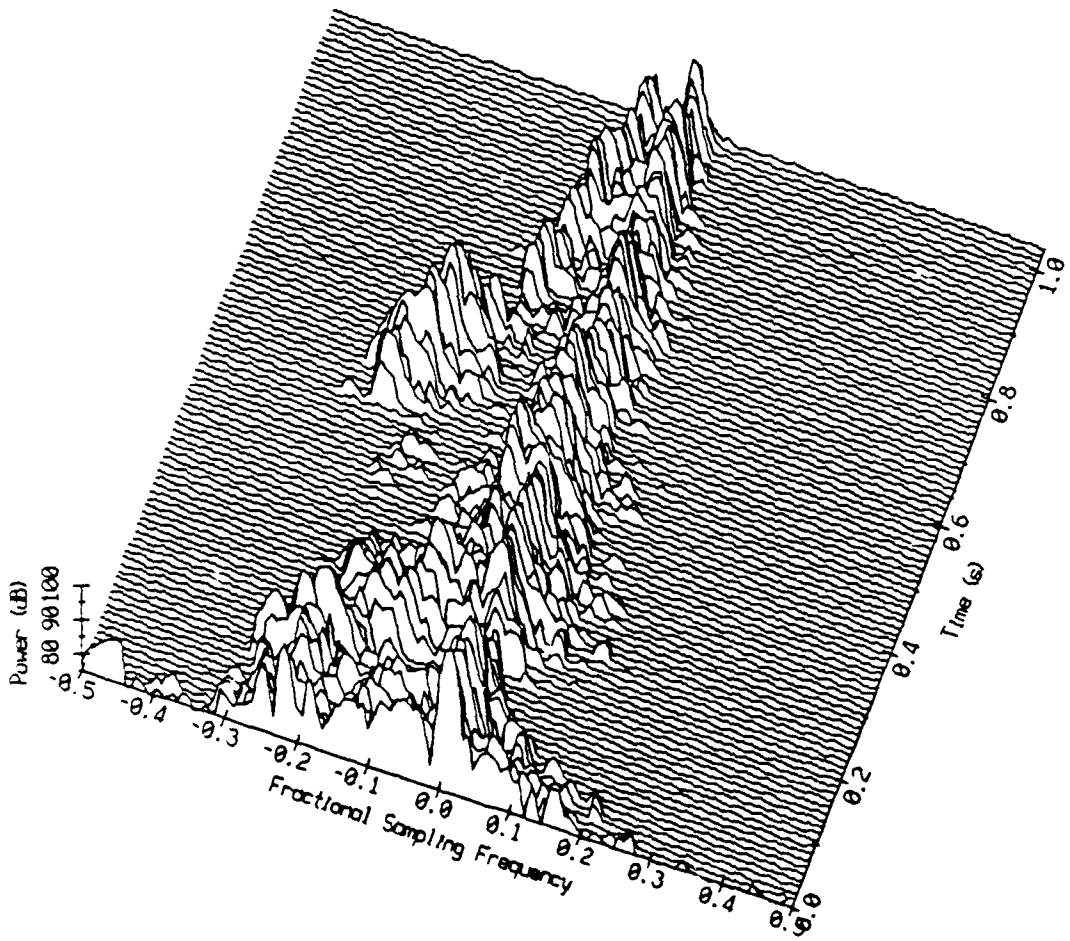

Figure 1.1. Typical range-Doppler map.

2. Element level reverberation time series synthesis

2.1. Introduction

The ocean's boundaries (surface and bottom) and particulate matter in the ocean volume scatter energy from an active sonar ping back to the transducer. The characteristics of this reverberation are highly non-stationary. A commonly-used display of the time-evolving frequency content of reverberation is the range-Doppler map. The expected range-Doppler map is useful in many instances for active sonar system performance characterization.

As depicted in Figure 2.1, one approach to estimating the expected range-Doppler map is to propagate the pulse outward and calculate the expected backscattered return at successive range increments[22]. At each range, the shell representing the ensonified portion of the ocean and its boundaries is split into cells subtending a small azimuth and elevation angle spread. The expected spectrum contributed by each cell is summed across all cells yielding the expected spectrum at that range (i.e. a slice of the range-Doppler map at a given range).

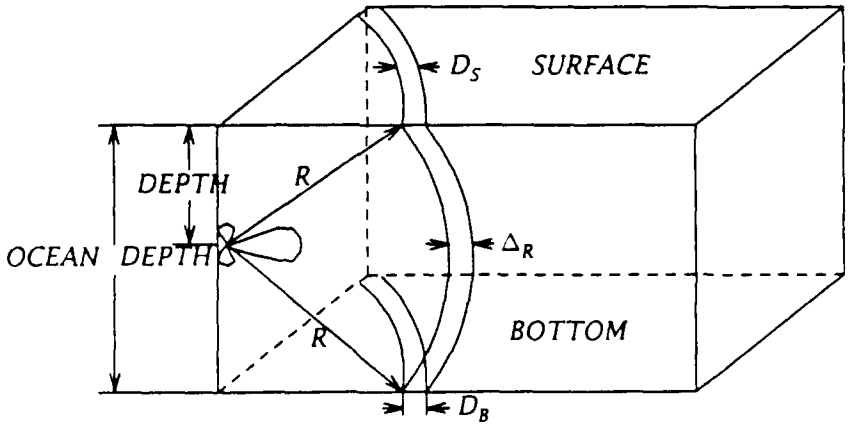

Figure 2.1. Reverberation model geometry

Although the expected range-Doppler map is useful in many instances for active sonar system performance characterization, often the actual reverberation time series is desired. Such reverberation time series are generated by REVGEN (REVerberation GENerator)[49,50]. REVGEN is a direct implementation of the point-scattering model of oceanic reverberation developed by Faure, Ol'shevskii, and Middleton[15,45,40,41,42,43]. The returns from a large number of discrete scatteres distributed randomly throughout the volume and on the boundaries are summed coherently to obtain the (complex basebanded) reverberation time series at the output of each hydrophone element or beam. The backscattering coefficient (strength) for each reverberation type (surface, volume, and bottom) is specified along with random scatterer motion, platform trajectory, absorption, boundary reflection losses, and transmitting/receiving beam patterns. REVGEN has proved very effective in the simulation of oceanic backscatter in a wide range of applications[7,63,19,2,3].

Although very good, REVGEN also is very computationally intensive and is not suitable for generating a large number of pings for a given environment as needed when performing Monte Carlo simulations for active sonar system performance characterization. Typically, generating a single sonar ping similar to the one synthesized in Section 2.3, will take REVGEN a few hours to run. In order to generate a large ensemble of pings, REVGEN would have to be run hundreds and maybe thousands of hours. An alternative to the point scattering approach taken in REVGEN is to synthesize reverberation by passing a vector white noise process through a multichannel IIR filter whose time-varying transfer function matches the time-evolving spectral characteristics of the expected auto and cross range-Doppler maps. Of specific interest is the generation of array element-level or beam-level reverberation time series which have appropriate element-to-

element or beam-to-beam crosscorrelations. Related approaches are discussed in[20,62,9,34]. Obviously, one run time investment here is in generating the multidimensional time-varying IIR filter coefficients. Surprisingly, this task in itself is relatively short, and typically takes a few minutes. Once the filter coefficients are available, generating each sonar ping takes a few minutes, as contrasted to a few hours using REVGEN. The time savings factor exceeds 100, and allows the synthesis of a complete sonar ping ensemble over the course of a few hours. This makes the use of a Monte Carlo simulation approach feasible.

Section 2.2 will describe one approach to the generation of the expected auto and cross range-Doppler maps and how to fit a time-varying, multichannel, autoregressive (AR) time series model to these range-Doppler maps. Then, a set of simulation results is provided in Section 2.3 and is compared with REVGEN's output.

2.2. Multichannel revereration time series synthesis

2.2.1. Expected range-Doppler map generation (RVMD)

There are several approaches which can be used to calculate the expected auto and cross range-Doppler maps. The specific environmental model used as the basis for the simulations presented in Section 2.3 is a multibeam extension of the approach discussed in[22]. Array elements can be viewed simply as beams with broad spatial response characteristics, when an element level Range-Doppler map is sought. The module whose function is to compute the scattering function resulting from the combined effects of the environment, vehicle dynamics and transmit and receive beam patterns is modified so it handles a pair of receive beams at a time. When the program is handling an auto-scattering function, both receive beams are identical, but when the program is dealing with a cross-

scattering function, the two receive beams are the ones whose cross scattering function is being computed. The programs run until all possible receive beam pairs are exhausted. The result is a multidimensional scattering function.

As shown in Figure 2.1, the reverberation model geometry consists of a spherical shell representing the portion of the ocean illuminated by the signal wavefront at the instant in time corresponding to a range R after transmit. The expected range-Doppler map is calculated in two stages.

First, the multidimensional scattering function is calculated following the steps outlined in Figure 2.2. The illuminated volume of the ocean is divided into cells. An evaluation of scatterer motion relative to the platform is made for a measure of spectral shifting and/or spreading due to the environment. For each cell, and each beam pair, the sonar equation is solved in order to determine the gross attenuation experienced by a transmitted signal during the scattering process. The total scattering function for each beam pair for surface, volume, and bottom reverberation is computed by summing the incremental contributions from all cells. These scattering functions include the effects of platform motion, transmit beampattern, both receive beam patterns, and the environment (surface, volume, and bottom backscattering strengths, scatterer velocity distributions, surface waves and current layers, and sound absorption). An isospeed sound speed profile is assumed and reflections at the surface and bottom boundaries are not permitted.

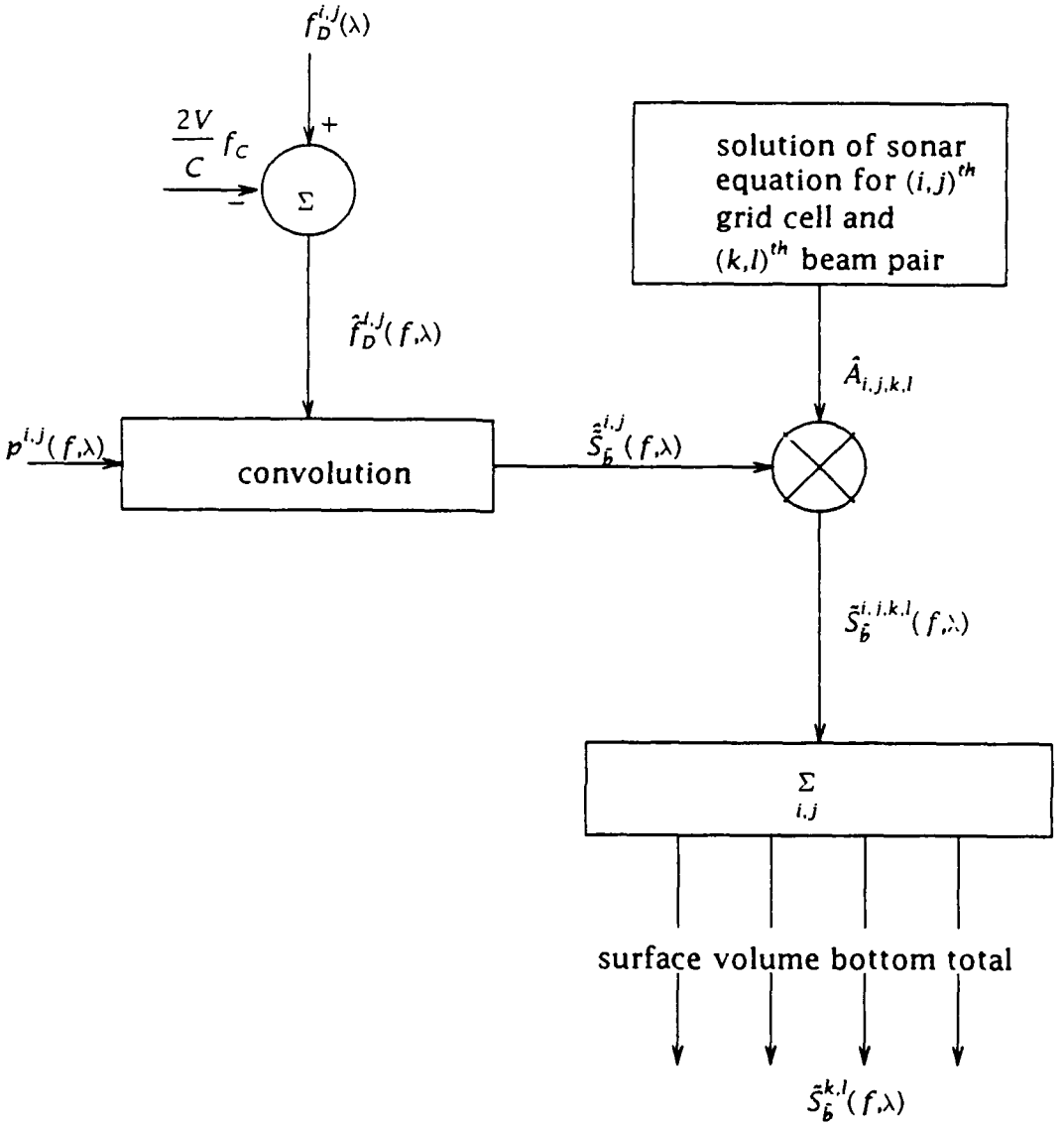

Figure 2.2. Scattering function calculation

In Figure 2.2, λ is a time delay (range) variable, $f_D^{i,j}(\lambda)$ is the Doppler shift accounting for vehicle motion relative to the $(i,j)^{th}$ grid cell and mean scatterer speed relative to a stationary vehicle, $\frac{2V}{C} f_C$ is the frequency offset such that a stationary target on vehicle axis has zero Doppler shift, $p^{i,j}(f,\lambda)$, is the zero-mean

Gaussian speed distribution of scatterers in $(i,j)^{th}$ grid cell, $\tilde{\tilde{S}}_{\hat{b}}^{i,j}(f,\lambda)$, is the Doppler shifted speed distribution of scatterers in $(i,j)^{th}$ grid cell, $\hat{A}_{i,j,k,l}$ is the scattering level (normalized to 1 s in range) from the $(i,j)^{th}$ grid cell, $(k,l)^{th}$ beam pair, $\tilde{S}_{\hat{b}}^{i,j,k,l}(f,\lambda)$ is the scattering function for the $(i,j)^{th}$ grid cell, $(k,l)^{th}$ beam pair, and $\tilde{S}_{\hat{h}}^{k,l}(f,\lambda)$ are the surface, volume, bottom and total scattering functions for the $(k,l)^{th}$ beam pair.

Outlined in Figure 2.3, the second stage completes the reverberation model by combining a detailed description of the transmit signal (i.e. pulse length, envelope shape, and source level) with the characterization of the environment provided by the multidimensional scattering function. The convolution of the scattering function with the transmitted spectrum yields the expected multi-beam range-Doppler map.

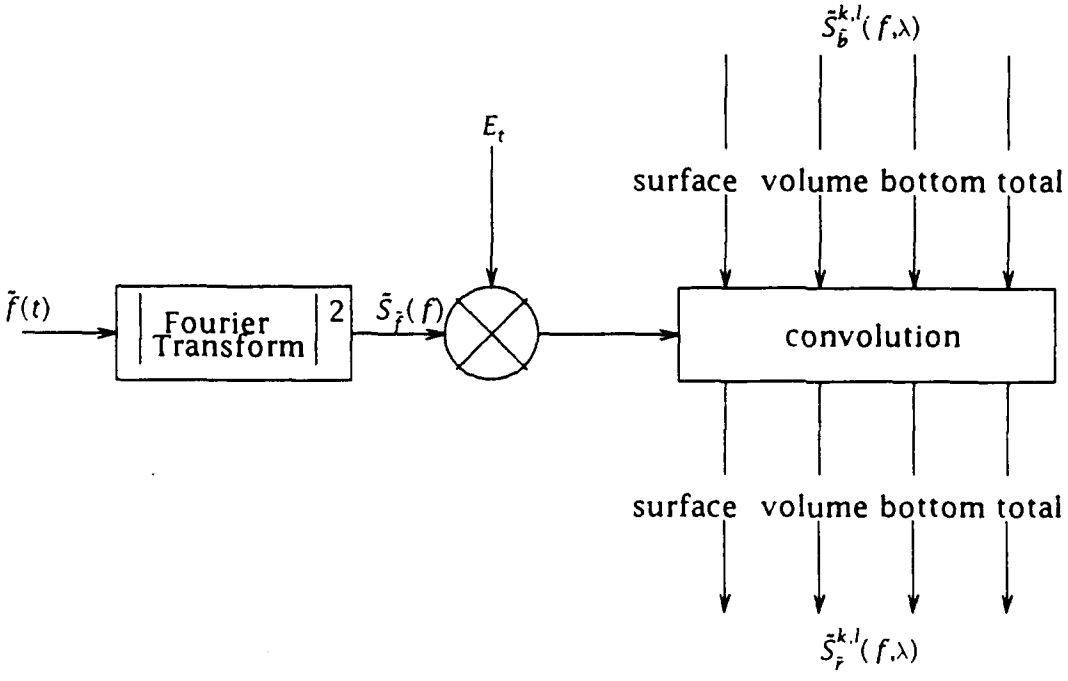

Figure 2.3. Convolution with the transmitted spectrum

In Figure 2.3 $\tilde{f}(t)$ is the complex envelope of transmit pulse, $\tilde{S}_{\tilde{f}}(f)$ is the normalized energy spectrum of the transmit pulse, E_t is the transmit pulse energy, $\tilde{S}_b^{k,l}(f,\lambda)$ are the surface, volume, bottom and total scattering functions for the $(k,l)^{th}$ beam pair, and $\tilde{S}_r^{k,l}(f,\lambda)$ are the surface, volume, bottom and total reverberation power spectra for the $(k,l)^{th}$ beam pair.

2.2.2. Time-varying IIR filter derivation

The classical linear minimum mean square error (MMSE) estimation problem has been developed by Kolmogorov[29] and Wiener[68], and has been since one of the foundations of estimation theory. It is discussed is standard estimation theory texts[54]. Its development is therefore left in this dissertation for an Appendix (A).

The end result of the linear MMSE problem are the well known *normal* equations, in this case, their multichannel version:

$$\begin{aligned} A_0R_0+A_0R_{-1}+ \ldots\ldots\ldots\ldots +A_pR_{-p} &= G_0 \\ A_0R_1+A_0R_0+ \ldots\ldots\ldots\ldots +A_pR_{-p+1} &= G_1 \\ \ldots\ldots\ldots\ldots & \\ A_0R_p+A_{p-1}R_0+ \ldots\ldots\ldots\ldots +A_pR_0 &= G_p \end{aligned} \tag{2.1}$$

or in their matrix form:

$$\begin{bmatrix} A_0 A_1 \ldots\ldots A_p \end{bmatrix} \begin{bmatrix} R_0 & R_1 & \cdots & R_p \\ R_{-1} & R_0 & \cdots & R_{p-1} \\ \cdot & \cdot & \cdots & \cdot \\ \cdot & \cdot & \cdots & \cdot \\ \cdot & \cdot & \cdots & \cdot \\ R_{-p} & R_{-p+1} & \cdots & R_0 \end{bmatrix} = \begin{bmatrix} G_0 G_1 \ldots\ldots G_p \end{bmatrix} \tag{2.2}$$

Since we are dealing with an N-input N-output system, A_i are all NxN matrices, and

so are R_i and G_i. Also, G_i are the crosscorrelation matrices between the input and the desired signal. In the specific problem of linear prediction, those reduce simply to the crosscorrelation between the input at time n and the input at time $(n-1)$, or the input autocorrelation at lag $(i+1)$:

$$G_i = R_{i+1} \tag{2.3}$$

In this case, the matrix form of the *normal* equations takes the form:

$$\begin{bmatrix} A_0, A_1 \ldots\ldots, A_p \end{bmatrix} \begin{bmatrix} R_0 & R_1 & \ldots & R_p \\ R_{-1} & R_0 & \ldots & R_{p-1} \\ . & . & \ldots & . \\ . & . & \ldots & . \\ . & . & \ldots & . \\ R_{-p} & R_{-p+1} & \ldots & R_0 \end{bmatrix} = \begin{bmatrix} R_1, R_2 \ldots\ldots, R_{p+1} \end{bmatrix} \tag{2.4}$$

Solving the above equations will yield the multichannel filter coefficients A_i.

Our goal is to pass a vector white uncorrelated noise process through a multichannel IIR filter as shown in Figure 2.4 yielding a vector time series at the output which approximates the time-evolving (auto and cross) spectral characteristics of reverberation as it would be seen at the output of the elements or beams of a transducer array. The time-varying coefficients of the multichannel one step forward prediction filter can be derived in a number of ways.

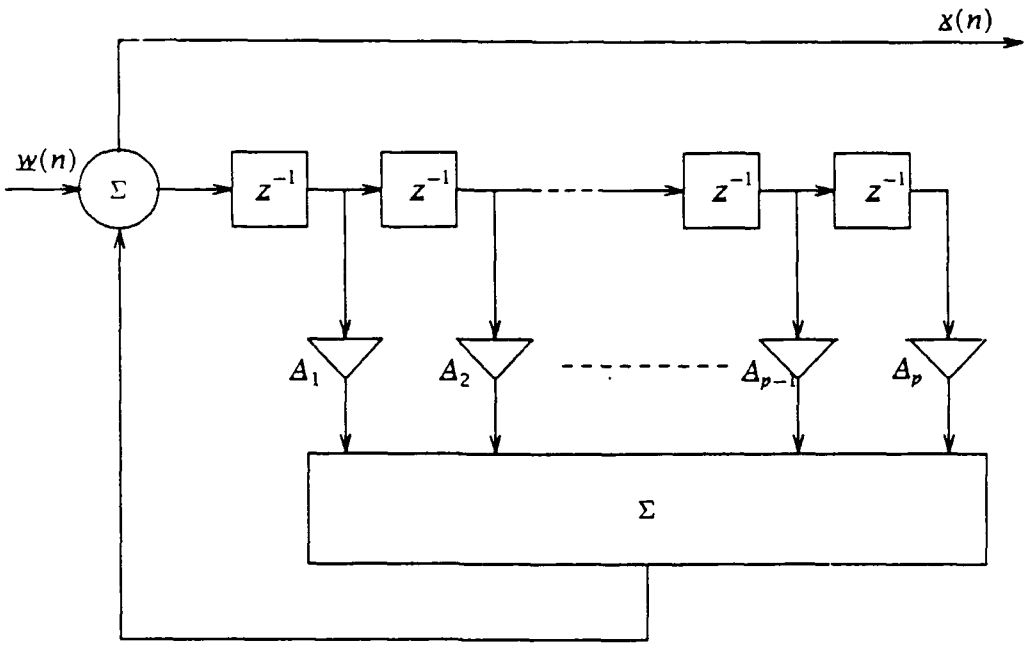

Figure 2.4. Autoregressive process generation model

Here, slices at a given range from the set of expected auto and cross range-Doppler maps will be viewed as the multichannel power spectrum of a stationary vector random process. First, the multichannel power spectrum is inverse Fourier transformed to yield the corresponding multichannel correlation function. Then, a multichannel extension of the Levinson-Durbin algorithm is used to derive the one-step forward prediction error (inverse) filter shown in Figure 2.5 which provides the IIR filter coefficients. The Levinson-Durbin algorithm has been discussed extensively in numerous publications[33,14,65,69,52,28], and its development will not be repeated here. It takes advantage of the special structure of the autocorrelation matrices, to achieve an efficient method of matrix inversion.

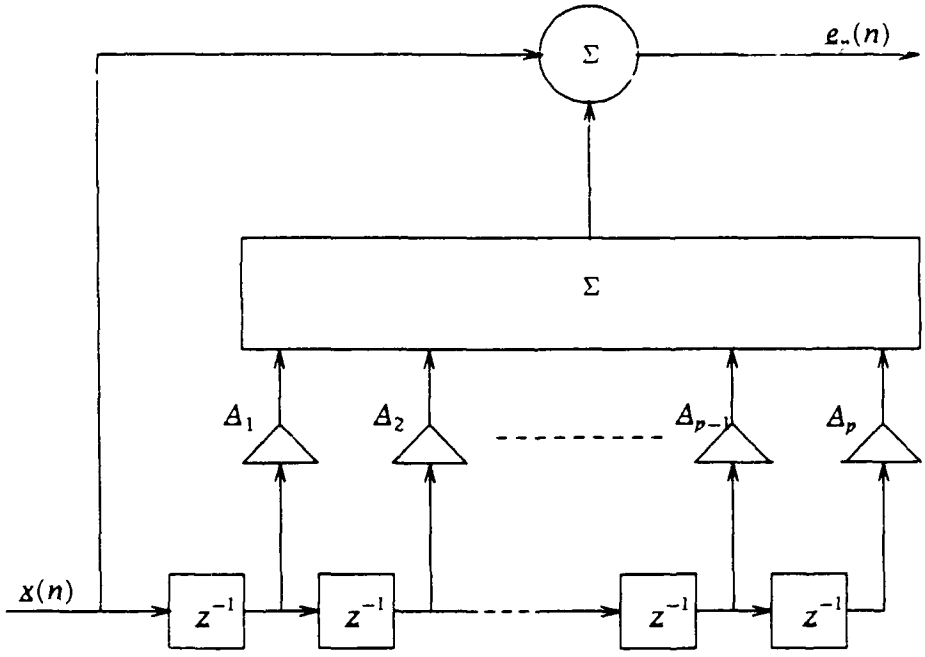

Figure 2.5. One step forward prediction error filter

Each increment in range is processed in exactly the same way yielding successive sets of IIR filter coefficients. The prediction error filter order is chosen such that it is of the smallest order large enough to accomplish emulating all of the spectral contents in the input data. In the type of problems encountered in this dissertation, where the input spectrum typically posesses two spectral humps, namely the main volume reverberation spectral hump, and another boundary reverberation spectral hump, experience shows that filter order can be kept to a low value (3-4), while preserving all spectral features of the input. This is well demonstrated in the simulations in Section 2.3.

2.2.3. Reverberation time series synthesis

The sets of IIR filter coefficients (one set per range increment) then are used as the coefficients of a time-varying, multichannel IIR filter. Since each

coefficient set represents a range slice, the range slices originally selected for RVMD have to be narrow enough so that the time varying spectra are relatively smooth from range slice to the next. A vector white uncorrelated noise process is passed through the filter yielding a vector output time series which simulates the outputs of a real transducer array in an ocean whose environmental parameters are those input to RVMD.

2.3. Active sonar simulation

As an example of this approach to reverberation time series synthesis, consider the following active sonar system. An array of 9 rows is mounted on a submerged vehicle as shown in Figure 2.6.

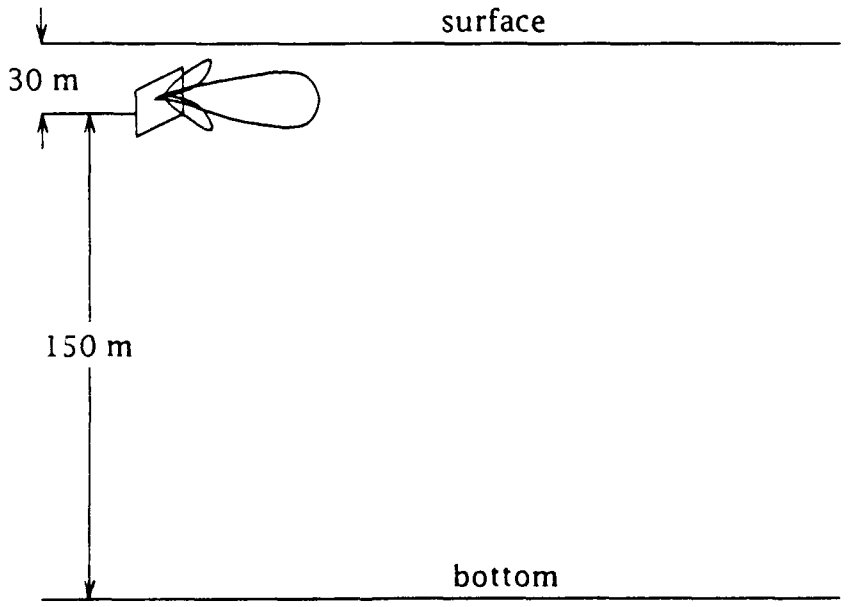

Figure 2.6. Submerged Array Example

The vehicle is traveling at 25 knots at a depth of 30 m. Ocean depth is 180 m. The sonar transmits a 180 ms, rectangularly windowed pulse.

The 9 row array has a sensor spacing of $\lambda/2$ at the operating frequency of the sonar. A conventional beam is formed by simply summing the outputs of all array rows. The corresponding beam pattern and a polar plot of a vertical slice through the beam pattern at 0° bearing are shown in Figure 2.7.

A difference beam is formed by subtracting the outputs of the 2 center rows of the array. The corresponding beam patterns similar to those in Figure 2.7 are shown in Figure 2.8.

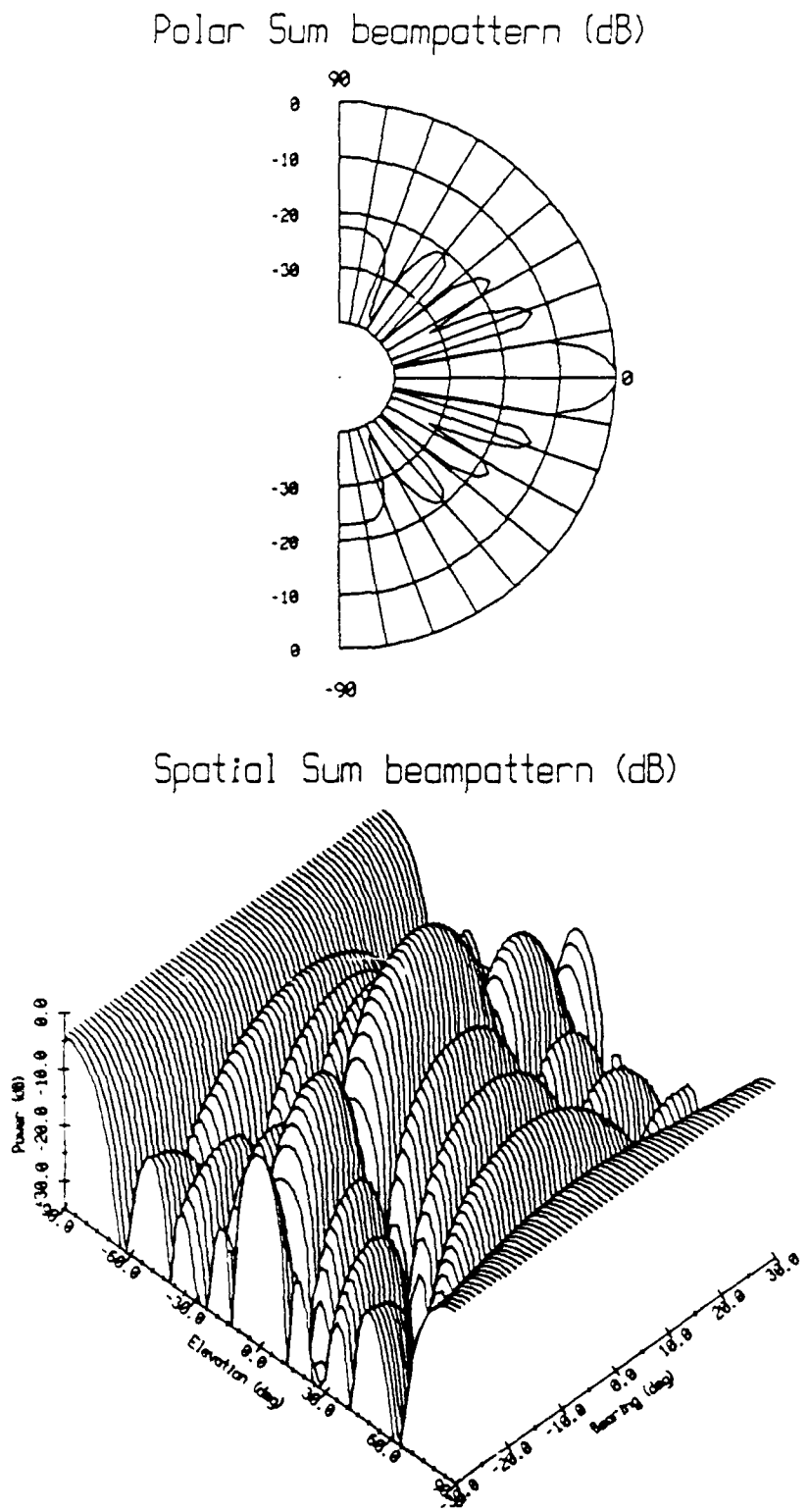

Figure 2.7. Sum Beam polar and spatial beampatterns.

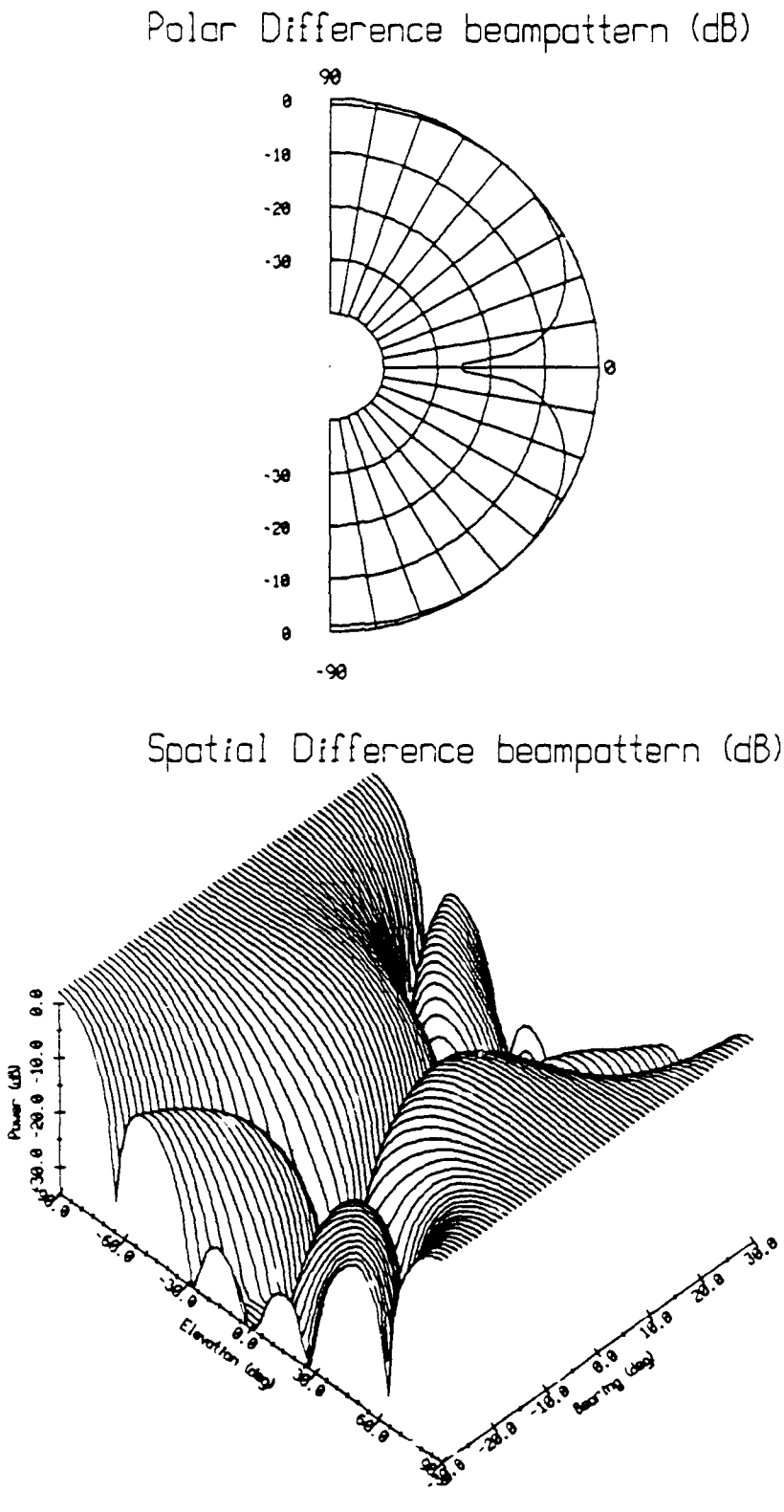

Figure 2.8. Difference Beam polar and spatial beampatterns.

A transmit beam is assumed which uniformly illuminates the medium over a sector $\pm 30°$ in bearing and $\pm 75°$ in elevation normal to the array plane.

The backscattered return to this sonar was simulated using REVGEN and the multichannel IIR filter approach discussed in Section 2.2. In this case, an isovelocity sound speed profile was assumed (c = 1500 m/s) along with the following parameters: (a) volume backscattering coefficient, s_v = -70 dB, (b) bottom backscattering coefficient, s_b = -20 dB, and (c) surface backscattering coefficient, s_s = -30 dB, and (d) attenuation due to absorption, α = 4 dB/km.

REVGEN range-Doppler maps of the returning reverberation for the conventional (sum) and difference beams as well as the the corresponding cross-power range-Doppler map are shown in Figure 2.9 (f_s = 1.27 kHz). These were generated by taking successive 128-point FFT's (Kaiser-Bessel window, α=2.5) overlapped by 87.5% (16 points). In addition, the range-Doppler maps have been left-shifted to compensate for platform velocity. In Figure 2.9a (sum beam), volume reverberation dominates early in the range-Doppler map. Later (at approximately 0.25 s in range), the onset of bottom reverberation arriving through the side lobes of the main beam is seen. In Figure 2.9b (difference beam), volume reverberation also dominates early in the range-Doppler map. The onset of bottom reverberation is more pronounced here than in Figure 2.9a due to the response characteristics of the difference beam pattern.

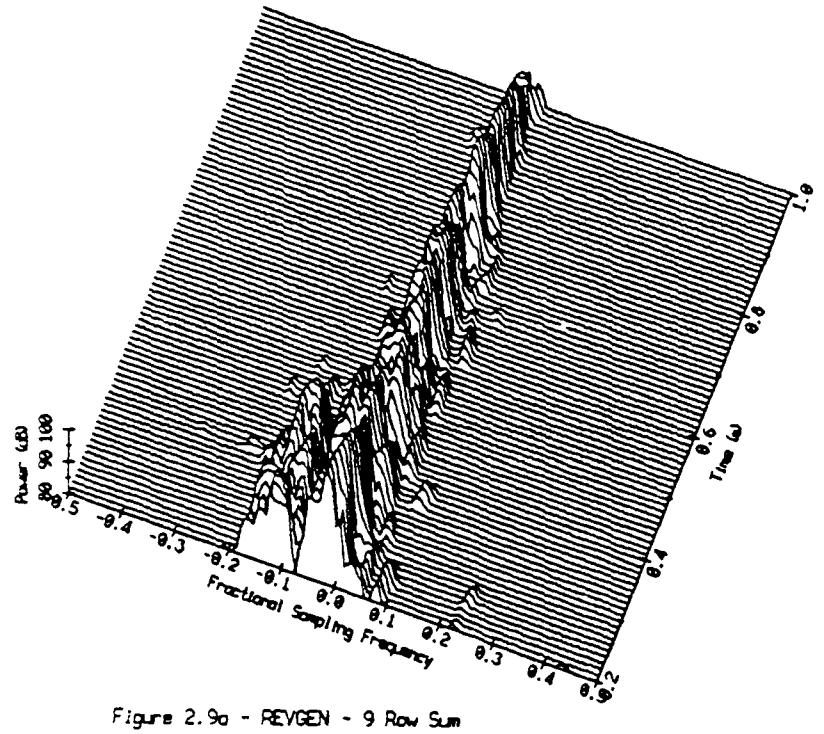

Figure 2.9a - REVGEN - 9 Row Sum

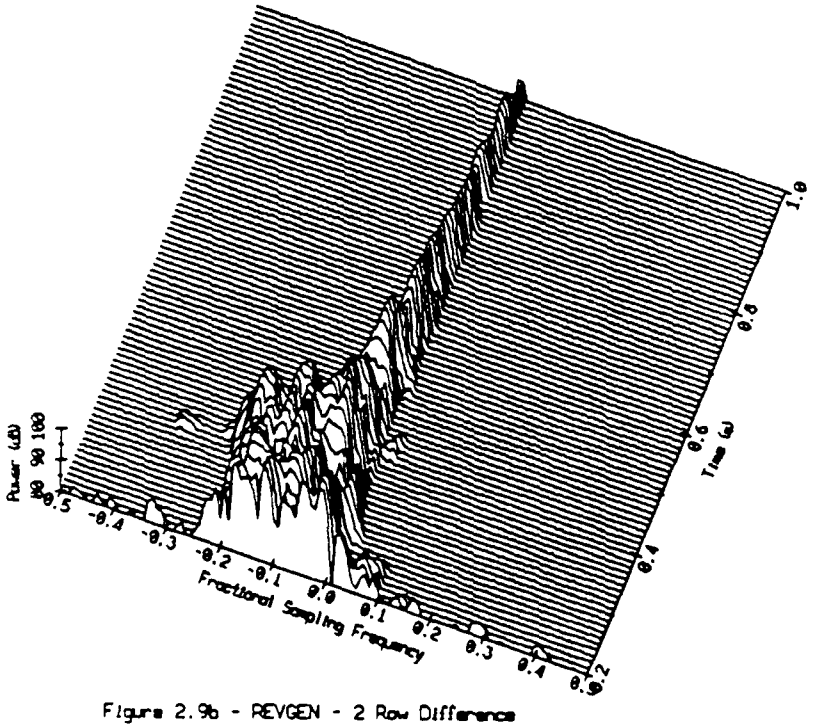

Figure 2.9b - REVGEN - 2 Row Difference

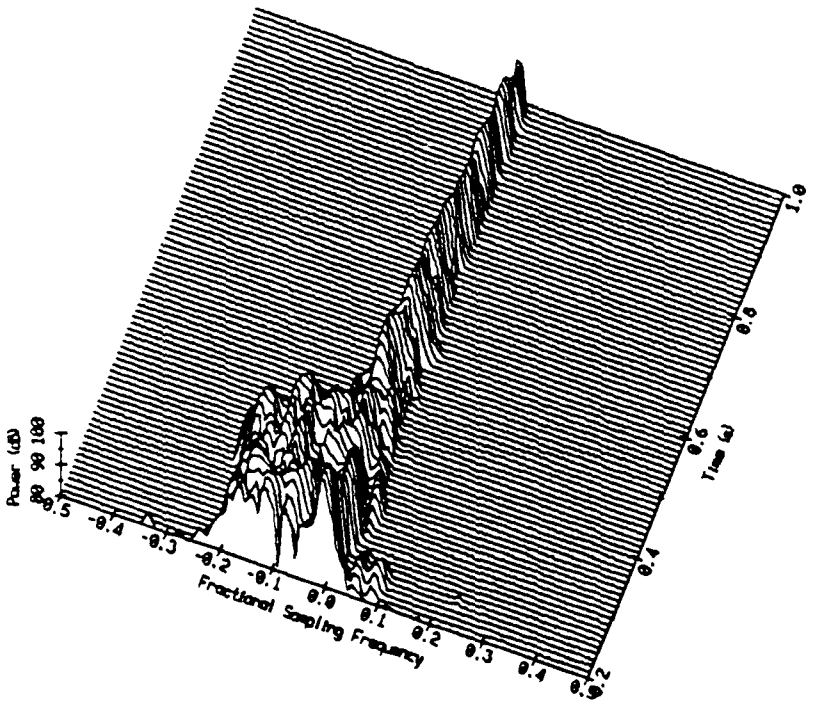

Figure 2.9c - REVGEN - Sum-Difference Cross

Figure 2.9. REVGEN - Sum, Difference and Cross range-Doppler maps.

The multichannel IIR filter results will be presented following the three steps discussed in Section 2.2. The RVMD parameters were identical to those used in the REVGEN simulation. First, Figure 2.10 shows the RVMD auto and cross range-Doppler maps. Note the "scallops" in the surface portion of the map, which are due to the sidelobes intersecting the ocean boundary. Second, the corresponding time-evolving inverse linear predictor spectral estimates (filter order p=4) are shown in Figure 2.11. They indicate how closely the derived IIR filter matches the expected auto and cross range-Doppler maps. Lastly, Figure 2.12 shows the results of passing a vector white noise process through the multichannel IIR filter and processing the output as done with the REVGEN time series. As is easliy seen, the results are quite similar to the REVGEN range-Doppler maps in Figure 2.9.

Figure 2.13 presents expanded high-resolution range-Doppler maps of the main beam, in order to further emphasize the similarity of REVGEN output (2.13a), RVMD output (2.13b), the linear predictor (2.13c), and finally REVSIM output (2.13d).

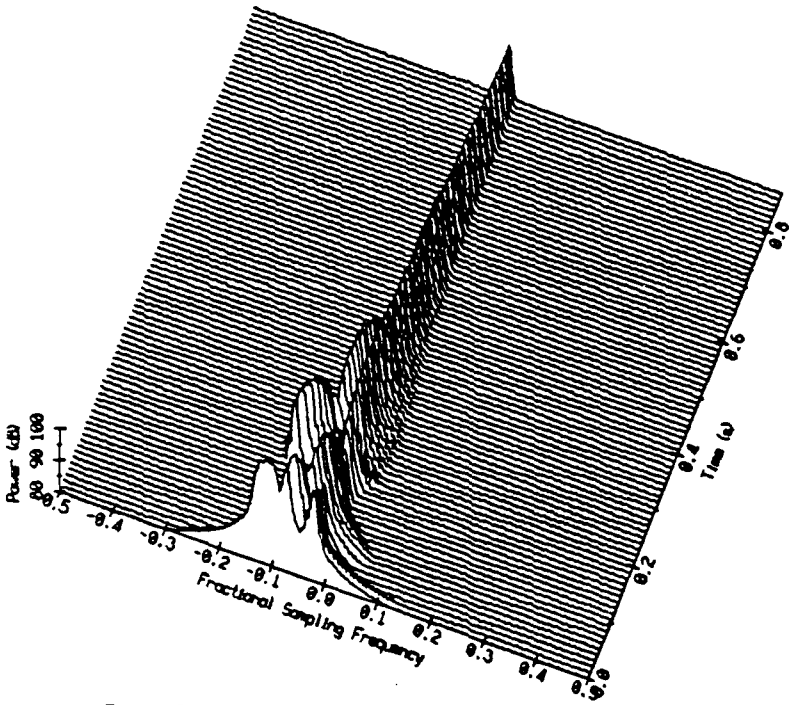

Figure 2.10a - RVMD - 9 Row Sum

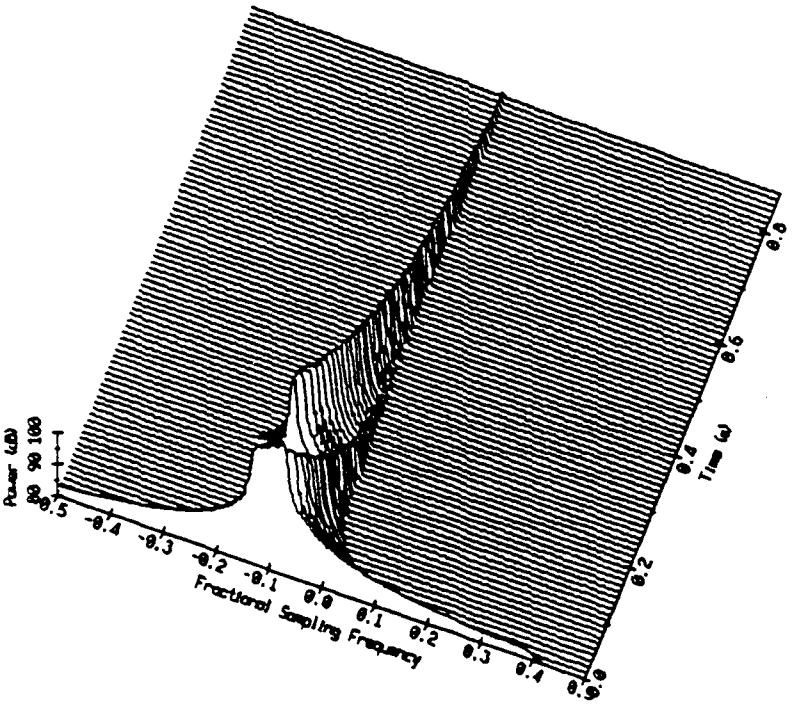

Figure 2.10b - RVMD - 2 Row Difference

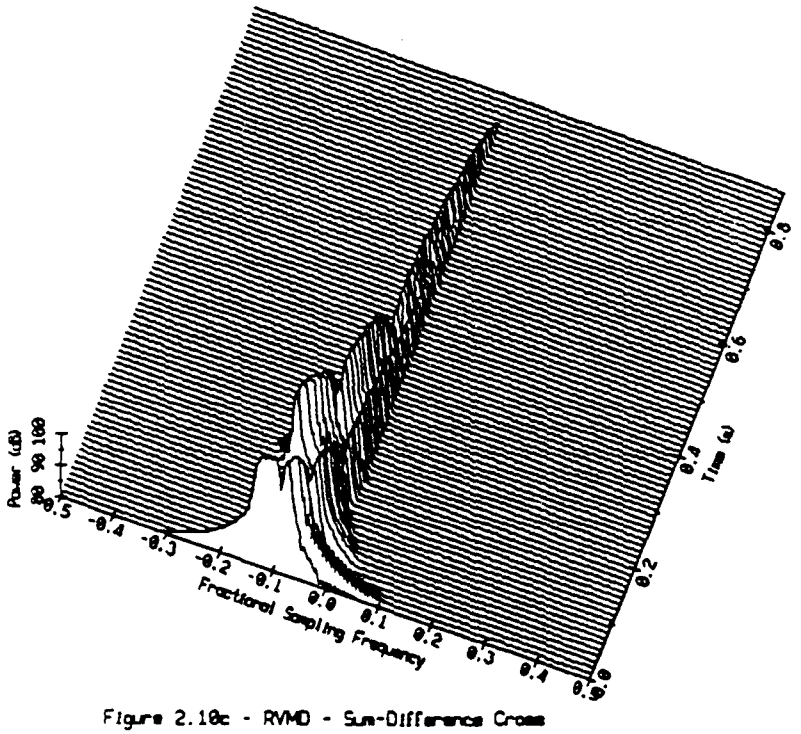

Figure 2.10c - RVMD - Sum-Difference Cross

Figure 2.10. RVMD - Auto and Cross range-Doppler maps.

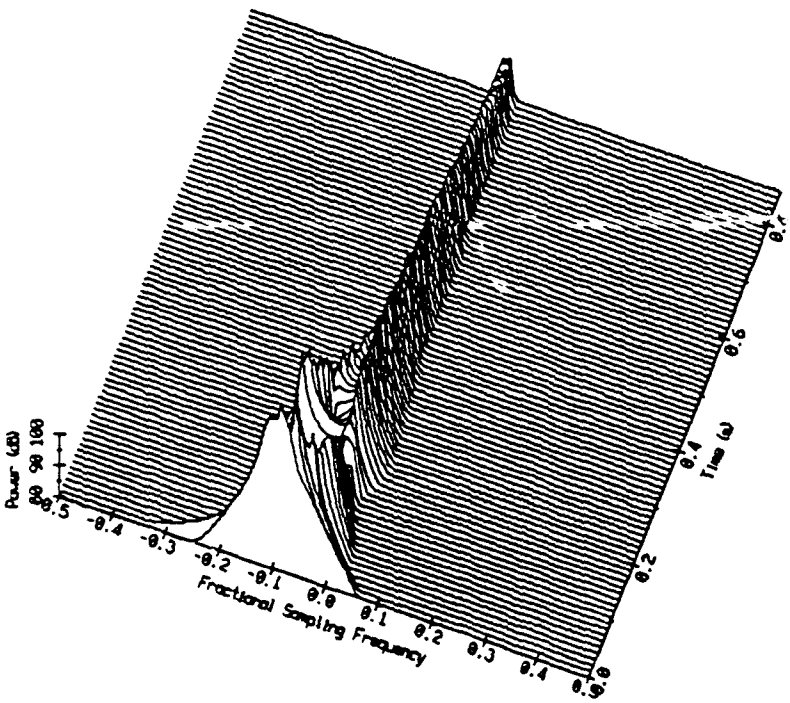

Figure 2.11a - Linear Predictor - 9 Row Sum

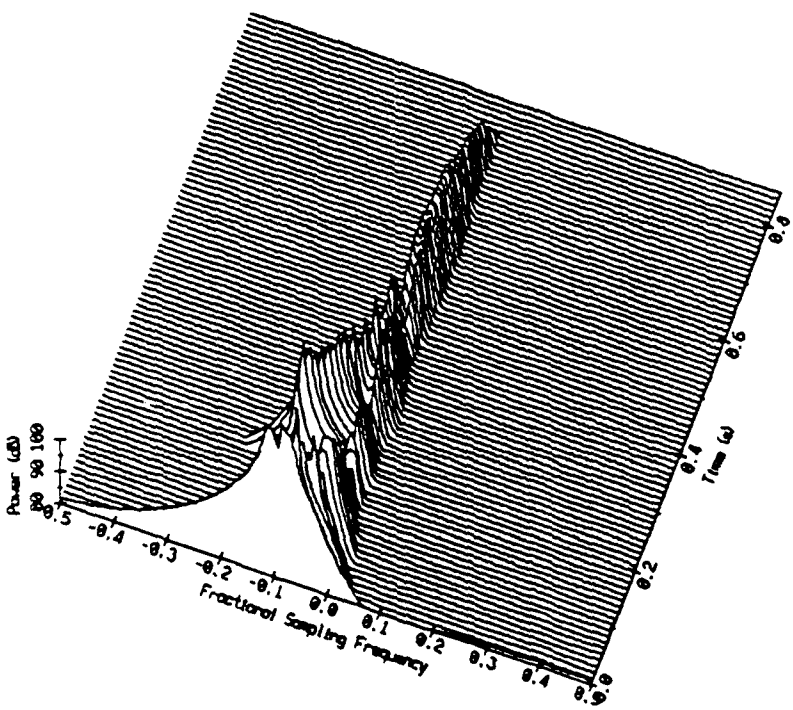

Figure 2.11b - Linear Predictor - 2 Row Difference

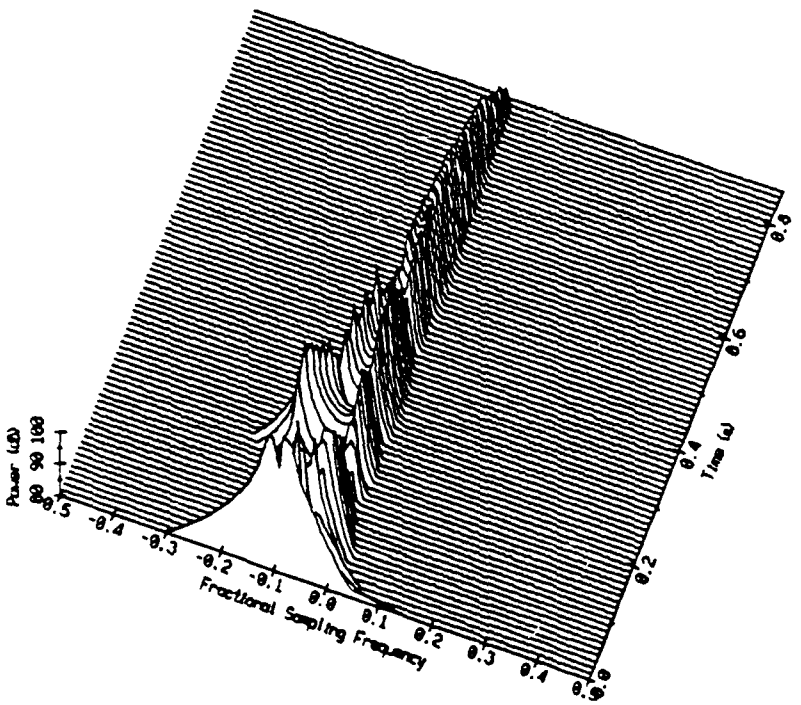

Figure 2.11c - Linear Predictor - Sum-Difference Cross

Figure 2.11. Inverse Linear Predictor - Auto and Cross range-Doppler maps.

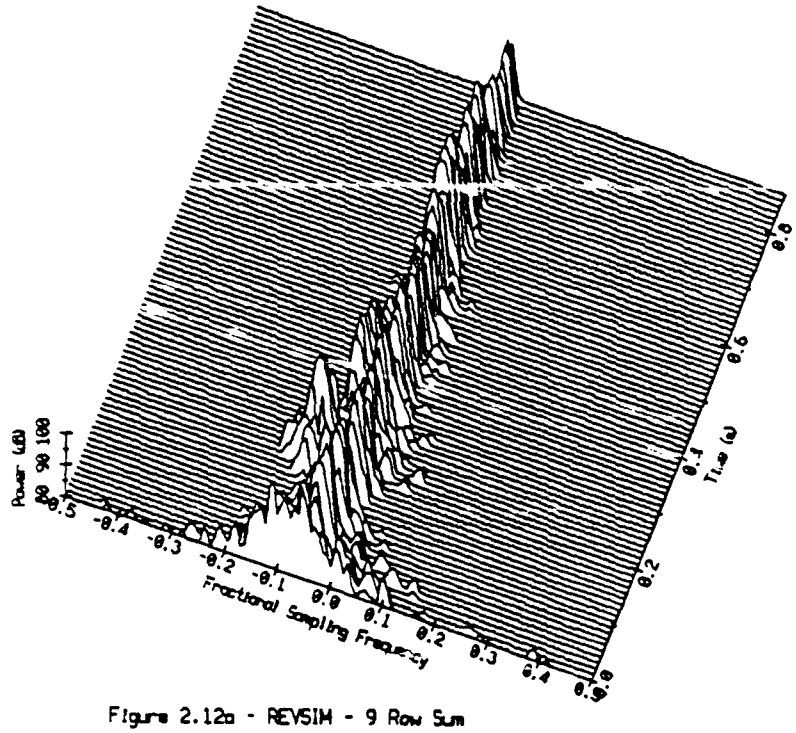

Figure 2.12a - REVSIM - 9 Row Sum

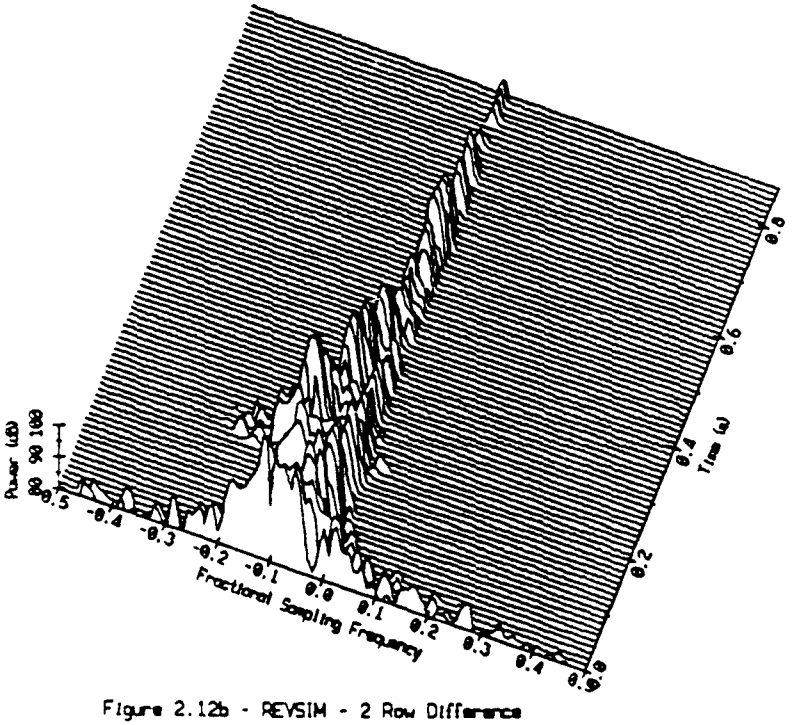

Figure 2.12b - REVSIM - 2 Row Difference

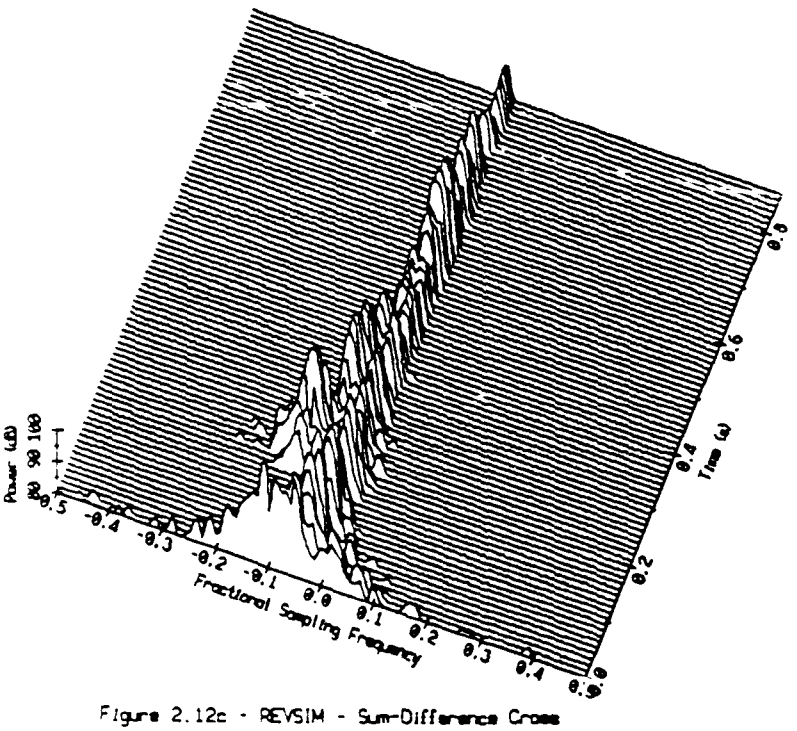

Figure 2.12c - REVSIM - Sum-Difference Cross

Figure 2.12. REVSIM - Auto and Cross range-Doppler maps.

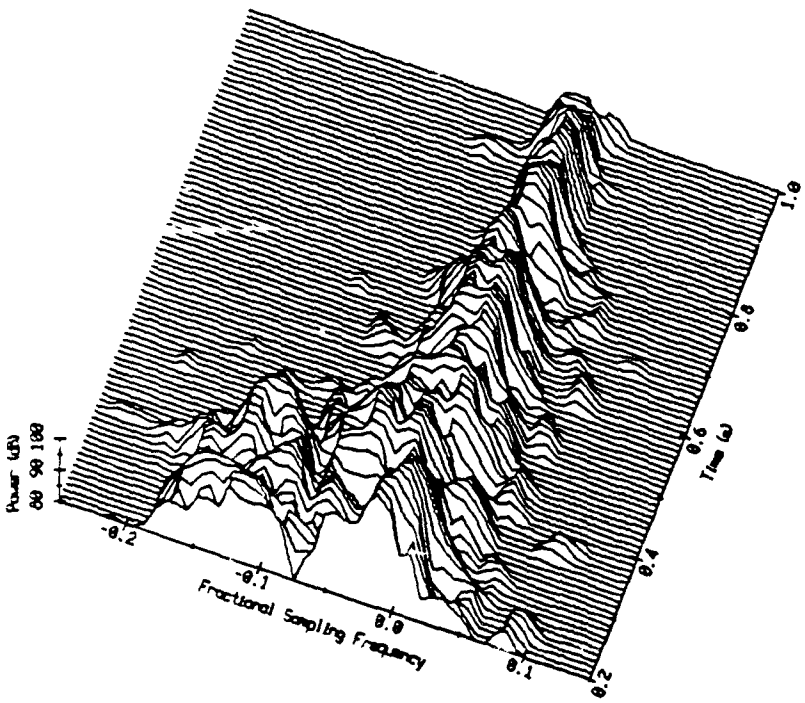

Figure 2.13a - REVGEN - 9 Row Sum

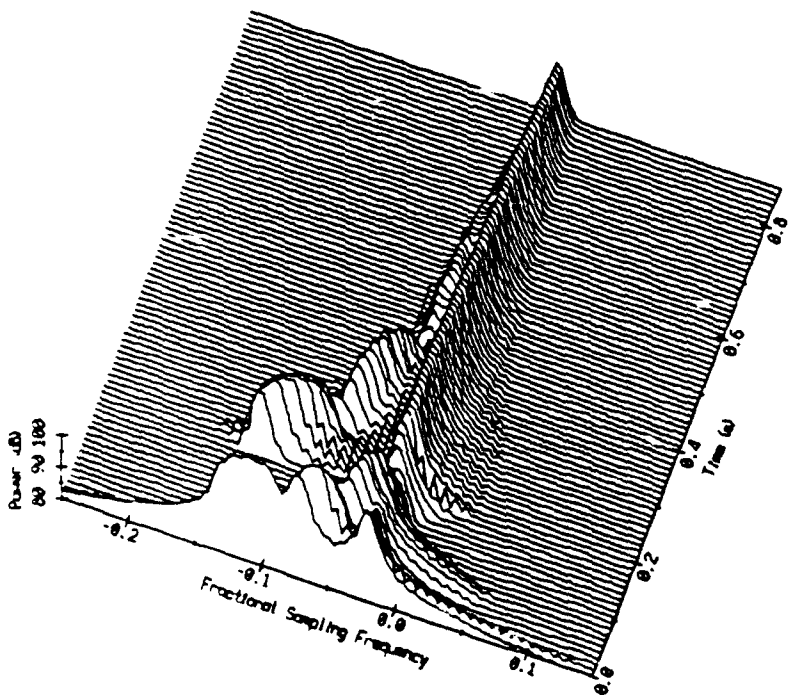

Figure 2.13b - RVMD - 9 Row Sum

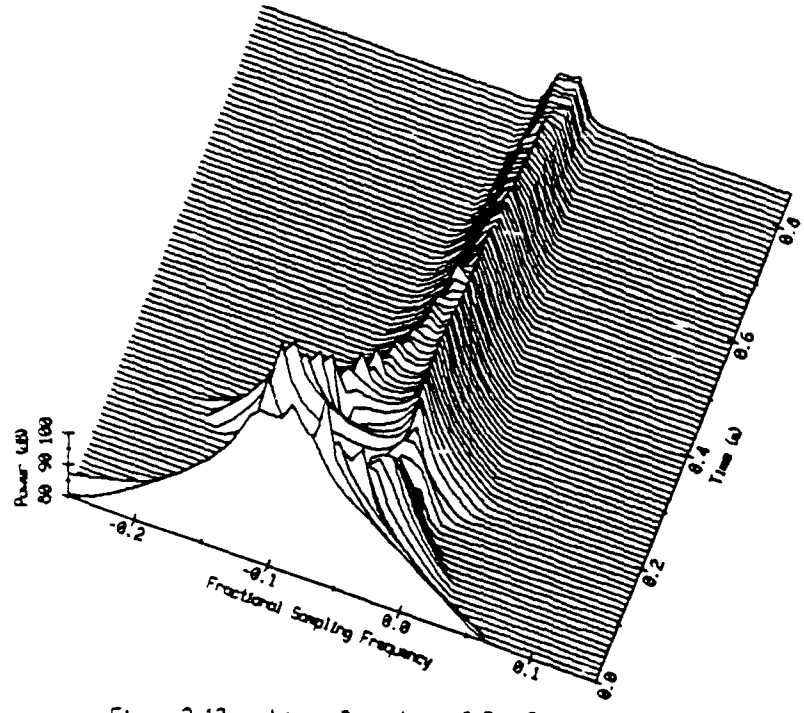

Figure 2.13c - Linear Predictor - 9 Row Sum

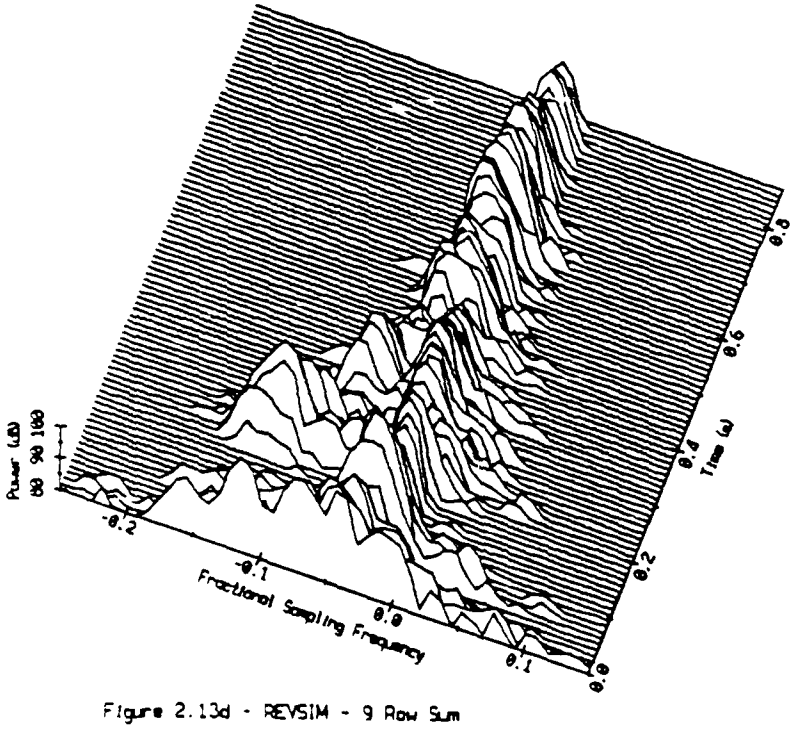

Figure 2.13d - REVSIM - 9 Row Sum

Figure 2.13. Main beam - high resolution range-Doppler maps.

3. Signal detection in boundary reverberation

As described in a previous chapter, ocean acoustic reverberation has a very complex nature, and a highly variable power spectrum. Reverberation is a source of interference which active sonar systems have to combat. In some situations, where the sonar array is fairly close to the ocean boundaries, the energy reflected off of these boundaries (bottom or surface), makes a significant contribution to the range-Doppler map. This contribution usually has a sudden onset, may appear at nonzero Doppler frequencies, and therefore may mask legitimate sonar echoes. The shape of the transmitting and receiving beams of the active sonar modify the time evolving range-Doppler map observed by the receiver. Traditionally, sonar systems have discriminated against boundary reverberation by forming fixed receiving beams which had low sidelobe characteristics in the direction of the ocean boundaries. However, the energy leaking through the low sidelobes may still be a major contributor to the overall noise background level. Furthermore, since the sonar system is typically moving and varying its depth in the water column, the direction of boundary reverberation is not fixed.

The above reasoning led many researchers to propose using an adaptive structure in order to track the interference direction and to place spatial beamformer nulls in that direction. Such a beamformer may continuously learn the boundary interference direction and adjust itself to cancel it out, thereby enhancing signal to noise ratio and improving the detection performance. Implementation of such an ad-hoc structure follows the lines of the well known adaptive noise canceler[66]. In addition to a main beam which receives well in the desired look direction, one or more reference beams are formed. The reference beams receive well in the direction of the boundary interference, and have spatial

nulls in the main look direction. The output of the main beam contains both the desired signal, and a contaminant which is the contribution of the boundary interference leaking through side lobes or the edges of the main lobe. Ideally, the reference beams contain only a replica of the interference. The output of the reference beam, or beams, is processed by an adaptive filter and then subtracted from the main beam. The adaptive filter tries to provide a good estimate of the interference portion of the main beam output, and the final error output ideally contains only the desired signal. Implementation of such adaptive reverberation cancellation schemes is reported by Hodgkiss and Alexandrou[23]. The boundary reverberation canceled output of the adaptive structure can now be treated as containing a known signal in noise (the volume reverberation), a classical, solved problem.

The proposed solution discussed so far is representative of an approach which is based on intuition. A typical conventional adaptive processor would combine one or more of the following building blocks in order to make a decision about target presence:

1. Fixed Beamformer.
2. Adaptive beamformer.
3. Adaptive nullformer.
4. Adaptive spectral whitener.
5. Matched filter.
6. Threshold detector.

Use of each of the above building blocks is intuitively reasonable, but it is not at all clear that any combination of these components yields an optimal processor (under any optimization criterion).

Another approach suggests treating the problem as a whole right from the

beginning without imposing intuitive components on the processor structure, and using all a-priori knowledge available. Detection theory provides us with a mathematical framework out of which optimum processors can be designed[54,64]. The processor will evolve out of the mathematical solution of the problem, and will not be restricted to using familiar structures.

Although Bayes optimal processors have been derived for the case of volume reverberation[55], little work has been done which takes advantage of a-priori knowledge of the time-evolving spatial characteristics of boundary reverberation. Related Bayes optimal work concerning interference sources of certain and uncertain (but not time varying) location is contained in[1] and [26,24,25] respectively.

Here, a classical detection theoretic approach is applied to the processing of a vector time series. That vector may be composed of the single array element outputs, or of some preformed beams. An optimality criterion is chosen, and then the processor structure is allowed to evolve freely out of the mathematical solution of the problem. Any uncertain parameters are treated as random variables and all knowledge about them is summarized in a-priori probability density functions.

3.1. The adaptive (noise canceling) ad-hoc detector

As previously mentioned, the time evolving nature of ocean acoustic boundary reverberation has led many researchers to try applying adaptive filtering schemes to an observed vector time series, in order to cancel out, or reduce the interference level present in it. The idea of adaptively canceling interference sources thereby enhancing the desired signal is intuitively reasonable, and seems very attractive. It is not at all clear, though, that using such a canceler as a building block, following it by another ad-hoc detection building

block is a globally optimal solution from any optimal detection criterion point of view.

As is implied from its name, an adaptive filter "adapts" to the changing conditions by varying its weights, and going through a learning process. Various mechanisms that control the variation of the filter weights have been proposed and implemented. Each one of these mechanisms is based on some optimality criterion (e.g. minimum mean square error), which is local to the adaptive filter structure, and does not necessarily conform to any global optimum detection criterion.

The adaptive filtering structures may be viewed as realizable approximate solutions to the classical optimal Wiener filtering problem, and can be developed both from a statistical point of view (assuming stationarity and ergodicity), or by using a deterministic least squares approach. Both approaches can be implemented through block processing or time-recursive techniques, and may be implemented in direct form, or through efficient lattice structures. Built into all of the adaptive filter implementations there is an adaptation coefficient which serves as a 'forgetting factor' (i.e. weighting less past in favor of more recent data).

There are three general classes of adaptive structures. The first class is based on the method of steepest descent and is generally referred to as the LMS algorithm. The work of Widrow and Hoff [67] has served as the basis to this method. The second class is the gradient lattice (GL), and the third is of the deterministic least squares type, and is referred to as the least squares lattice (LSL). A comparison between these three classes is beyond the scope of this work, and Alexandrou[4] is a good reference in that regard. Due to its superior behavior during abrupt changes in the processed data, the LSL class of adaptive filters has been typically selected by researchers dealing with the ocean boundary

reverberation problem. Hodgkiss and Alexandrou[23] and Alexandrou[5] have shown how the LSL filter can be used to cancel or reduce sea surface reverberation interference. LSL class adaptive filters are used in this dissertation as part of an ad-hoc detection scheme. In fact, a new structure of a joint process pole-zero adaptive LSL filter is developed in the next chapter, and its performance is compared to that of the standard all-zero LSL filter.

The ad-hoc detection scheme, then, accepts as inputs a main beam output which contains the signal contaminated by interference, and one or more reference outputs, which contain the interference alone. The adaptive filter tries to cancel the interference, and the filter's output is then presumed to be interference free, and is presented to a signal known exactly in noise known exactly Bayes optimum detector for making the decision. Figure 3.1 illustrates the structure of the ad-hoc detector.

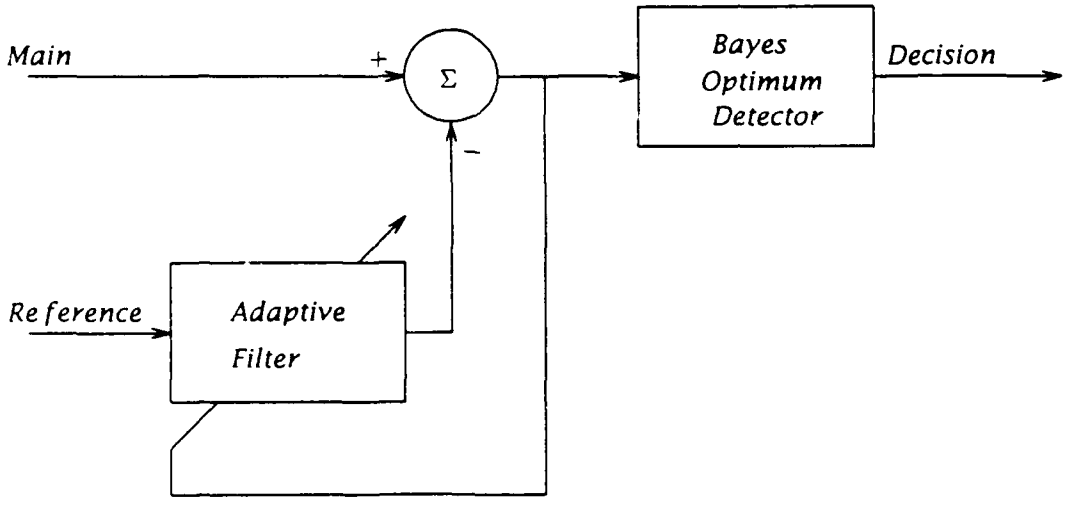

Figure 3.1 The ad-hoc detector

3.2. Complex exponential Fourier series representation of signals

In order to be able to use classical statistical techniques and apply those to optimal detection theory, we need to obtain a finite dimensional observation vector which is then used in computing the joint probability density functions under the true and the null hypotheses. These probability density functions, in turn, are used to form the likelihood ratio. Typically, the vector of observables available for processing is that of the array element outputs, or some preformed beam outputs. In any case, this is a vector of continuous time waveforms, which means that some mapping technique is required in order to collapse this space into a finite dimensional space. There are three well known techniques to perform this transformation, namely time sampling, Karhunen-Loeve expansion, and trigonometric Fourier series. The best selection of the mapping technique usually depends on the problem one is faced with, and a good choice can often reduce the complexity of writing the likelihood ratio expressions.

Adams and Nolte[1] have shown that using the trigonometric Fourier series mapping technique leads to significant mathematical tractability, and Hodgkiss[27] derived the conditions that have to be met in order to be able to represent the observed vector in terms of its Fourier coefficients. Certainly, with the advent of fast computers, and the availability of fast Fourier transformation algorithms, using this approach seems very attractive. The mathematical derivations of optimal Bayes detectors in this dissertation follow similar derivations made by Adams and Nolte[1] and Hodgkiss[27] except that their derivations dealt with the passive sonar problem, where this work is dealing with its active counterpart. The trigonometric Fourier series mapping is used, then, throughout this work.

It is well known that a well behaved function $f(t)$ on $\left(-\frac{T}{2}, \frac{T}{2}\right)$ can be

represented as:

$$f(t) = \lim_{N \to \infty} \sum_{-N}^{N} a(n) \left(\frac{1}{T}\right)^{1/2} \exp(jn\omega_0 t) \tag{3.1}$$

where $\omega_0 = \frac{2\pi}{T}$, and

$$a(n) = \left(\frac{1}{T}\right)^{1/2} \int_{-T/2}^{T/2} f(t)\exp(-jn\omega_0 t)dt \tag{3.2}$$

If $f(t)$ is bandlimited and has no dc component then on $\left(-\frac{T}{2}, \frac{T}{2}\right)$ $f(t)$ can be expressed as:

$$f(t) = 2 \text{ Re} \sum_{N_1}^{N_2} a(n) \left(\frac{1}{T}\right)^{1/2} \exp(jn\omega_0 t) \tag{3.3}$$

Then $f(t)$ is mapped into a finite-dimensional vector $\underline{f}$.

$$\underline{f}^T = [a(N_1), a(N_1+1), \ldots\ldots\ldots\ldots, a(N_2)] \tag{3.4}$$

The above can also be shown for a stationary random process $r(t)$, with power spectral density $R(\omega)$. It can be expressed on $\left(-\frac{T}{2}, \frac{T}{2}\right)$ as:

$$r(t) = \lim_{N \to \infty} \sum_{-N}^{N} z(n)\left(\frac{1}{T}\right)^{1/2} \exp(jn\omega_0 t) \tag{3.5}$$

where $z(n)$ is a random variable defined as in (3.2) above.

If r(t) is bandlimited and has no dc component then:

$$r(t) = 2 \text{ Re} \sum_{N_1}^{N_2} z(n)\left(\frac{1}{T}\right)^{1/2} \exp(jn\omega_0 t) \tag{3.6}$$

i.e. every realization of the random process $r(t)$ can be mapped into a vector:

$$z^T = [z(N_1), z(N_1+1), \ldots\ldots\ldots, z(N_2)] \tag{3.7}$$

If $r(t)$ is a Gaussian random process, then $z(n)$, which is a linear functional of $r(t)$ is a Gaussian random variable. For zero mean noise processes, z has the zero vector as its mean. For large T, Papoulis[47] has shown that the components of (3.7) are approximately uncorrelated and $z(n)$ has a variance $R(n\omega_0)$. The covariance matrix of z is therefore diagonal. It can also be shown that z is a complex Gaussian vector, i.e. is a $(N_2 - N_1 + 1)$-tuple of complex random variables such that the vector of real and imaginary parts is $(N_2 - N_1 + 1)$-variate Gaussian.

3.3. The array detection problem

An array of receiver elements observes a vector of time waveforms as follows:

$$r^T(t) = [r_0(t), r_1(t), \ldots\ldots\ldots r_{K-1}(t)] \tag{3.8}$$

where subscript denotes the array element.

If all the received waveforms are bandlimited then according to (3.2) one can express them in a Fourier expansion, as follows:

$$r_k(t) = \lim_{N \to \infty} \sum_{-N}^{N} z_k(n) \left(\frac{1}{T}\right)^{1/2} \exp(jn\omega_0 t) \tag{3.9}$$

The Fourier coefficients are:

$$z_k(n) = \left(\frac{1}{T}\right)^{1/2} \int_{-T/2}^{T/2} r_k(t) \exp(-jn\omega_0 t)\, dt \tag{3.10}$$

One can now group the Fourier coefficients for a single frequency index but from

all the array elements in a K dimensional vector as follows:

$$Z^T(n) = [z_0(n), z_1(n), \ldots\ldots\ldots, z_{K-1}(n)] \tag{3.11}$$

and group now vectors from all the frequency indices:

$$Z^T = [Z^T(N_1), Z^T(N_1 + 1), \ldots\ldots\ldots, Z^T(N_2)] \tag{3.12}$$

In this way the time waveform observed on the K elements is mapped into a $K(N_2 - N_1 + 1)$ dimensional vector. It can be shown that Z is a complex Gaussian vector, and that its covariance matrix (for large T), is block diagonal. There are $(N_2 - N_1 + 1)$ KxK blocks, each representing the correlation between array elements at a specific frequency.

3.4. Hypothesis testing

The theory of hypothesis testing began with the work of Bayes[6] on conditional probability. The notions of cost and risk were introduced by Wald[61], who initiated much of the recent theoretical work along the lines of the theory of games. Communications receivers based on the ideas of conditional probability were proposed by Kotel'nikov[30] in a dissertation from 1947, published in 1956 and translated into English in 1959. At the same time Woodward and Davies[70], and Woodward[71] suggested applying conditional probability to signal detection. An analysis of signal detection within the framework of conditional probability was performed by Middleton[39], and Peterson, Birdsall and Fox [48] were at the same time designing receivers based on the likelihood ratio. The following summarizes the thought process developed by the above mentioned researchers.

A processor which has available an observed vector time series z, has to be designed. The processor is forced to make a binary decision between two mutually exclusive and exhaustive hypotheses, namely, signal absent or signal present:

$$H_0 : \underline{z} = \underline{n}(\underline{\ell}_0) \tag{3.13}$$

$$H_1 : \underline{z} = \underline{s}(\underline{\ell}_1) + \underline{n}(\underline{\ell}_1) \tag{3.14}$$

where $\underline{n}(\underline{\ell}_0)$, $\underline{s}(\underline{\ell}_1)$ and $\underline{n}(\underline{\ell}_1)$ are noise and signal vectors written as functions of parameter vectors $\underline{\ell}_0$ and $\underline{\ell}_1$. The parameter vectors determine the shape and character of the noise and signal vectors, and may be fully known, partially known, or even completely unknown.

The processor's choice results in one of four different outcomes, i.e a false alarm, a miss, a detection or a null decision. Their corresponding probabilities are:

$$\textit{False Alarm}: \quad Q_{10} = \int_{R1} p_0(\underline{z})d\underline{z} \tag{3.15}$$

$$\textit{Miss}: \quad Q_{01} = \int_{R0} p_1(\underline{z})d\underline{z} \tag{3.16}$$

$$\textit{Detection}: \quad Q_{11} = \int_{R1} p_1(\underline{z})d\underline{z} \tag{3.17}$$

$$\textit{Null Decision}: \quad Q_{00} = \int_{R0} p_0(\underline{z})d\underline{z} \tag{3.18}$$

where $p_0(\underline{z})$ and $p_1(\underline{z})$ are the probability density functions of the observed vector under the two hypotheses.

A cost is attached to every one of the outcomes, and consequently a cost matrix is defined:

$$\underline{C} = \begin{bmatrix} C_{00} & C_{01} \\ C_{10} & C_{11} \end{bmatrix} \tag{3.19}$$

Where C_{ij} is the cost of choosing H_i when H_j is true. The cost selection depends heavily on the scenario of the problem, but usually the costs for making a correct

decision are chosen lower than those for an incorrect decision. A negative cost means a reward (conceivable for a correct decision).

A risk function is also attached to every outcome, and is defined as follows:

$$R=C_{ij}Q_{ij} \tag{3.20}$$

This function is the product of the cost and the probability of an outcome, and represents the risk incurred in case that outcome materializes.

3.5. The Bayes Criterion

The Bayes criterion attempts to minimize the average risk, and seems a natural approach for an observer forced to make a large number of decisions under repetitive circumstances. If ς is the probability that H_0 is true, the average risk is:

$$\bar{R} = \varsigma[C_{00}Q_{00} + C_{10}Q_{10}] + (1-\varsigma)[C_{01}Q_{01} + C_{11}Q_{11}] \tag{3.21}$$

$$= \varsigma[C_{00}\int_{R_0} p_0(z)dz + C_{10}\int_{R_1} p_0(z)dz] + (1-\varsigma)[C_{01}\int_{R_0} p_1(z)dz + C_{11}\int_{R_1} p_1(z)dz]$$

Now, since $\int_{R_0} p_i(z)dz = 1 - \int_{R_1} p_i(z)dz \quad i=0,1$

Then

$$\bar{R} = \varsigma[C_{00} + (C_{10} - C_{00})\int_{R_1} p_0(z)dz] + (1-\varsigma)[C_{01} + (C_{01} - C_{11})\int_{R_1} p_1(z)dz] \tag{3.22}$$

$$= \varsigma C_{00} + (1-\varsigma)C_{01} - (1-\varsigma)(C_{01} - C_{11})\int_{R_1}[p_1(z) - \Lambda_0 p_0(z)]dz$$

Where:

$$\Lambda_0 = \frac{\varsigma(C_{10} - C_{00})}{(1 - \varsigma)(C_{01} - C_{11})} \tag{3.23}$$

Furthermore, since $(C_{01} - C_{11})$ is positive, minimizing $\bar{R}$ means to select R_1 such that the integral is as large as possible. In other words, choose R_1 such that all points for which the expression $p_1(z) - \Lambda_0 p_0(z)$ is positive are included.

This leads to the following decision rule:

$$R_1 = [z : \Lambda(z) = \frac{p_1(z)}{p_0(z)} > \Lambda_0] \tag{3.24}$$

$$R_0 = [z : \Lambda(z) = \frac{p_1(z)}{p_0(z)} < \Lambda_0]$$

The optimum Bayes detector in the least risk sense is implemented, therefore, in forming the ratio $\Lambda(z) = \frac{p_1(z)}{p_0(z)}$ which is called the likelihood ratio. The likelihood ratio is compared to a prescribed threshold, and the decision is made based on the comparison's outcome. The above procedure serves as the basis for all the optimum detector derivations in this dissertation.

3.6. Implementing the Bayes criterion for the detection of a known signal in spatially correlated Gaussian noise

The following outlines the procedure used when deriving Bayes optimum detectors. This case is a very simple one, in which everything is known about the signal and the noise, and there is no boundary interference. Such may be the case in the deep ocean, where the boundaries are far enough from the array so that the reflections off of them are highly absorbed. Also, if an interference canceling scheme is used prior to the Bayes detector, the processor may assume that interference was canceled out completely, and implement the following approach:

The processor observes a vector time series as follows:

$$\underline{r}^T(t) = [r_0(t), r_1(t), \ldots\ldots\ldots, r_{K-1}(t)] \qquad \frac{-T}{2} < t < \frac{T}{2} \tag{3.25}$$

Under H_1 :

$$r_k(t) = s_k(t) + n_k(t) \qquad \frac{-T}{2} < t < \frac{T}{2} \tag{3.26}$$

Under H_0 :

$$r_k(t) = n_k(t) \qquad \frac{-T}{2} < t < \frac{T}{2} \tag{3.27}$$

As shown before, one can write:

$$n_k(t) = 2 \text{ Re} \sum_{N_1}^{N_2} a_k(n) \left(\frac{1}{T}\right)^{1/2} \exp(j2n\omega_0 t) \qquad \frac{-T}{2} < t < \frac{T}{2} \tag{3.28}$$

$$s_k(t) = 2 \text{ Re} \sum_{N_1}^{N_2} b_k(n) \left(\frac{1}{T}\right)^{1/2} \exp(j2n\omega_0 t) \qquad \frac{-T}{2} < t < \frac{T}{2} \tag{3.29}$$

and

$$r_k(t) = 2 \text{ Re} \sum_{N_1}^{N_2} z_k(n) \left(\frac{1}{T}\right)^{1/2} \exp(j2n\omega_0 t) \qquad \frac{-T}{2} < t < \frac{T}{2} \tag{3.30}$$

When noise alone is observed, $\underline{Z}$, defined before, is a zero mean complex Gaussian vector with covariance matrix $\underline{Q}$.

When a signal is present, $\underline{Z}$ is a complex Gaussian random vector with covariance matrix $\underline{Q}$ and mean:

$$m^T = [b_0(N_1), b_1(N_1), \ldots\ldots, b_{K-1}(N_1), b_0(N_1+1), \ldots\ldots, b_{K-1}(N_1+1), \ldots\ldots, b_{K-1}(N_2)] \quad (3.31)$$

The probability density functions are then:

$$p(Z/H_1) = \frac{1}{\pi^K |Q|} \exp[-(Z-m)^* Q^{-1}(Z-m)] \quad (3.32)$$

$$p(Z/H_0) = \frac{1}{\pi^K |Q|} \exp[-Z^* Q^{-1} Z] \quad (3.33)$$

Form the likelihood functional:

$$\Lambda(Z) = \frac{p(Z/H_1)}{p(Z/H_0)} = \exp[-(Z-m)^* Q^{-1}(Z-m) + Z^* Q^{-1} Z] \quad (3.34)$$

Any monotone function of the likelihood functional can serve as a sufficient statistic:

$$\ln\Lambda(Z) = -(Z-m)^* Q^{-1}(Z-m) + Z^* Q^{-1} Z \quad (3.35)$$

$$= -Z^* Q^{-1}(Z-m) + m^* Q^{-1}(Z-m) + Z^* Q^{-1} Z$$

$$= -Z^* Q^{-1} Z + Z^* Q^{-1} m + m^* Q^{-1} Z - m^* Q^{-1} m + Z^* Q^{-1} Z$$

$$= Z^* Q^{-1} m + m^* Q^{-1} Z - m^* Q^{-1} m$$

since $m^* Q^{-1} m$ isn't related to the observed vector Z, another sufficient statistic is:

$$\frac{1}{2}[Z^* Q^{-1} m + m^* Q^{-1} Z] = \mathrm{Re}\,[Z^* Q^{-1} m] \quad (3.36)$$

$$= \mathrm{Re} \sum_{N_1}^{N_2} Z^*(n) Q^{-1}(n) [b_0(n), \ldots\ldots, b_{K-1}(n)]^T$$

where $Q^{-1}(n)$ is the inverse of the nth block $Q(n)$ of the block diagonal matrix Q.

Thus, the resultant optimum detector instructs us to implement a matched filter where we correlate the observed vector with the signal mean vector.

The above derivation serves as an 'example recipe', which is repeated in this work in order to arrive at Bayes optimum detectors which apply to various scenarios and statistical assumptions.

4. JCLSL and JCARMA - all-zero and pole-zero adaptive filters

One approach to the problem of interference rejection in an array processing context is the use of an adaptive beamforming structure which dynamically steers a spatial null towards the source of undesirable signal. Interference leaks into the output of a conventionally formed beam through sidelobes pointing towards the source of interference. One or more reference beams can be constructed which receive well the interference but are prevented from passing signals propagating from the desired look direction. The outputs of these reference beams are adaptively filtered to provide a good estimate of the contaminant, and are then subtracted from the output of the conventional beam. Such a structure is performing a noise canceling operation.

Since a beamformer weights and sums the outputs from a finite number of array elements, it implements a spatial FIR digital filter. The response characteristics of a beamformer will exhibit nulls as a function of either: (1) source arrival angle at a given frequency or (2) source frequency at a given arrival angle. Beam based adaptive beamformers can perform poorly due to nulls in the response characteristics of the reference channel beamformer. A reference channel adaptive filter implementing poles can partially compensate for these nulls.

4.1. An all-zero adaptive filter

The all-zero, joint process, least squares lattice structure (JCLSL) used in this dissertation has been discussed in detail elsewhere[21,2] along with applications to the adaptive array processing problem. Figure 4.1 depicts the general structure of this adaptive filter, and Figure 4.2 details the single stage structure.

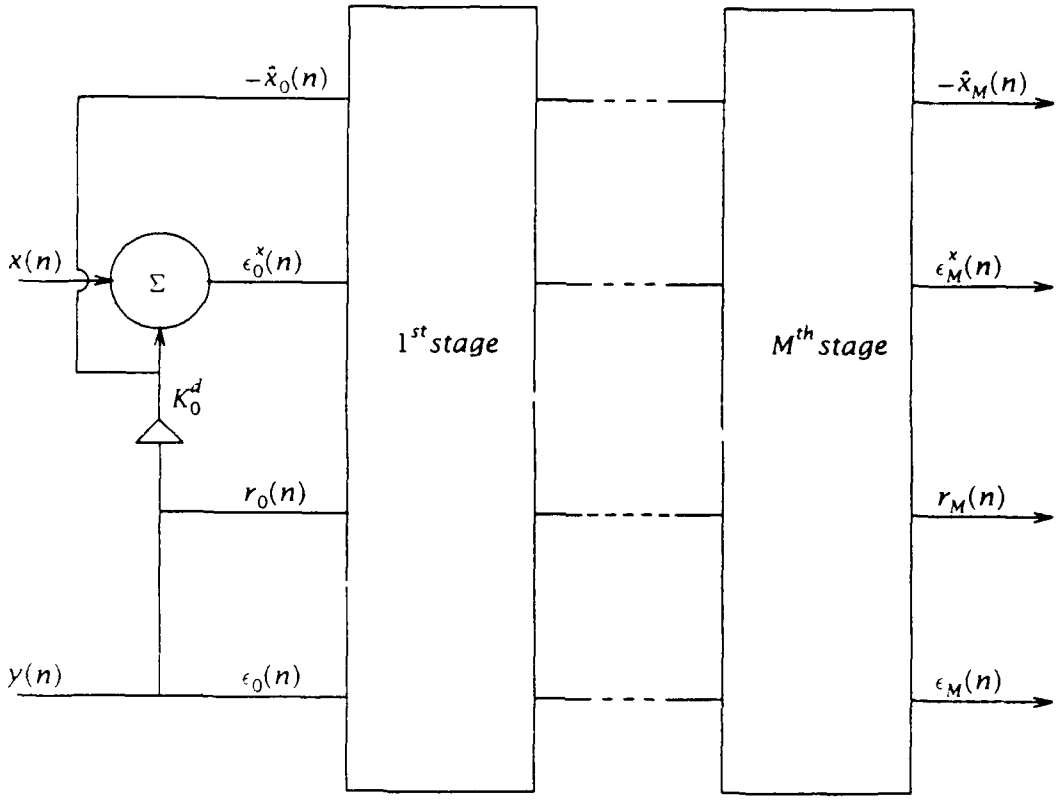

Figure 4.1. All-zero, joint process, least squares lattice filter

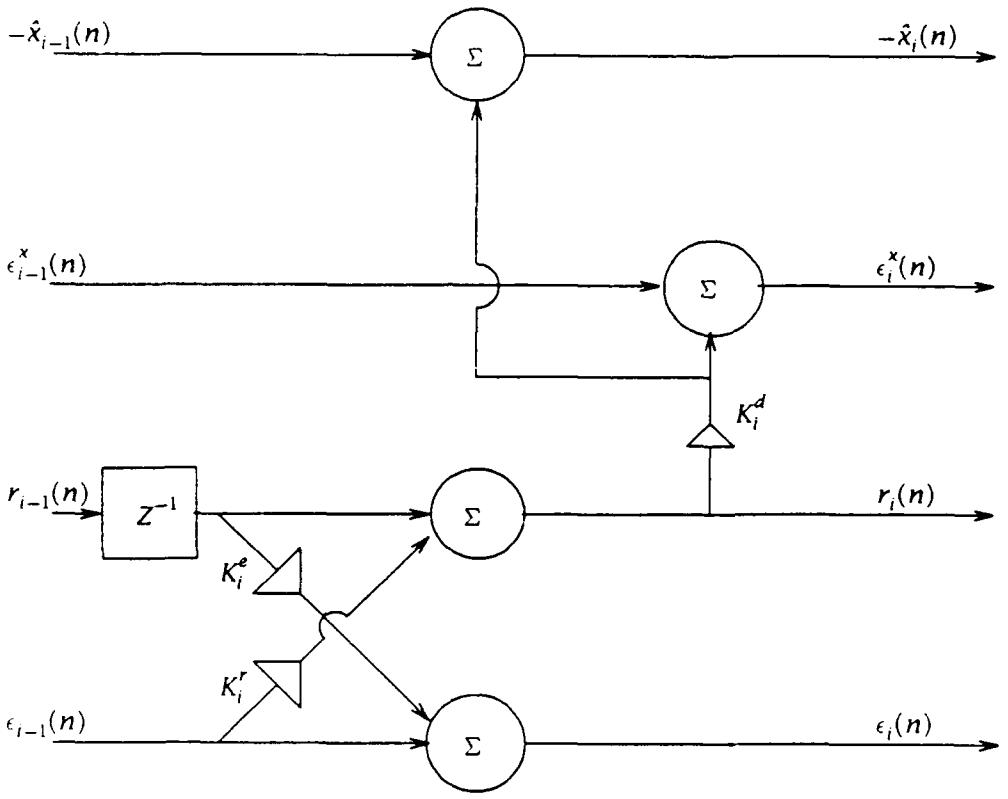

Figure 4.2. i^{th} stage of the filter

The reference channel process $y(n)$ is filtered to form an estimate of the primary channel process $x(n)$ (the desired signal). Of particular importance in noise canceling applications is the residual $e^x_M(n)$ obtained by adding the filtered reference channel to the primary channel. In an adaptive beamforming application $x(n)$ is the output of a conventional beam containing an interference contamination, and $y(n)$ is the output of the formed reference beam. The filter attempts to form a good estimate of the contaminant present in $x(n)$.

4.2. The pole-zero complex adaptive joint process least squares lattice

This section will formulate and solve the joint process estimation problem, where the estimated process is assumed to be an ARMA process, and therefore the

linear predictor takes the form of a pole-zero structure. The single channel all-zero linear predictor and the all-zero joint process estimator, as well as the pole-zero linear predictor have all been developed and documented[21,2,32,17,16,53]. An embedding approach is taken, where a scalar ARMA process is embedded into a vector AR process, and the previously developed AR recursions are utilized to produce the pole-zero joint process estimator recursions. The benefit of using the more complex adaptive filter possessing both poles and zeros is finally demonstrated through a simulation example.

4.3. The input-output ARMA process model:

Consider a scalar data sequence $y(n)$ which is assumed to be an M^{th} order ARMA process of the form:

$$y(n)+a_{M,1}y(n-1)+.....+a_{M,M}y(n-M) = b_{M,0}u(n)+.....+b_{M,M}u(n-M) \quad (4.1)$$

where the orders of the AR and MA parts of the ARMA process are chosen to be equal for presentation convenience, and u(n) is the input to the ARMA filter. Note that by simply dividing equation (4.1) by $b_{M,0}$, it can be turned around to form:

$$u(n)+d_{M,1}u(n-1)+.....+d_{M,M}u(n-M) = c_{M,0}y(n)+.....+c_{M,M}y(n-M) \quad (4.2)$$

Here, $u(n)$ is also represented as an ARMA process.

The innovations of $y(n)$ and $u(n)$ are, respectively:

$$\epsilon_M^y(n) = y(n)-\hat{y}(n) \quad (4.3)$$

$$\epsilon_M^u(n) = u(n)-\hat{u}(n) \quad (4.4)$$

where

$$\hat{y}(n) = -a_{M,1}y(n-1)-.....-a_{M,M}y(n-M)+b_{M,1}u(n-1)+.....+b_{M,M}u(n-M) \quad (4.5)$$

and

$$\hat{u}(n) = -d_{M,1}u(n-1)-.....-d_{M,M}u(n-M)+c_{M,1}y(n-1)+.....+c_{M,M}y(n-M) \quad (4.6)$$

4.4. The embedding approach:

Equations (4.3)-(4.6) can be combined into a single matrix equation in the form of a 2-dimensional AR linear predictor equation:

$$\begin{bmatrix}\epsilon_M^y(n)\\ \epsilon_M^u(n)\end{bmatrix} = \begin{bmatrix}y(n)\\ u(n)\end{bmatrix} + \sum_{i=1}^{M}\begin{bmatrix}a_{M,i} & -b_{M,i}\\ -c_{M,i} & d_{M,i}\end{bmatrix}\begin{bmatrix}y(n-i)\\ u(n-i)\end{bmatrix} \quad (4.7)$$

The backward linear prediction equation can also be written in terms of an embedded ARMA process in a vector AR process:

$$\begin{bmatrix}r_M^y(n)\\ r_M^u(n)\end{bmatrix} = \begin{bmatrix}y(n-M-1)\\ u(n-M-1)\end{bmatrix} + \sum_{i=1}^{M}\begin{bmatrix}e_{M,M+1-i} & -f_{M,M+1-i}\\ -g_{M,M+1-i} & h_{M,M+1-i}\end{bmatrix}\begin{bmatrix}y(n-i)\\ u(n-i)\end{bmatrix} \quad (4.8)$$

where $r_M^y(n)$ and $r_M^u(n)$ are the M^{th} order backward prediction error signals. Equations (4.7) and (4.8) are then just AR forward and backward linear prediction equations for the 2-dimensional process:

$$\underline{w} = \begin{bmatrix}y(n)\\ u(n)\end{bmatrix} \quad (4.9)$$

The most crucial assumption made here is that $u(n)$ can indeed be represented by equation (4.2). Lee[31] shows that in most cases this assumption is valid. Furthermore, implicit in this approach is the availability of the innovation process $u(n)$ to the ARMA filter. Since this input is unavailable, a bootstrapping approach is taken, in which ϵ_M^y, the best estimate of $u(n)$, is fed back to the input, and used

instead. Now one can use the previously derived AR process recursions to compute the ARMA process linear predictor recursions and also the joint ARMA process recursions. The ARMA process linear predictor recursions are well documented[31,53,32] and we will not repeat them here. Instead, we will extend the joint process AR estimator recursions to get the joint ARMA process estimator recursions. The notation used in the following equations is: $y(n)$ represents the reference process being filtered to predict the "desired" signal $x(n)$. $u(n)$ is the reference signal innovation process. The first index always represents order number, and the second represents time.

The recursion for the desired signal prediction error in the joint AR process estimator is[31] :

$$\epsilon^{x}_{i+1,n} = \epsilon^{x}_{i,n} - \Delta^{x}_{i+1,n} R^{-r}_{i+1,n} r_{i+1,n} \tag{4.10}$$

where Δ_M is the M^{th} order AR process cross correlation coefficient, and R^{-r}_M is the M^{th} order AR process backward prediction error covariance inverse. Using the embedding approach, we now have in the ARMA case:

$$r_{i+1,n} = \begin{bmatrix} r^{y}_{i+1,n} \\ r^{u}_{i+1,n} \end{bmatrix} \tag{4.11}$$

where, again, $u(n)$ is the innovation process of the reference signal $y(n)$. Now, combining (4.10) and (4.11) we get:

$$\epsilon^{x}_{i+1,n} = \epsilon^{x}_{i,n} - \Delta^{x^T}_{i+1,n} R^{-r}_{i+1,n} r_{i+1,n} \tag{4.12}$$

where

$$\Delta^{x^T}_{i+1,n} = (\Delta^{xy}_{i+1,n} , \Delta^{xu}_{i+1,n}) \tag{4.13}$$

$$R_{i+1,n}^{-r} = \frac{\begin{bmatrix} R_{i+1,n}^{ruu} & -R_{i+1,n}^{ryu} \\ -R_{i+1,n}^{ruy} & R_{i+1,n}^{ryy} \end{bmatrix}}{R_{i+1,n}^{ryy} R_{i+1,n}^{ruu} - R_{i+1,n}^{ryu} R_{i+1,n}^{ruy}}$$

It follows then that:

$$\epsilon_{i+1,n}^{x} = \epsilon_{i,n}^{x} - \frac{1}{\Delta_{i+1,n}} (\Delta_{i+1,n}^{xy}, \Delta_{i+1,n}^{xu}) \begin{bmatrix} R_{i+1,n}^{ruu} & -R_{i+1,n}^{ryu} \\ -R_{i+1,n}^{ruy} & R_{i+1,n}^{ryy} \end{bmatrix} \begin{bmatrix} r_{i+1,n}^{y} \\ r_{i+1,n}^{u} \end{bmatrix} \tag{4.14}$$

where

$$\Delta_{i+1,n} = R_{i+1,n}^{ryy} R_{i+1,n}^{ruu} - R_{i+1,n}^{ryu} R_{i+1,n}^{ruy}$$

Further:

$$\begin{aligned} \epsilon_{i+1,n}^{x} = \epsilon_{i,n}^{x} &- \frac{1}{\Delta_{i-1,n}} (\Delta_{i+1,n}^{xy} R_{i+1,n}^{ruu} - \Delta_{i+1,n}^{xu} R_{i+1,n}^{ruy}) r_{i+1,n}^{y} \\ &- \frac{1}{\Delta_{i+1,n}} (-\Delta_{i+1,n}^{xy} R_{i+1,n}^{ryu} - \Delta_{i+1,n}^{xu} R_{i+1,n}^{ryy}) r_{i+1,n}^{u} \end{aligned} \tag{4.15}$$

Now define the joint process reflection coefficients as:

$$K_{i+1,n}^{dxy} = \Delta_{i+1,n}^{xy} R_{i+1,n}^{ruu} - \Delta_{i+1,n}^{xu} R_{i+1,n}^{ruy} \tag{4.16}$$

$$K_{i+1,n}^{dxu} = \Delta_{i+1,n}^{xy} R_{i+1,n}^{ryu} - \Delta_{i+1,n}^{xu} R_{i+1,n}^{ryy}$$

and finally the desired signal prediction error recursion is:

$$\epsilon_{i+1,n}^{x} = \epsilon_{i,n}^{x} - K_{i+1,n}^{dxy} r_{i+1,n}^{y} - K_{i+1,n}^{dxu} r_{i+1,n}^{u} \tag{4.17}$$

The recursions for Δ^{xy} and Δ^{xu} are given by:

$$\Delta_{i+1,n+1}^{xy} = (1-\alpha)\Delta_{i+1,n}^{xy} + \frac{\epsilon_{i,n+1}^{x} r_{i+1,n+1}^{y^*}}{1-\gamma_{i,n+1}} \tag{4.18}$$

$$\Delta^{xu}_{i+1,n+1} = (1-\alpha)\Delta^{xu}_{i+1,n} + \frac{\epsilon^{x}_{i,n+1} r^{u^*}_{i+1,n+1}}{1-\gamma_{i,n+1}}$$

where $(1-\alpha)$ is the exponential weighting factor, and γ is the likelihood variable. The recursions for R^{ryy}, R^{ruy}, R^{ryu} and R^{ruu} are given by:

$$R^{ryy}_{i+1,n+1} = (1-\alpha)R^{ryy}_{i+1,n} + \frac{r^{y}_{i+1,n+1} r^{y^*}_{i+1,n+1}}{1-\gamma_{i,n+1}} \tag{4.19}$$

$$R^{ryu}_{i+1,n+1} = (1-\alpha)R^{ryu}_{i+1,n} + \frac{r^{y}_{i+1,n+1} r^{u^*}_{i+1,n+1}}{1-\gamma_{i,n+1}}$$

$$R^{ruy}_{i+1,n+1} = (1-\alpha)R^{ruy}_{i+1,n} + \frac{r^{u}_{i+1,n+1} r^{y^*}_{i+1,n+1}}{1-\gamma_{i,n+1}}$$

$$R^{ruu}_{i+1,n+1} = (1-\alpha)R^{ruu}_{i+1,n} + \frac{r^{u}_{i+1,n+1} r^{u^*}_{i+1,n+1}}{1-\gamma_{i,n+1}}$$

And all the above recursions yield the joint ARMA process estimator structure shown in Figure 4.3. Figure 4.4 details the single stage structure.

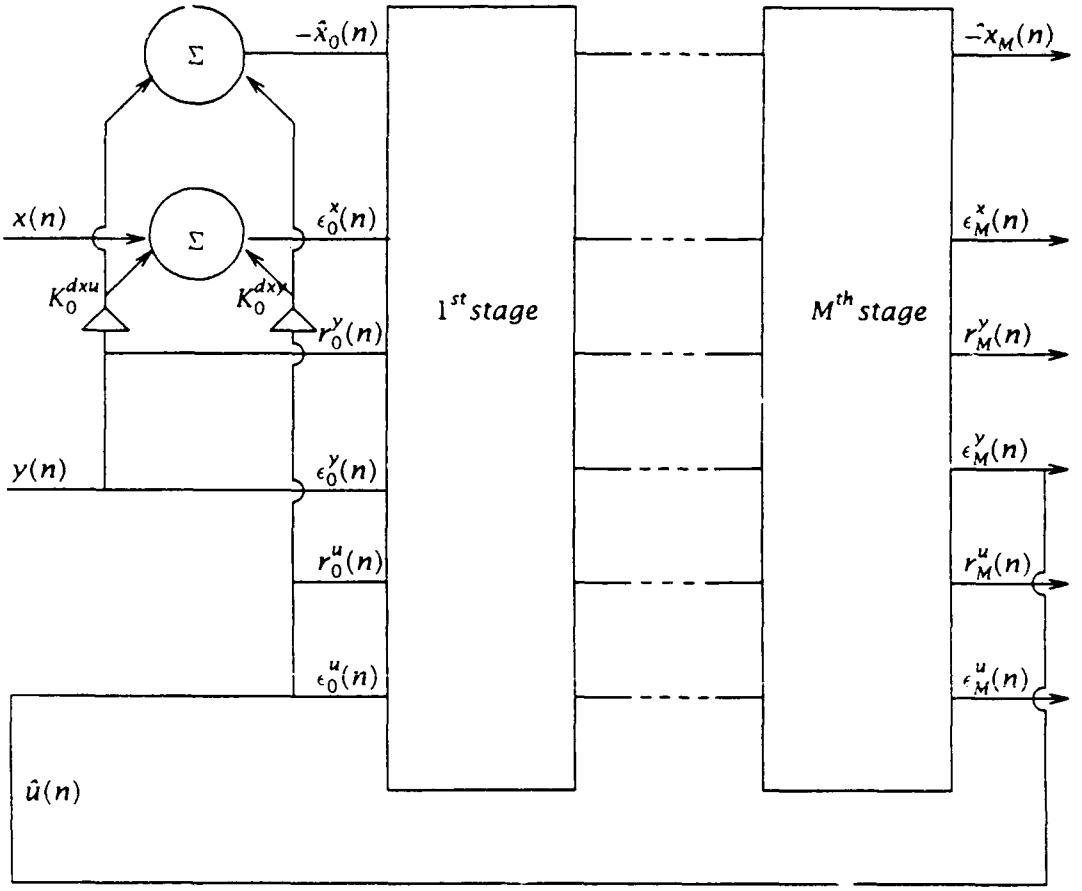

Figure 4.3. Pole-zero, joint process, least squares lattice filter

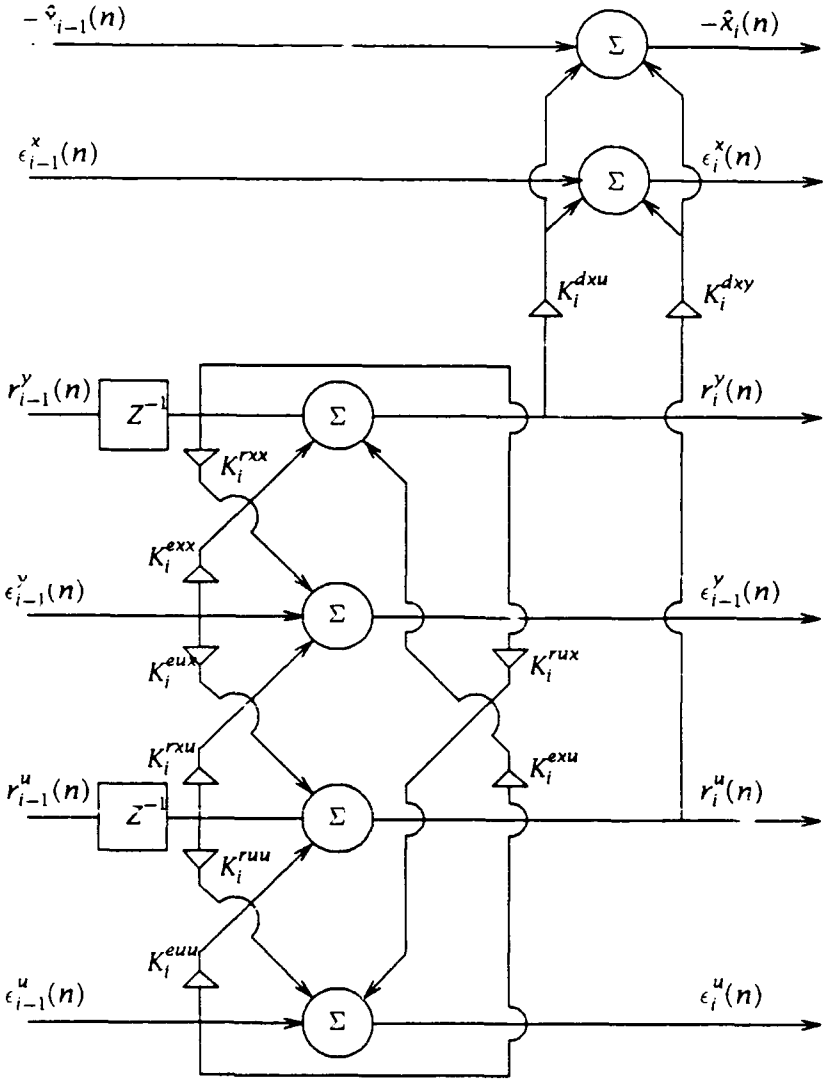

Figure 4.4. i^{th} stage of the structure

4.5. Simulations

Two sets of simulations will be used to compare the performance of the all-zero (JCLSL) and the pole-zero (JCARMA) least square lattice adaptive noise canceling structures.

Figure 4.5 describes how the input data was generated for the first simulation.

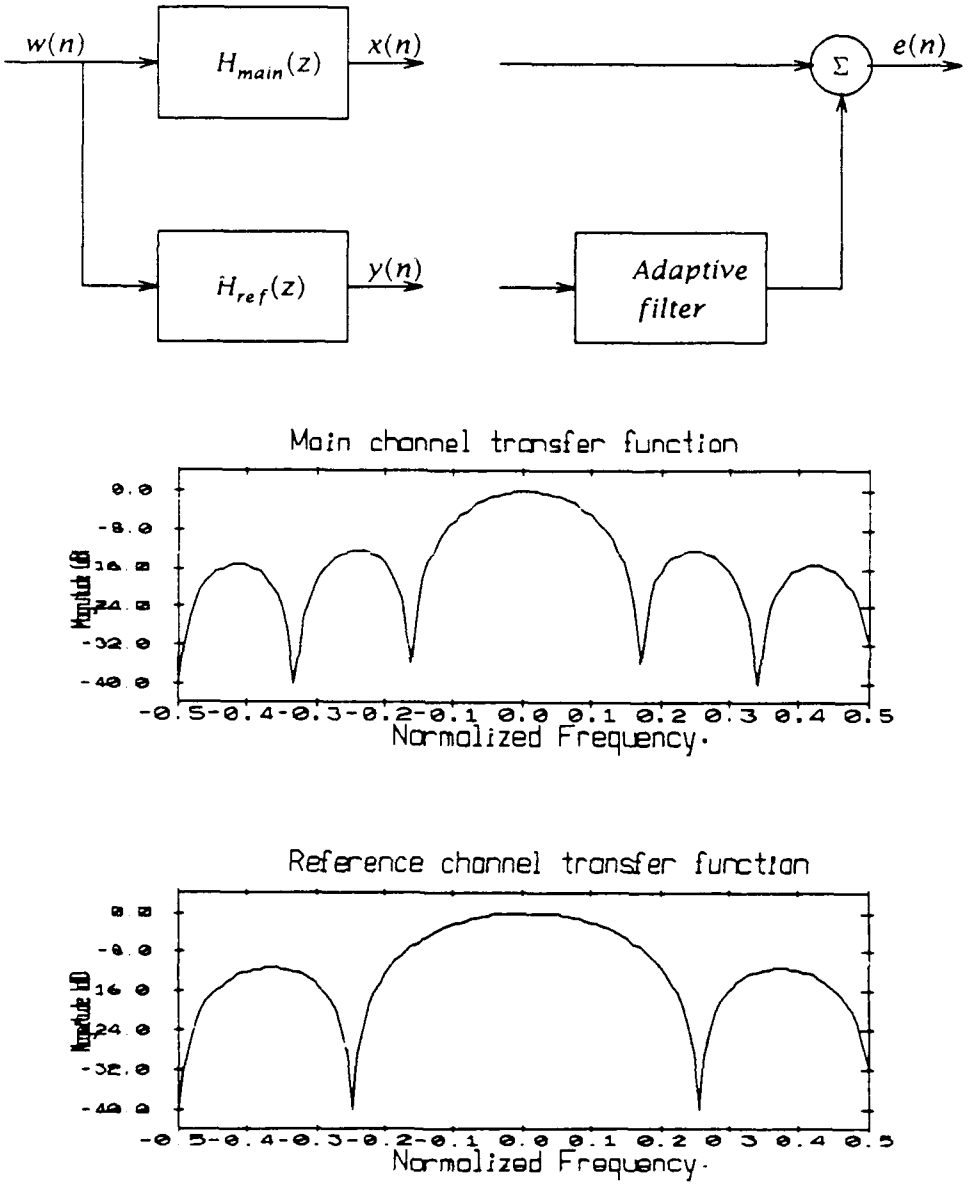

Figure 4.5. Data generation model.

A white noise time series $w(n)$ has been passed through two simple FIR digital filters. $H_{main}(z)$, generating the main channel data $x(n)$, consists of a 6-point rectangular window. $H_{ref}(z)$, generating the reference channel data $y(n)$, consists

of a 4-point rectangular window. Since the goal of the adaptive filter is to invert the characteristics of the reference channel transfer function, $H_{ref}(z)$, and to model the characteristics of the main channel transfer function, $H_{main}(z)$, this example presents a case where the ability to adapt poles is important.

Figure 4.6 displays error power as a function of time at the output of JCLSL and JCARMA for filter order p=4. The results show that JCARMA has a several dB lower error signal power than JCLSL.

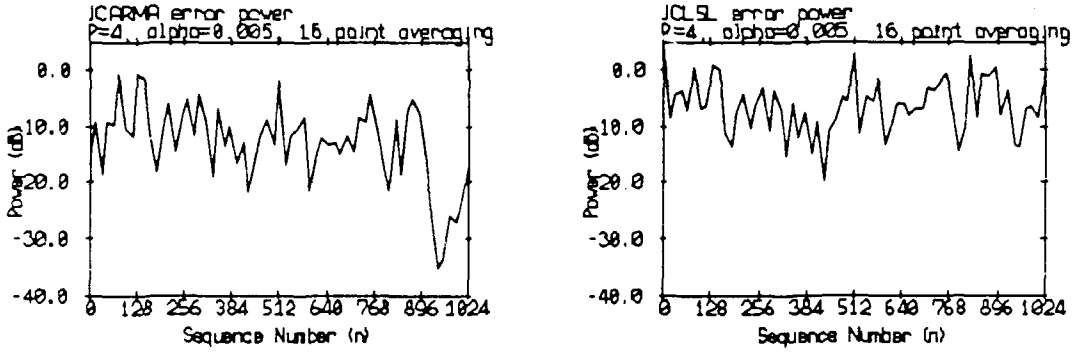

Figure 4.6. JCARMA vs. JCLSL error power vs. time (p=4)

Additional insight is gained by looking at the power spectra in Figure 4.7 (JCLSL), and Figure 4.8 (JCARMA). The left hand pair of panels are estimates of the main and reference channel input power spectra (white noise passed through H_{main} and H_{ref}). Note the dip in the reference channel spectrum which is centered on the first sidelobe of the main channel power spectrum. It is in this particular region that the adaptive filter can use the ability to adapt poles. The right hand pair of panels are estimates of the adaptive filter output and error $e(n)$ power spectra. As can be seen, JCARMA is able to properly match the spectral characteristics of the main channel where JCLSL cannot.

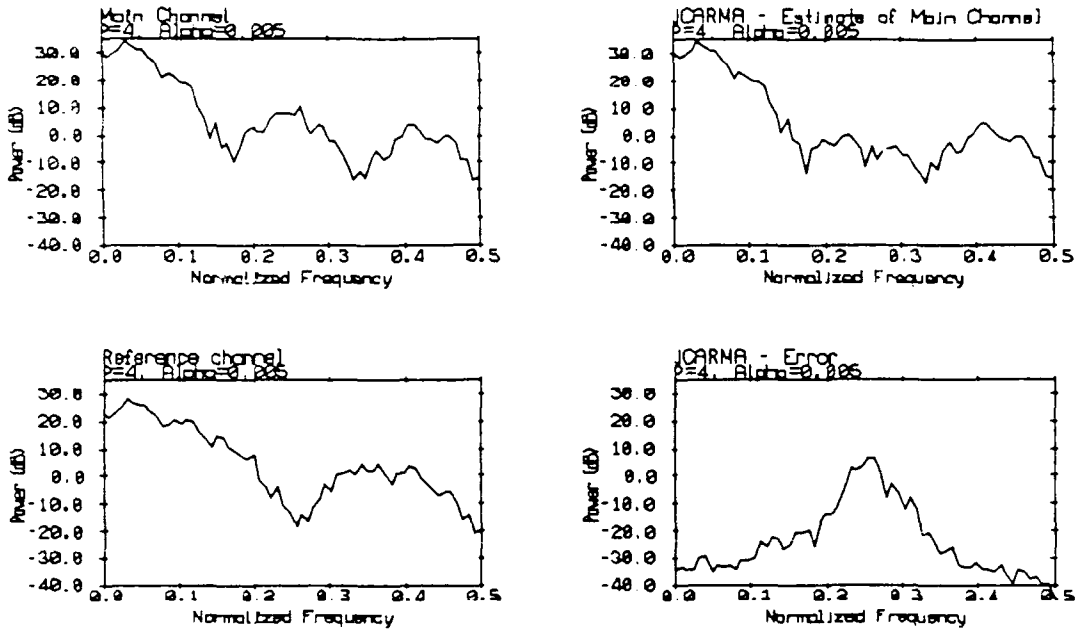

Figure 4.7. JCARMA, p=4

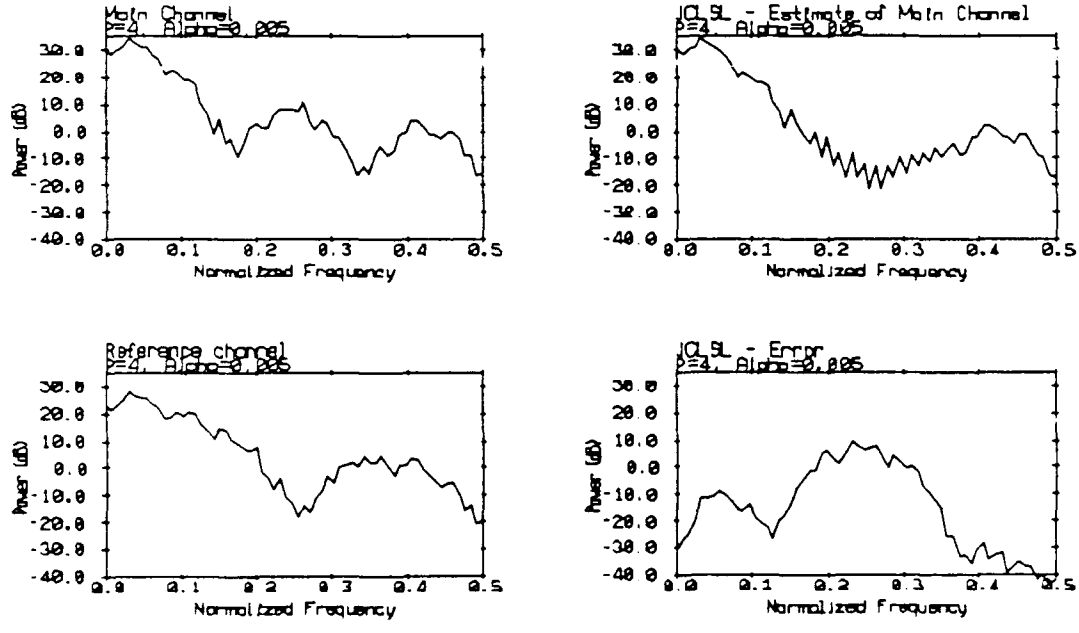

Figure 4.8. JCLSL, p=4

Figures 4.9, 4.10 and 4.11 repeat the simulation with filter order p=8. Note that even with the additional degrees of freedom, JCLSL for p=8 is unable to perform

as well as JCARMA for p=4.

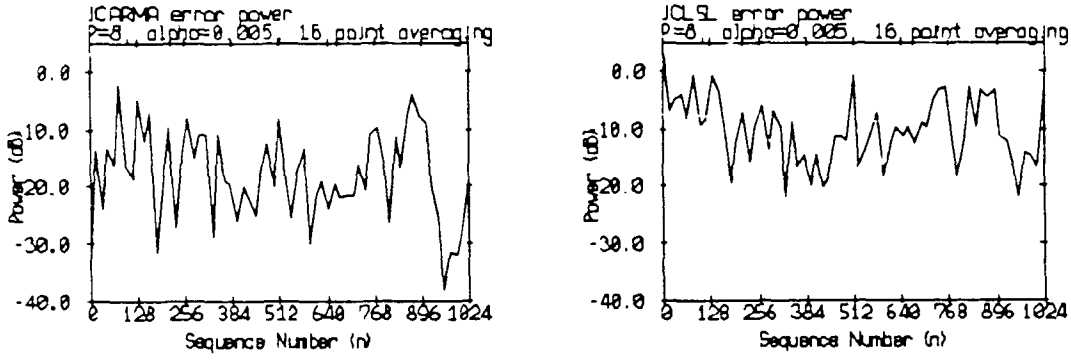

Figure 4.9. JCARMA vs. JCLSL error power vs. time (p=8)

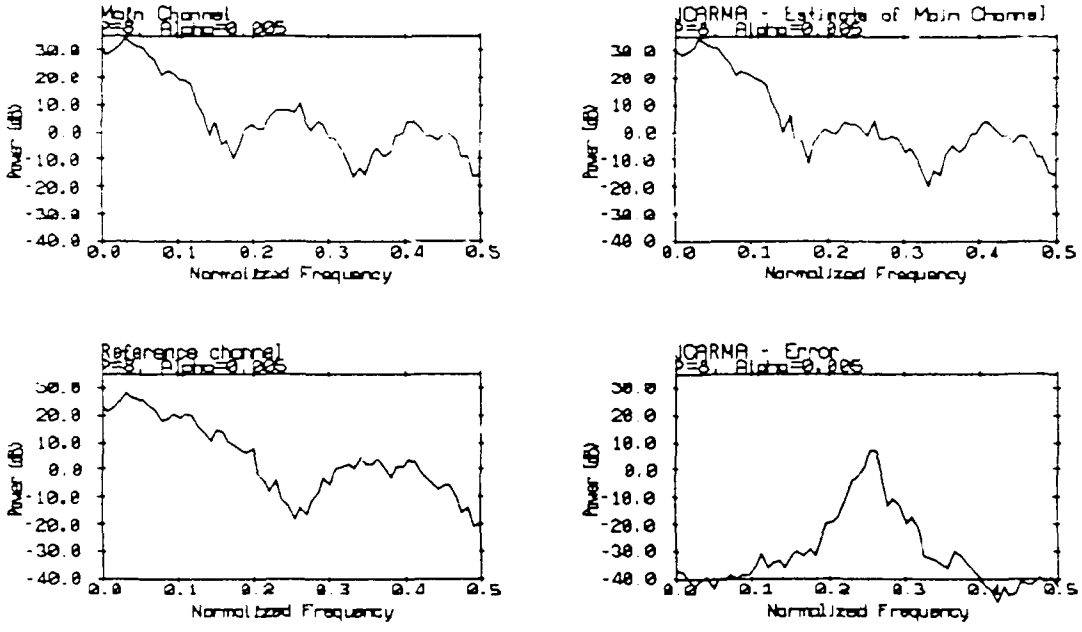

Figure 4.10. JCARMA, p=8

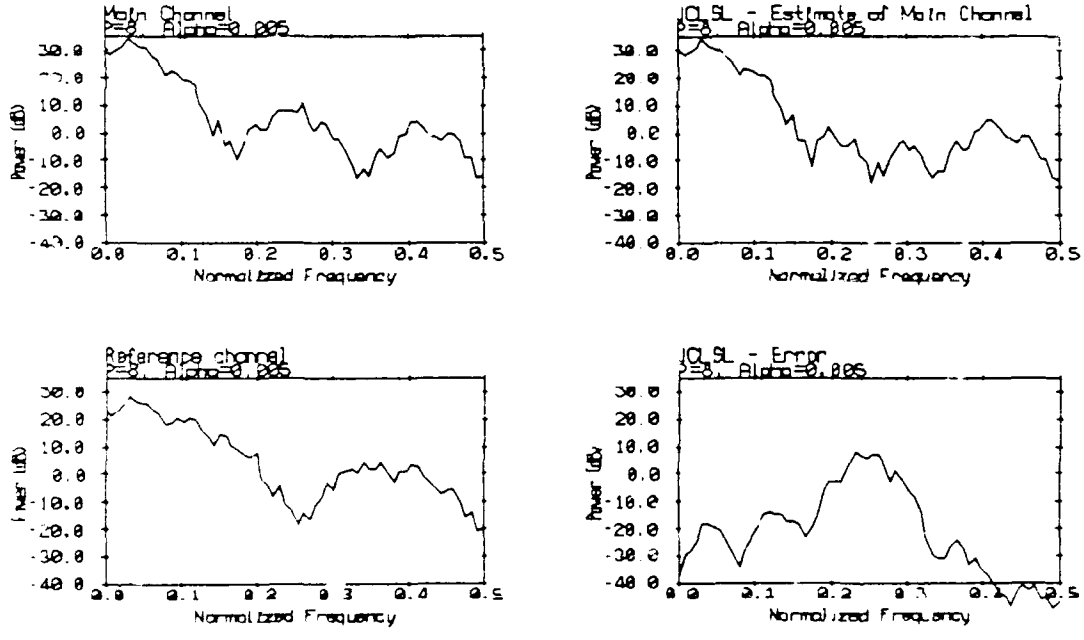

Figure 4.11. JCLSL, p=8

4.6. REVGEN simulation

The second simulation was set up using a real ocean environment, and REVGEN, a REVerberation GENerator discussed in Chapter 2. This is a reverberation simulation package which implements directly the point scattering model[50]. The returns from a large number of discrete scatterers, distributed randomly throughout the ocean volume and boundaries, are summed coherently to obtain the reverberation time series.

The sonar receiving array is made of four elements, and is placed at a depth of 150m, in water which is 450m deep. The array platform is moving at 12.5 knots. A pure tone, 180 msec pulse is transmitted and propagated through the water column. The transmit beampattern is uniform over 60 azimuthal degrees and 150 vertical degrees. The return volume, surface and bottom reverberation time series for each of the array elements is generated by REVGEN. Two conventional beams are formed, a primary beam using the sum of all four array element time series, and a reference beam using the difference between the two middle element time series.

It is clear from the above description, and from examining the beampatterns that the sonar array will receive boundary reverberation which might hinder its ability to receive well from the desired look direction (straight ahead). An adaptive filter continuously steering a spatial null in the direction of the interference may improve the sonar's performance. Here, the performance of JCARMA will be compared again to that of JCLSL, under the described scenario.

Figure 4.12 details the polar beampatterns of the main and reference channels along a vertical cross-section. Figure 4.13 details the spatial beampatterns of the main and reference channels. Figure 4.14 depicts range-

Doppler maps of the main and reference channel time series, after the platform's own speed has been compensated for by shifting the entire range-Doppler map by the proper amount. The surface reverberation return is clearly seen, peaking around 0.5 sec and -0.2 cycles/sample.

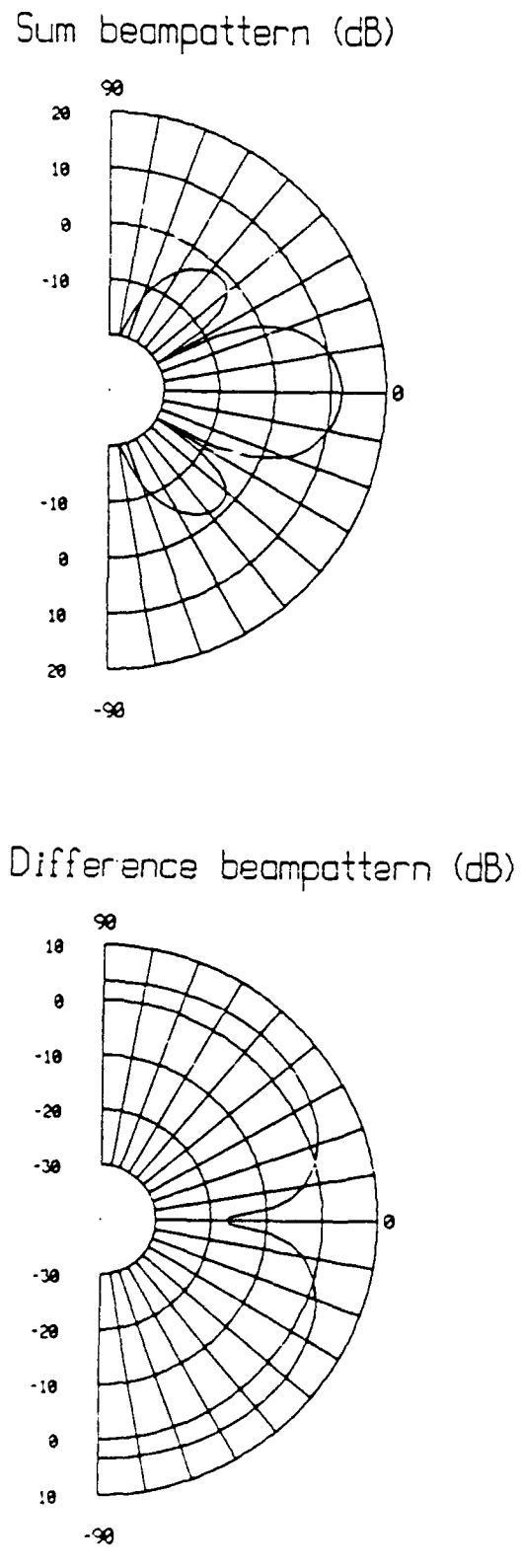

Figure 4.12. Main and Reference channels polar beampatterns.

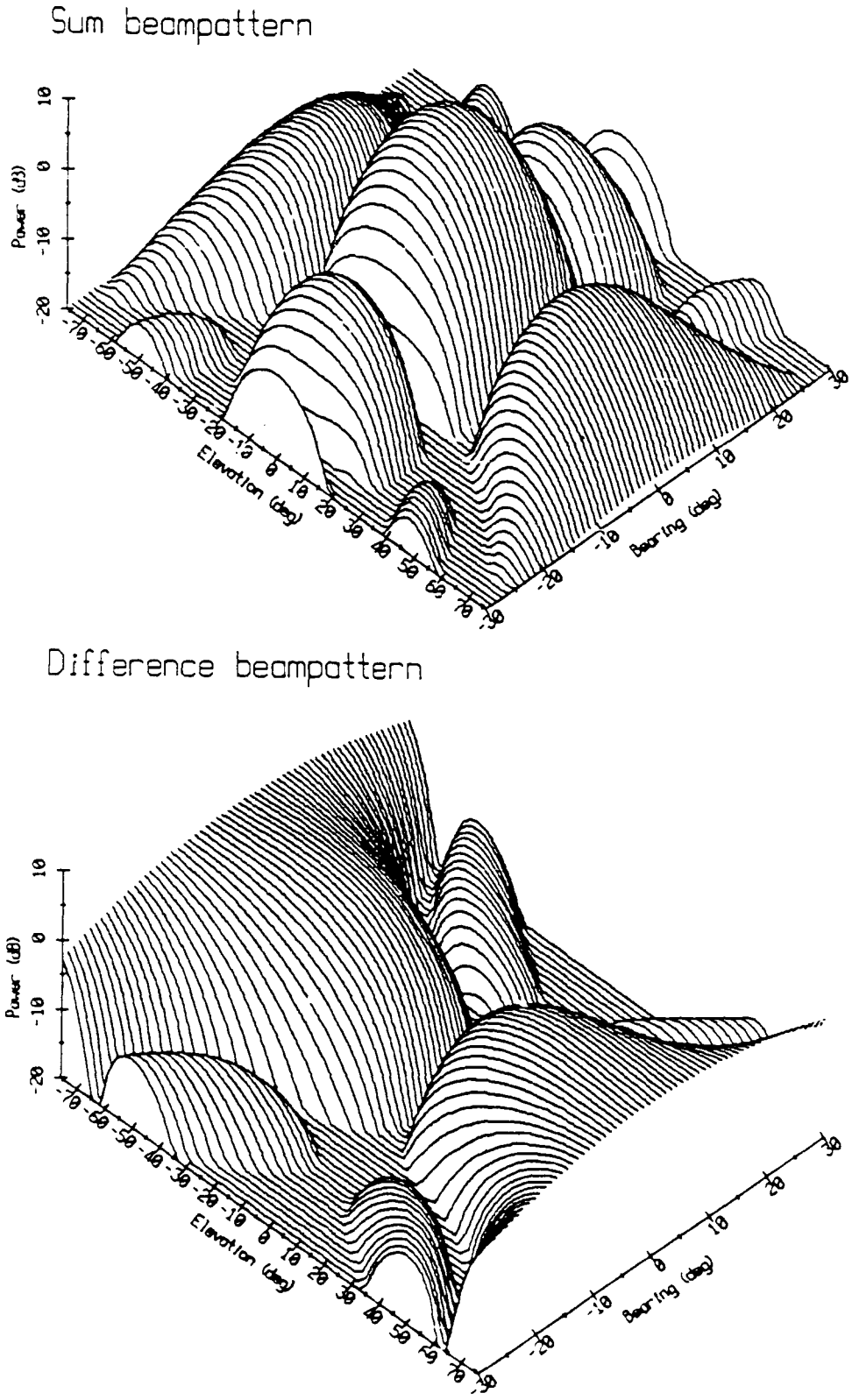

Figure 4.13. Main and Reference channels spatial beampatterns.

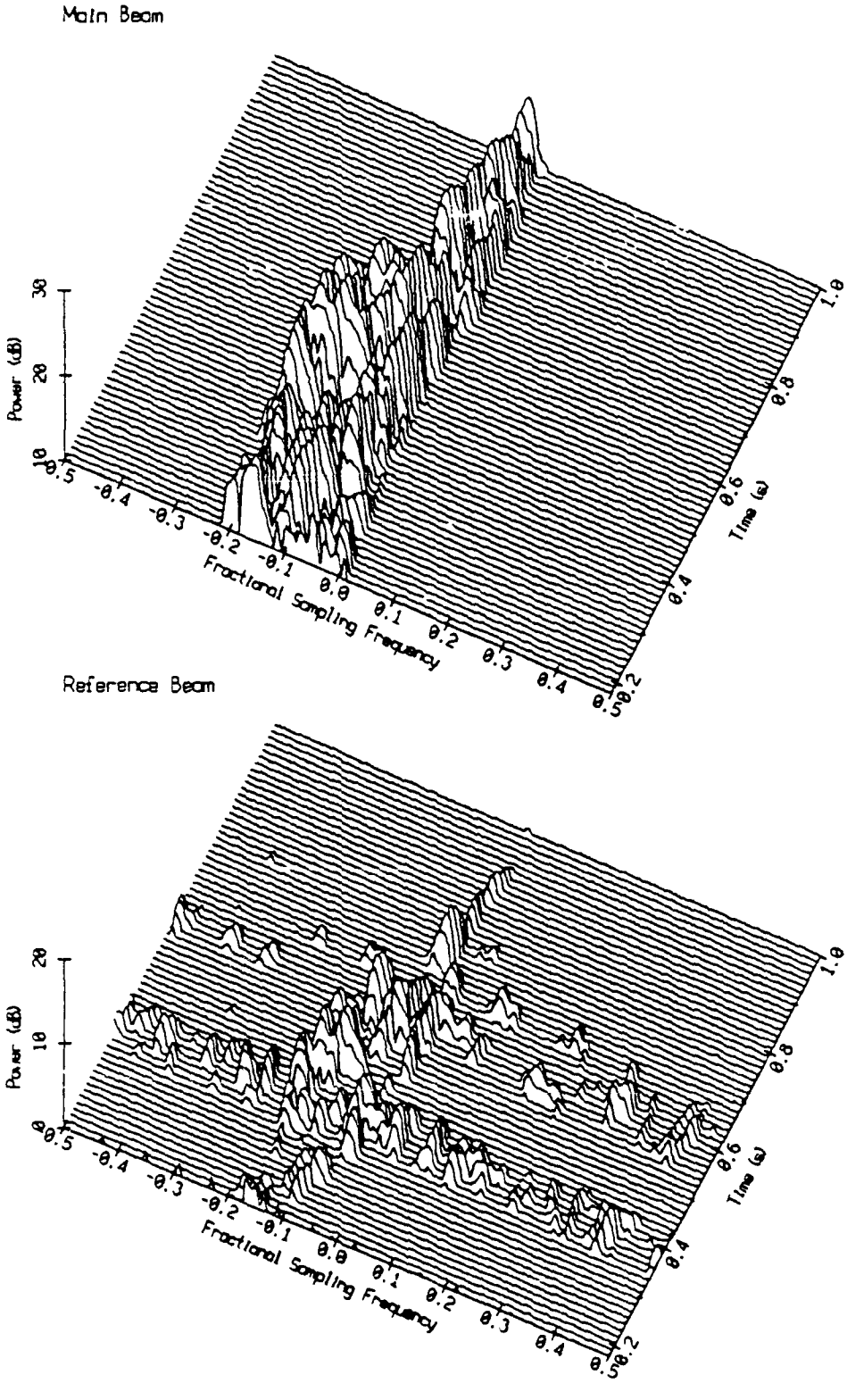

Figure 4.14. Main and Reference channels range-Doppler maps.

Now we pass the 2-beam vector time series through the two adaptive filtering structures (JCLSL and JCARMA), and examine the results. For both filters, filter order was set to 3, and α to 0.02. Figure 4.15 depicts the two adaptive filter outputs. Though it is clear that both filters have done a good job of reducing the surface interference level, thereby allowing better reception from the look direction, it is not clear in this case that JCARMA performs better than JCLSL. Plotting the overall time evolving power levels (Figure 4.16) and the JCLSL/JCARMA error power ratio (Figure 4.17) further reveals that in this scenario there is only a slight performance advantage for JCARMA over JCLSL. The error power ratio departs 0 towards the positive side wherever JCARMA does better than JCLSL. The scenario used above will be used again in this dissertation to test and compare the performance of different detectors. The above serves as an indicator, which has been confirmed in other simulations, that in these scenarios, the slight performance advantage of JCARMA over JCLSL, does not justify the higher algorithmic complexity, and the higher run-time investment.

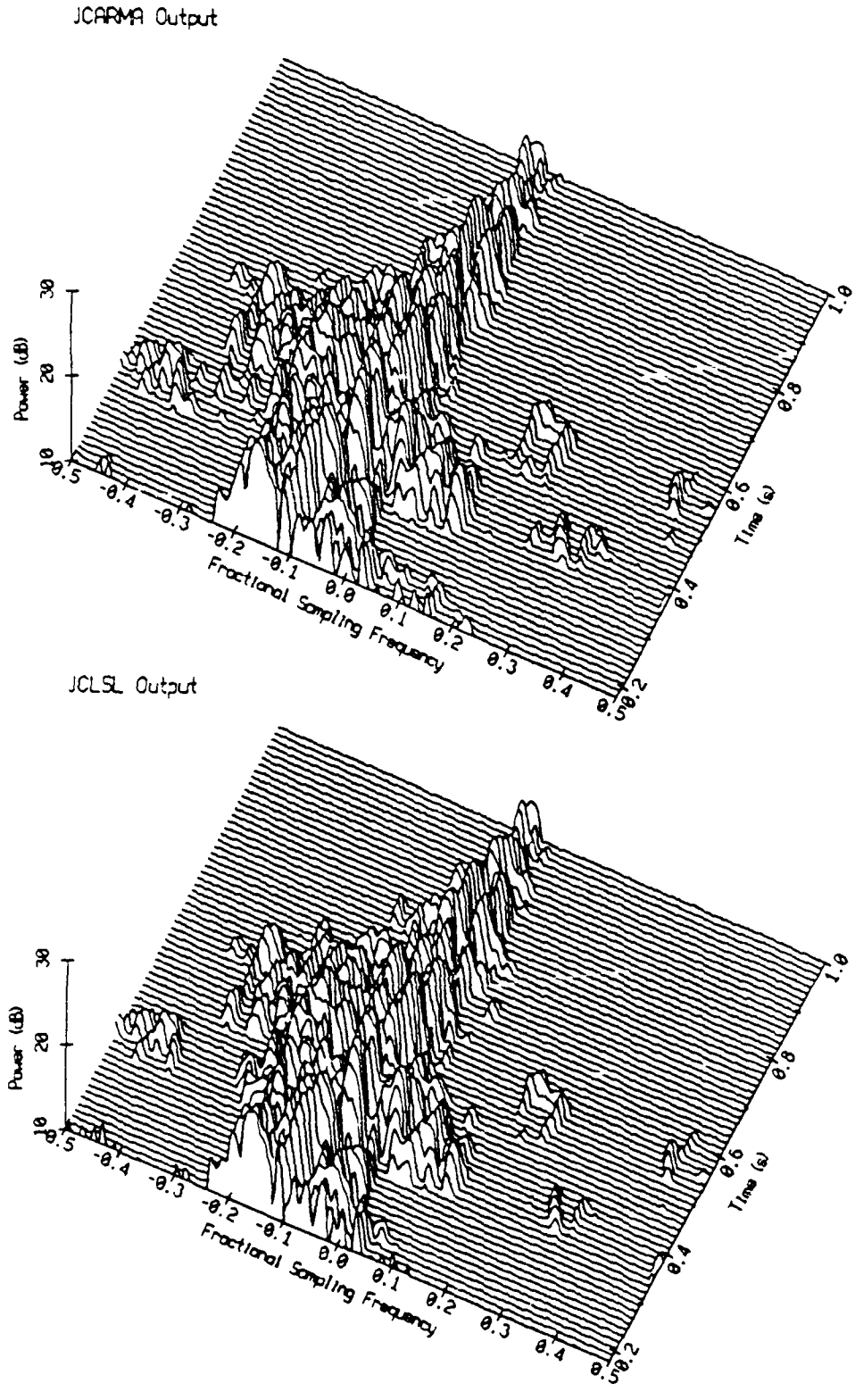

Figure 4.15. JCLSL vs. JCARMA filter output range-Doppler maps.

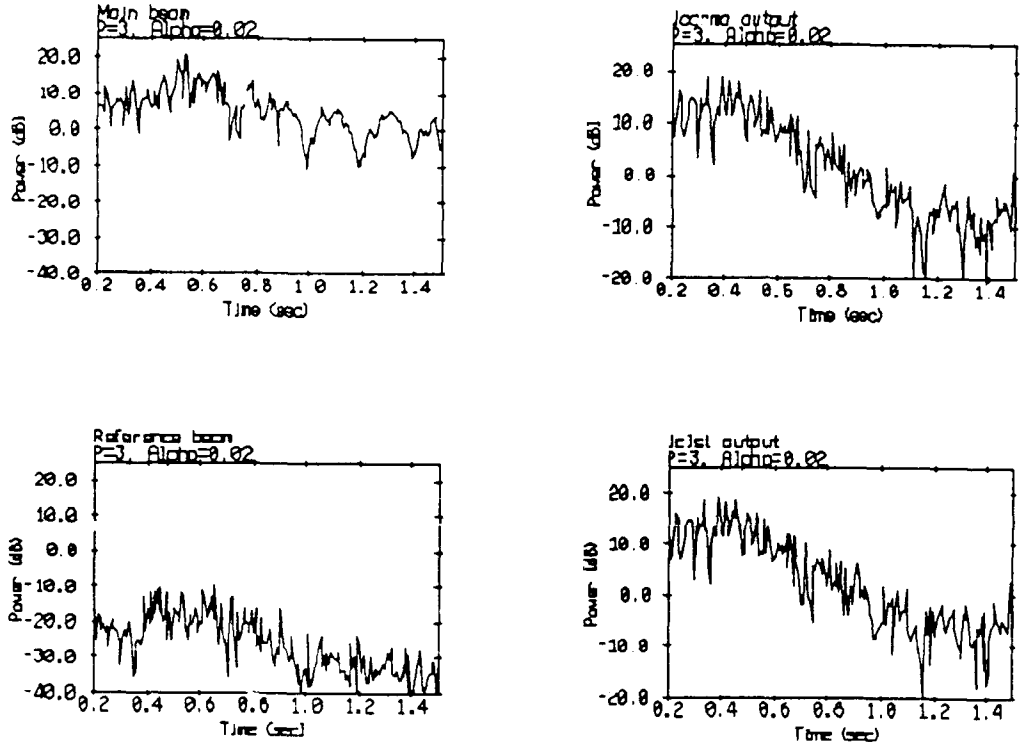

Figure 4.16. REVGEN simulation - power levels.

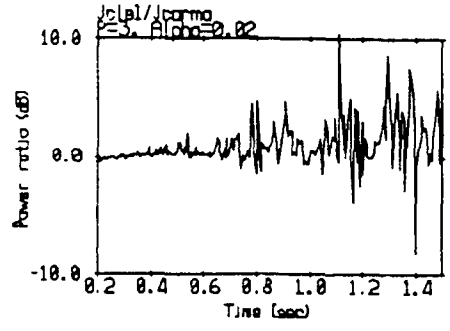

Figure 4.17. REVGEN simulation - JCLSL/JCARMA error power ratio.

5. Three specific problems and their corresponding Bayes optimum detectors

This chapter deals with a specific scenario which an active sonar system may encounter. Bayes optimum detectors are developed for three different sub-scenarios, whose level of uncertainty is ever increasing. The setting is as follows: an active sonar system is mounted on an underwater platform which is submerged in shallow ocean water. In this context shallow water means that the first reflection of acoustic energy back into the receiver is significant. The ocean depth is chosen such that there is a significant no-overlap zone between the two boundary (surface and bottom) interferences, and therefore only one of them is considered, meaning detection is performed in the no-overlap zone. The platform's depth in the water column is either known, or has a known probability density function. Sound speed profiles are assumed isovelocity, i.e. acoustic energy propagates through the medium in straight lines. The platform is completely stationary in the water column, i.e. the effective own Doppler speed is zero. The sonar's front end is a four element sensor array whose preformed beam outputs are available to the processor in the form of a sampled vector time series. The preformed beam ensemble contains a sum beam which is formed by summing all element outputs, and one or more difference beams formed by subtracting two adjacent element outputs. It is further assumed that the transmission pulse is narrowband, that the incoming signal characteristics are completely known, and that the target is stationary. The sonar is assumed to be limited in performance by acoustic reverberation and not by ambient ocean noise. This assumption is typically valid in medium and high frequency systems, certainly when dealing with relatively short ranges.

The three sub-scenarios are as follows:

1. Platform is at a fixed, precisely known depth.

2. Platform is at an unknown depth, but the depth probability density function is known precisely.

3. Platform is at an unknown depth, but the depth probability density function is known precisely. Also, there is a fixed interference source whose direction probability density function is known precisely.

Since the transmitted energy is propagating through the water, the boundary interference direction is changing constantly. In the case where platform depth is known exactly, the interference direction is also known exactly. When there is uncertainty in platform depth, it translates to uncertainty in the direction of the incoming boundary interference.

In the first two sub-scenarios, a sum-difference beam arrangement is sufficient, since there are two degrees of freedom, namely signal and boundary interference. In the third sub-scenario, another interference source is introduced, and therefore another degree of freedom is required. That is why in this scenario another difference beam is formed and used, and the problem's dimension increases.

As discussed in Chapter 1, ocean acoustic reverberation has been the subject of numerous studies[36,35,13,46]. These studies clearly show that the complex envelope magnitude of acoustic reverberation is Rayleigh distributed, and that the real and imaginary components of this envelope are jointly Gaussian distributed. This property of reverberation justifies using Gaussian probability density functions in all the derivations of the Bayes optimum detectors in this dissertation.

In Chapter 3, a general expression was derived for the likelihood function in the case of a known signal in spatially correlated Gaussian noise:

$$\Lambda(Z) = \frac{p(Z/H_1)}{p(Z/H_0)} = \exp[-(Z-m)^{*}Q^{-1}(Z-m) + Z^{*}Q^{-1}Z] \qquad (5.1)$$

Equation (5.1) will serve as the basis for computing the Bayes optimum detectors in the three sub-scenarios addressed in this chapter. It is clear that key to this derivation is our ability to precisely and accurately arrive at the covariance matrix inverse expressions.

Figure 5.1 depicts the power spectrum of a typical sonar ping at the range where detection is attempted.

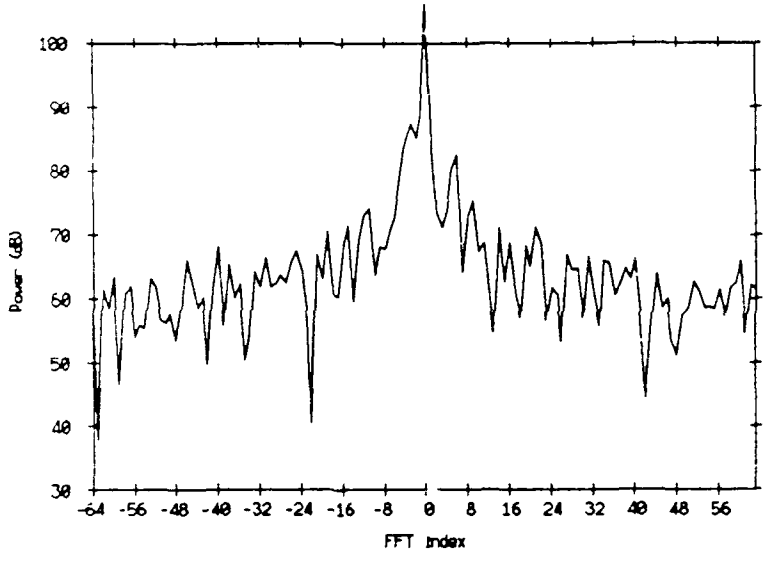

Figure 5.1. Sum beam power spectrum

It is apparent that due to this problem's setting (i.e. a narrowband transmission pulse, 0 vehicle speed, 0 target speed), almost all the spectral content is located in frequency index 0, or DC. For this reason, it is sufficient to use a single frequency term in computing the received signal Fourier transform vector Z, the covariance matrix Q, which ends up containing a single block, and the signal mean vector m.

5.1. Derivation of the two beam covariance matrix

Typically, active sonar systems operating at medium and high frequencies, are reverberation limited. The detection ranges of these systems are usually such that reverberation dominates the ambient ocean noise which is therefore ignored[60]. The ability to precisely evaluate the total reverberation (volume, surface and bottom) covariance matrix, is the foundation to the correct derivation of the likelihood functional. That will lead to the design of a true optimal detector in the "Bayesian" sense.

Consider the four element array which we use. We have available two beams: sum and difference. The sum beam is a sum of all four channels, and the difference beam is a difference between the two center channels. Figure 5.2 depicts this arrangement:

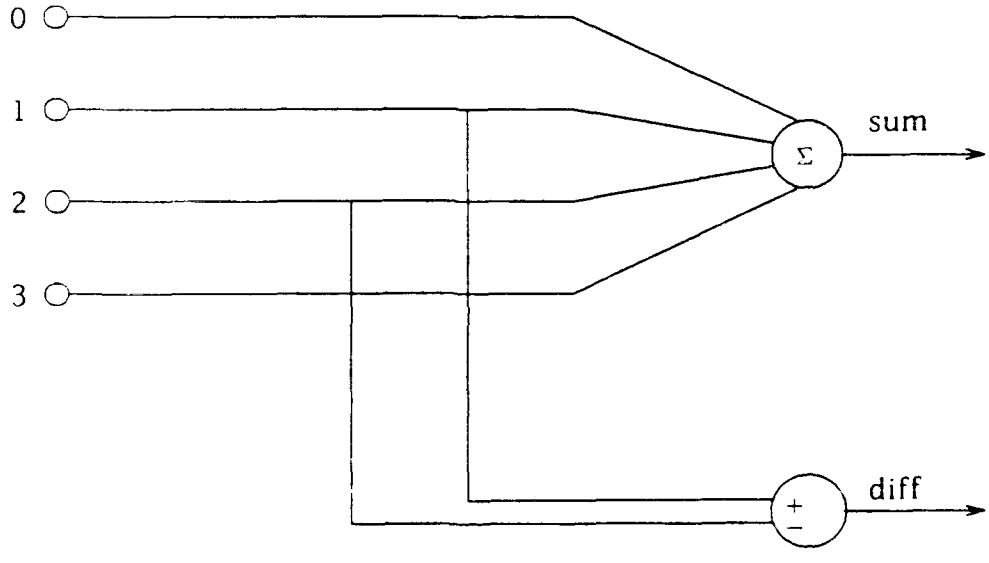

Figure 5.2. Sum and difference beams

Since in this work, the mapping used to reduce the received signal to a finite dimensional space is the Fourier transform, the matrix sought here represents the covariance between Fourier coefficients of all frequency indices, and all array indices. Here, only a single frequency Fourier coefficient is used, and therefore the covariance matrix is block diagonal, and only one block of it needs to be calculated. Since the sonar is reverberation limited, we need consider only the reverberation components' contribution to the covariance matrix.

Volume reverberation results from the scattering of acoustic energy by marine life and particulate matter distributed in the water. Its element to element cross-power spectrum depends heavily on the cross-element spatial response overlap, but by no means is white. Array element to element covariance is therefore far from being negligible. It will be shown here, though, that in the particular case of sum-difference beams, volume reverberation can be assumed as uncorrelated element to another element.

Denote the k-th element received waveform by $r_k(t)$.

Then the sum beam waveform $s(t)$ is:

$$s(t) = r_0(t)+r_1(t)+r_2(t)+r_3(t) \tag{5.2}$$

and the difference beam waveform is:

$$d(t) = r_1(t)-r_2(t) \tag{5.3}$$

The cross-covariance between the sum and difference beams is:

$$Q_{sd}(t) = E[s(t)d^*(t)] = E\left[\left(r_0(t)+r_1(t)+r_2(t)+r_3(t)\right)\left(r_1^*(t)-r_2^*(t)\right)\right] \tag{5.4}$$

where $E[\ ]$ represents the expected value operator, and * represents complex conjugation.

Dropping the time dependence in the notation:

$$Q_{sd} = E\left[r_0 r_1^* + r_1 r_1^* + r_2 r_1^* + r_3 r_1^* - r_0 r_2^* - r_1 r_2^* - r_2 r_2^* - r_3 r_2^*\right] \tag{5.5}$$

On the average, and certainly when the reverberating volume is in the far field (i.e its range is much larger than the array length), it is true that:

$$\begin{aligned} E\left[r_1 r_1^*\right] &\approx E\left[r_2 r_2^*\right] \\ E\left[r_3 r_1^*\right] &\approx E\left[r_0 r_2^*\right] \\ E\left[r_0 r_1^*\right] &\approx E\left[r_3 r_2^*\right] \\ E\left[r_2 r_1^*\right] &\approx E\left[r_1 r_2^*\right] \end{aligned} \tag{5.6}$$

and therefore:

$$Q_{sd} \approx 0 \tag{5.7}$$

We see that in the particular case of sum-difference beams, far field volume reverberation is essentially uncorrelated, and its only contribution to the covariance matrix is along the main diagonal.

Consider now the boundary reverberation. Denote the n^{th} Fourier coefficient at the 0^{th} array element due to the boundary reverberation as $d_0(n)$. Then the Fourier coefficient at the p^{th} array element is:

$$d_p(n) = d_0(n)\exp\left(-jn\omega_0\delta_p\right) \quad P=0,...,3 \tag{5.8}$$

where δ_p is the time delay between element 0 and element p. The sum Fourier coefficient is then:

$$d_s(n) = \sum_{p=0}^{3} d_0(n)\exp\left(-jn\omega_0\delta_p\right) \tag{5.9}$$

and the difference Fourier coefficient is:

$$d_d(n) = d_0(n)\left(\exp\left(-jn\omega_0\delta_1\right)-\exp\left(-jn\omega_0\delta_2\right)\right) \tag{5.10}$$

Consider now the covariance matrix. let $\exp(jn\omega_0\delta_1) \equiv W$, and note that $\delta_p = p\delta_1$, then the cross covariance is:

$$Q_{sd} = E\left[d_s(n)d_d^*(n)\right] = |\, d_0(n)\,|^2\left(1+W^{-1}+W^{-2}+W^{-3}\right)\left(W^1-W^2\right) \tag{5.11}$$

$$= |\, d_0(n)\,|^2\left(W^{-2}-W^2\right)$$

$$= -2j\,|\, d_0\,|^2\sin(2n\omega_0\delta_1)$$

In general, if there are k (even) elements in the array, and the middle two are subtracted to form the difference beam:

$$E\left[d_s(n)d_d^*(n)\right] = -2j\,|\, d_0\,|^2\sin(n\omega_0\frac{k}{2}\delta_1) \tag{5.12}$$

When k is odd, and elements subtracted are $\frac{k-1}{2}$ and $\frac{k-1}{2}+1$:

$$E\left[d_s(n)d_d^*(n)\right] = |\, d_0\,|^2\left(\exp\left(-jn\omega_0\delta_{\frac{k-1}{2}}\right)-\exp\left(+jn\omega_0\delta_{\frac{k-1}{2}+1}\right)\right) \tag{5.13}$$

The sum beam autocovariance is:

$$Q_{ss} = E\left[d_s(n)d_s^*(n)\right] = \sum_{p=0}^{3} d_0(n)W^{-p}\sum_{p=0}^{3} d_0(n)W^p \tag{5.14}$$

$$= |\, d_0\,|^2\left(W^3+2W^2+3W^1+4+3W^{-1}+2W^{-2}+W^{-3}\right)$$

$$= 2 \mid d_0 \mid^2 \left(4+3\cos(n\omega_0\delta_1)+2\cos(2n\omega_0\delta_1)+\cos(3n\omega_0\delta_1)\right)$$

And in general:

$$E\left[d_s(n)d_s^*(n)\right] = 2 \mid d_0 \mid^2 \sum_{i=0}^{k-1}(k-i)\cos(in\omega_0\delta_1)$$

The difference beam autocovariance is:

$$Q_{dd} = E\left[d_d(n)d_d^*(n)\right] = \mid d_0 \mid^2 \left((W^{-1}-W^{-2})(W^1-W^2)\right) \tag{5.15}$$

$$= 2 \mid d_0 \mid^2 \left(1-\cos(n\omega_0\delta_1)\right)$$

The covariance matrix can now be inverted and used in the likelihood ratio expression.

5.2. Signal known exactly in correlated Gaussian interference of precisely known direction

The covariance matrix elements computed are all functions of δ_1, the basic element to element time delay. When depth is known precisely, figuring out δ_1 requires a trigonometric computation which is illustrated in Figure 5.3:

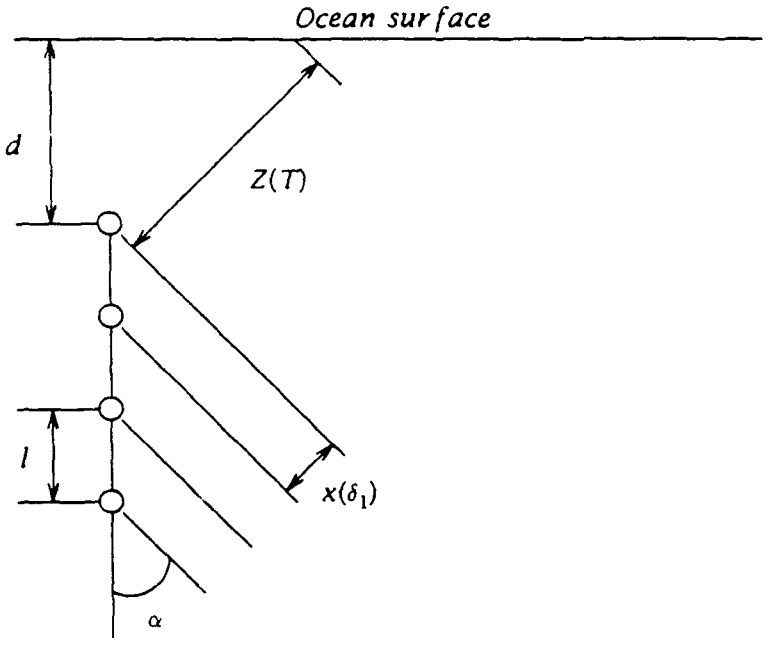

Figure 5.3. Element to element time delay computation

$$\sin\alpha = \frac{d}{Z(T)} \tag{5.16}$$

$$Z(T) = cT$$

$$\sin\alpha = \frac{d}{cT}$$

$$x(\delta_1) = l\sin\alpha \tag{5.17}$$

and therefore:

$$\delta_1 = \frac{x(\delta_1)}{c} = \frac{l\sin\alpha}{c} = \frac{ld}{c^2T} \tag{5.18}$$

where l is the inter-element spacing, d is the array depth, c is the speed of sound, and T is the observation time.

The following summarizes our findings relative to a representative block of the block diagonal reverberation covariance matrix:

$$Q(n,\delta_1) = \begin{bmatrix} 2\,|\,d_0\,|^2 \sum_{i=0}^{k-1}(k-i)\cos(n\omega_0 i\delta_1)+V_s & -2j\,|\,d_0\,|^2\sin(n\omega_0\frac{k}{2}\delta_1) \\ 2j\,|\,d_0\,|^2\sin(n\omega_0\frac{k}{2}\delta_1) & V_d+2\,|\,d_0\,|^2\left[1-\cos(n\omega_0\delta_1)\right] \end{bmatrix} \quad (5.19)$$

Where V_s and V_d are the sum and difference volume reverberation powers.

Now one can invert the covariance matrix, and use it in the previously computed likelihood ratio expression derived for this case of signal known exactly in correlated Gaussian interference of known location.

$$\Lambda(Z) = \frac{p(Z/H_1)}{p(Z/H_0)} = \exp[-(Z-\underline{m})^* Q^{-1}(Z-\underline{m}) + Z^* Q^{-1} Z] \quad (5.20)$$

5.3. Signal known exactly in correlated Gaussian interference of uncertain direction

Boundary interference in this case is coming from an uncertain direction since vehicle depth is uncertain. We do have some limited knowledge about depth, though, in the form of a probability density function (pdf) of it. This pdf is translated directly (through a simple transformation) to a pdf of the element to element delay δ_1. The same covariance matrix expressions developed for the previous case still apply, but now computing the likelihood ratio involves integration over the uncertain parameter. When H_0 is in force, the conditional probability density function is:

$$p(Z/H_0,\delta_1) = (\pi^k\,|\,Q(n,\delta_1)\,|\,)^{-1}\exp\left[-Z^*(n)Q^{-1}(n,\delta_1)Z(n)\right] \quad (5.21)$$

In our case Z is 2-dimensional (sum-difference), and only one frequency index is used. Therefore:

$$Z = \begin{bmatrix} z_1 \\ z_2 \end{bmatrix} \tag{5.22}$$

The covariance matrix, which is a function of δ_1 has been derived previously. Let:

$$Q(\delta_1) = \begin{bmatrix} Q_{11} & Q_{12} \\ Q_{21} & Q_{22} \end{bmatrix} \tag{5.23}$$

then:

$$E_0 \equiv -Z^* Q^{-1}(\delta_1) Z = -\frac{1}{\Delta}\left(|\, z_1 \,|^2 Q_{22} + |\, z_2 \,|^2 Q_{11} - 2\mathrm{Re}(z_2^* z_1 Q_{21}) \right) \tag{5.24}$$

where Δ is the determinant of Q. Note that Δ , and Q_{ij} are all functions of δ_1. Now the conditional pdf under H_0 assuming δ_1 is known can be written as:

$$p(Z/H_0,\delta_1) = \frac{1}{\pi^2 \Delta} \exp(E_0) \tag{5.25}$$

The knowledge about the distribution of the element to element delay can now be utilized to form the pdf under H_0:

$$p(Z/H_0) = \frac{1}{\pi^2 \Delta} \int_{\delta_{1i}}^{\delta_{1f}} \exp(E_0) p(\delta_1) d\delta_1 \tag{5.26}$$

where δ_{1i} and δ_{1f} represent the boundaries in between which $p(\delta_1)$ is defined. Finally, when assuming uniform distribution on δ_1, as will be assumed here:

$$p(Z/H_0) = \frac{1}{\pi^2 \Delta (\delta_{1f} - \delta_{1i})} \int_{\delta_{1i}}^{\delta_{1f}} \exp(E_0) d\delta_1 \tag{5.27}$$

When H_1 is in force, the conditional probability density function is:

$$p(Z/H_1,\delta_1) = (\pi^k \mid Q(n,\delta_1) \mid)^{-1}\exp\left(-\left(Z(n)-b_0(n)\underline{u}(n)\right)^{\cdot}\right. \qquad (5.28)$$
$$\left. Q^{-1}(n,\delta_1)\left(Z(n)-b_0(n)\underline{u}(n)\right)\right)$$

where $b_0(n)$ is the signal mean vector, and $\underline{u}(n)$ is the signal "pointing" vector. The signal direction is assumed precisely forwards, i.e.:

$$\underline{u} = \begin{bmatrix}1\\1\end{bmatrix} \qquad (5.29)$$

Using the same steps used to derive $p(Z/H_0,\delta_1)$:

$$E_1 \equiv -\left(Z-b_0\underline{u}\right)^{\cdot} Q^{-1}(\delta_1)\left(Z-b_0\underline{u}\right) \qquad (5.30)$$
$$= \frac{1}{\Delta}\left\{-\left(\mid z_1 \mid^2 Q_{22}+\mid z_2 \mid^2 Q_{11}-2\mathrm{Re}(z_2^{\cdot} z_1 Q_{21})\right)\right.$$
$$\left.+2b_0\mathrm{Re}(z_1^{\cdot}Q_{22}-z_2^{\cdot}Q_{21}-z_1^{\cdot}Q_{12}+z_2^{\cdot}Q_{11})-\mid b_0 \mid^2(Q_{22}-Q_{21}-Q_{12}+Q_{11})\right\}$$

The conditional pdf under H_1 assuming δ_1 is known can be written now as:

$$p(Z/H_1,\delta_1) = \frac{1}{\pi^2\Delta}\exp(E_1) \qquad (5.31)$$

Using what's known about the distribution of δ_1:

$$p(Z/H_1) = \frac{1}{\pi^2\Delta}\int_{\delta_{1i}}^{\delta_{1f}} \exp(E_1)p(\delta_1)d\delta_1 \qquad (5.32)$$

and when the uniform distribution is incorporated:

$$p(Z/H_1) = \frac{1}{\pi^2\Delta(\delta_{1f}-\delta_{1i})}\int_{\delta_{1i}}^{\delta_{1f}} \exp(E_1)d\delta_1 \qquad (5.33)$$

We are now finally ready to compute the likelihood ratio for the case of signal

known exactly in correlated Gaussian interference of uncertain direction:

$$\Lambda = \frac{p(Z/H_1)}{p(Z/H_0)} = \frac{\int_{\delta_{1i}}^{\delta_{1f}} \exp(E_1)d\delta_1}{\int_{\delta_{1i}}^{\delta_{1f}} \exp(E_0)d\delta_1} \tag{5.34}$$

5.4. Derivation of the three beam covariance matrix

When we consider a more complex case, in which, in addition to the boundary reverberation interference we have another fixed interference source (e.g. a jammer), we need another degree of freedom in the system. Therefore, another difference beam is formed, and we have three beams: one sum beam and two difference beams. Figure 5.4 depicts this arrangement:

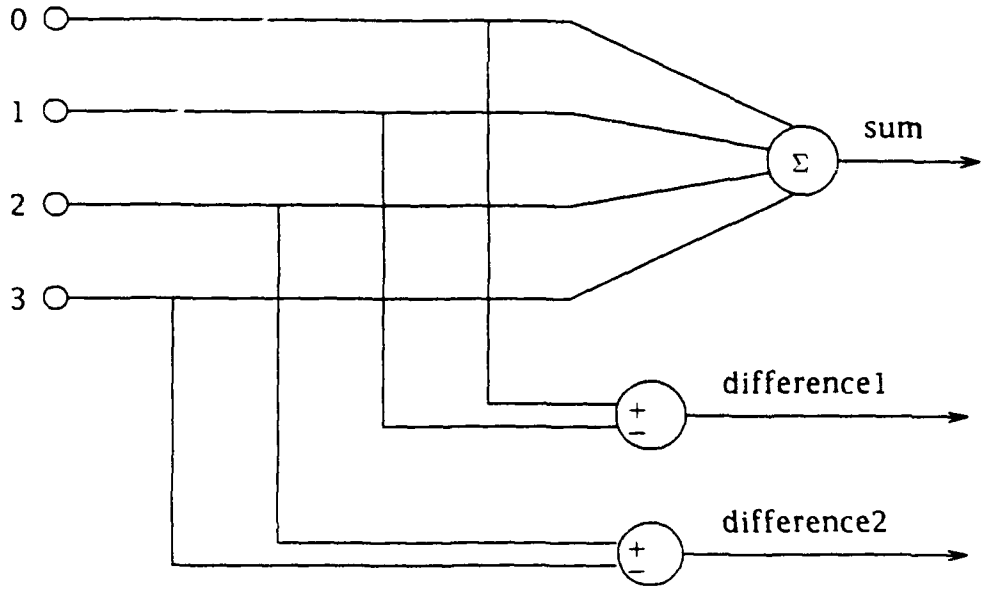

Figure 5.4. Sum and difference beams

Now we can attempt to compute the increased order covariance matrix. Denote the n^{th} Fourier coefficient at the 0^{th} array element due to the boundary reverberation as $d_0(n)$. Then the Fourier coefficient at the p^{th} array element is:

$$d_p(n) = d_0(n)\exp\left(-jn\omega_0\delta_p\right) \quad P=0,...,3 \tag{5.35}$$

where δ_p is the time delay between element 0 and element p. The sum Fourier coefficient is then:

$$d_s(n) = \sum_{p=0}^{3} d_0(n)\exp\left(-jn\omega_0\delta_p\right) \tag{5.36}$$

and the difference Fourier coefficients are:

$$d_{d1}(n) = d_0(n)\left(\exp\left(-jn\omega_0\delta_0\right)-\exp\left(-jn\omega_0\delta_1\right)\right) \tag{5.37}$$

$$d_{d2}(n) = d_0(n)\left(\exp\left(-jn\omega_0\delta_2\right)-\exp\left(-jn\omega_0\delta_3\right)\right) \tag{5.38}$$

Consider now the covariance matrix. let $\exp(jn\omega_0\delta_1) \equiv W$, and note that $\delta_p = p\delta_1$, then the first cross-covariance is:

$$Q_{sd1} = E\left[d_s(n)d_{d1}^{*}(n)\right] = |\, d_0(n)\,|^2\left(1+W^{-1}+W^{-2}+W^{-3}\right)\left(1-W^{1}\right) \tag{5.39}$$

$$= |\, d_0(n)\,|^2\left(W^{-3}-W^{1}\right)$$

The second cross-covariance is:

$$Q_{sd2} = E\left[d_s(n)d_{d2}^{*}(n)\right] = |\, d_0(n)\,|^2\left(1+W^{-1}+W^{-2}+W^{-3}\right)\left(W^{2}-W^{3}\right) \tag{5.40}$$

$$= |\, d_0(n)\,|^2\left(W^{-1}-W^{3}\right)$$

The sum be. .tocovariance (calculated previously) is:

$$Q_{ss} = E\left[d_s(n)d_s^*(n)\right] = 2 \mid d_0 \mid^2 \sum_{i=0}^{k-1}(k-i)\cos(in\omega_0\delta_1) \tag{5.41}$$

The difference beam autocovariances (calculated previously) are:

$$Q_{d1d1} = E\left[d_{d1}(n)d_{d1}^*(n)\right] = E\left[d_{d2}(n)d_{d2}^*(n)\right] = 2 \mid d_0 \mid^2 \left(1-\cos(n\omega_0\delta_1)\right) \tag{5.42}$$

The difference beam cross covariances is:

$$\begin{aligned} Q_{d1d2} = E\left[d_{d1}(n)d_{d2}^*(n)\right] &= \mid d_0(n) \mid^2 \left(1-W^{-1}\right)\left(W^2-W^3\right) \\ &= \mid d_0(n) \mid^2 \left(2W^2-W^1-W^3\right) \end{aligned} \tag{5.43}$$

When a fixed interference is introduced, the structure of the resulting covariance matrix is identical to the boundary reverberation covariance matrix. The only difference is that the time delay variable δ does not vary with range, but is fixed. The fixed time delay is denoted δ_f. The combined covariance matrix is then the sum of the range variable boundary interference matrix, the fixed interference matrix, and the diagonal volume reverberation matrix:

$$Q = Q(n,\delta_1,\delta_f) = \begin{bmatrix} Q_{11} & Q_{12} & Q_{13} \\ Q_{21} & Q_{22} & Q_{23} \\ Q_{31} & Q_{32} & Q_{33} \end{bmatrix} \tag{5.44}$$

5.5. Signal known exactly in correlated Gaus.ian interference of uncertain direction, plus a fixed interference of uncertain direction

Fixed interference, as well as boundary reverberation in this case are coming from uncertain directions. Again, we do have some limited knowledge about fixed

interference direction in the form of a probability density function (pdf) of it. Here, computing the likelihood functional involves integration over both uncertain parameters, namely δ_1 and δ_f. When H_0 is in force, the conditional probability density function is:

$$p(Z/H_0,\delta_1,\delta_f) = (\pi^k \mid Q(n,\delta_1,\delta_f) \mid)^{-1}\exp\left(-Z^*(n)Q^{-1}(n,\delta_1,\delta_f)Z(n)\right) \tag{5.45}$$

In our case Z is 3-dimensional, and only one frequency index is used. Therefore:

$$Z = \begin{bmatrix} z_1 \\ z_2 \\ z_3 \end{bmatrix} \tag{5.46}$$

The covariance matrix, which is a function of δ_1 has been derived previously. Let:

$$Q^{-1}(\delta_1,\delta_f) \equiv H(\delta_1,\delta_f) = \begin{bmatrix} H_{11} & H_{12} & H_{13} \\ H_{21} & H_{22} & H_{23} \\ H_{31} & H_{32} & H_{33} \end{bmatrix} \tag{5.47}$$

then:

$$E_0 \equiv -Z^* H(\delta_1,\delta_f)Z \tag{5.48}$$

$$= -\left(\mid z_1 \mid^2 H_{11} + \mid z_2 \mid^2 H_{22} + \mid z_3 \mid^2 H_{33} + 2\mathrm{Re}(z_2^* z_1 H_{21}) + 2\mathrm{Re}(z_3^* z_1 H_{31}) + 2\mathrm{Re}(z_3^* z_2 H_{32}) \right)$$

Note that H_{ij} are functions of δ_1 and δ_f. Now the conditional pdf under H_0 when δ_1 and δ_f are known can be written as:

$$p(Z/H_0,\delta_1,\delta_f) = \frac{1}{\pi^2 \Delta}\exp(E_0) \tag{5.49}$$

Where Δ is the determinant of Q, and:

$$\Delta = \Delta(\delta_1, \delta_f) \tag{5.50}$$

$$E_0 = E_0(\delta_1, \delta_f)$$

The knowledge about the distribution of δ_1 and δ_f can now be utilized to form the pdf under H_0. Assuming that the two time delays are independent, which is reasonable:

$$p(Z/H_0) = \frac{1}{\pi^3 \Delta} \int_{\delta_{1i}}^{\delta_{1f}} \int_{\delta_{fi}}^{\delta_{ff}} \exp(E_0) p(\delta_1) p(\delta_f) d\delta_1 d\delta_f \tag{5.51}$$

where δ_{1i} and δ_{1f} represent the boundaries in between which $p(\delta_1)$ is defined, and δ_{fi} and δ_{ff} represent the boundaries in between which $p(\delta_f)$ is defined. Finally, when assuming that both delays are uniformly distributed, as will be assumed here we get:

$$p(Z/H_0) = \frac{1}{\pi^3 \Delta (\delta_{1f} - \delta_{1i})(\delta_{ff} - \delta_{fi})} \int_{\delta_{1i}}^{\delta_{1f}} \int_{\delta_{fi}}^{\delta_{ff}} \exp(E_0) d\delta_1 d\delta_f \tag{5.52}$$

When H_1 is in effect, the probability density function is:

$$p(Z/H_1, \delta_1, \delta_f) = (\pi^k \Delta)^{-1} \exp\left\{ -\left[Z(n) - b_0(n)\underline{u}(n)\right]^* \right. \tag{5.53}$$
$$\left. Q^{-1}(n, \delta_1, \delta_f)\left[Z(n) - b_0(n)\underline{u}(n)\right] \right\}$$

where $b_0(n)$ is the signal mean vector, and $\underline{u}(n)$ is the signal "pointing" vector. The signal direction is assumed precisely forwards, i.e.:

$$\underline{u} = \begin{bmatrix} 1 \\ 1 \\ 1 \end{bmatrix} \tag{5.54}$$

Using the same steps used to derive $p(Z/H_0, \delta_1, \delta_f)$:

$$E_1 \equiv -\left(Z-b_0\underline{u}\right)^{\cdot} Q^{-1}(\delta_1,\delta_f)\left(Z-b_0\underline{u}\right) \tag{5.55}$$

$$= -E_0+2b_0\mathrm{Re}\left\{z_1^{\cdot}(H_{11}+h_{12}+H_{13})+z_2^{\cdot}(H_{21}+H_{22}+H_{23})+z_3^{\cdot}(H_{31}+H_{32}+H_{33})\right\}$$
$$-|\,b_0\,|^2\sum_{i=1}^{3}\sum_{j=1}^{3}H_{ij}$$

The conditional pdf under H_1 when both delays are known can be written now as:

$$p(Z/H_1,\delta_1,\delta_f) = \frac{1}{\pi^3\Delta}\exp(E_1) \tag{5.56}$$

Using what is known about the distribution of δ_1:

$$p(Z/H_1) = \frac{1}{\pi^3\Delta}\int_{\delta_{1i}}^{\delta_{1f}}\int_{\delta_{fi}}^{\delta_{ff}}\exp(E_1)p(\delta_1)p(\delta_f)d\delta_1 d\delta_f \tag{5.57}$$

and when the uniform distributions are incorporated:

$$p(Z/H_1) = \frac{1}{\pi^3\Delta(\delta_{1f}-\delta_{1i})(\delta_{ff}-\delta_{fi})}\int_{\delta_{1i}}^{\delta_{1f}}\int_{\delta_{fi}}^{\delta_{ff}}\exp(E_1)d\delta_1 d\delta_f \tag{5.58}$$

We are now finally ready to compute the likelihood ratio for the case of signal known exactly in correlated Gaussian interference of uncertain direction plus an interference of uncertain direction:

$$\Lambda = \frac{p(Z/H_1)}{p(Z/H_0)} = \frac{\int_{\delta_{1i}}^{\delta_{1f}}\int_{\delta_{fi}}^{\delta_{ff}}\exp(E_1)d\delta_1 d\delta_f}{\int_{\delta_{1i}}^{\delta_{1f}}\int_{\delta_{fi}}^{\delta_{ff}}\exp(E_0)d\delta_1 d\delta_f} \tag{5.59}$$

We have developed in this chapter three different Bayes optimum detectors for three different ocean environments. These will be used later in this dissertation in the detector comparisons.

6. Block processing and time sequential approaches to Bayes optimum detection

The general expressions developed in the previous chapter for the three different cases are indirectly all time dependent. As the transmission pulse propagates through the water, it ensonifies different regions of the ocean, and the return signal varies therefore with time. The time dependence enters the optimum detector expressions through the element to element delay δ_1, and through the signal and boundary reverberation powers.

There are at least two approaches to processing the data. The simpler approach is to divide the incoming data stream into equal length blocks, and to process each block separately, without carrying over any information from the processing of one block to the next. This approach is called block processing, and is obviously sub-optimal in a sense, since it takes a look at only part of the available information at any given point in time. Despite its apparent flaw, this approach is many times easier to implement, and is well suited for real time applications. The second approach is to store all the incoming data, and then process it at once and make a decision. This approach is called one-shot, and it is optimal in the sense that it makes use of all the available data. A variant of this approach is the time sequential approach. Here, the processor operates on a block of observations at a time, but through updating the a-priori probability density functions of the uncertain parameters, it carries over acquired information from block to block. This approach is mathematically equivalent to the one-shot approach, and produces exactly the same decisions, but in some respects is more attractive since it demonstrates the inherent learning nature of the detector, and lends itself to comparisons with other adaptive structures. Both the block processing and the time sequential approaches have been implemented in this

dissertation, and are both used in the comparisons with ad-hoc detectors

6.1. The time sequential processor design equations

Consider the vector $\underline{r}^T(t)$ of time waveforms observed by the receiver array as in (3.20). $\underline{r}^T(t)$ is broken into time sequences of length T_{inc}, and the vectors of Fourier coefficients $Z_i^T(n)$ are formed, where i represents the i^{th} increment. Thus, for a total observation period of $T = LT_{inc}$, $\underline{r}(t)$ will be represented by L vectors of Fourier coefficients, $(Z_1,.....,Z_L)$.

When using the block processing approach, each one of vectors Z_i^T represents a block, and is being processed separately from all the others. When using time sequential processing, the approach is as follows. In order to form the likelihood ratio, we need the marginal distributions of the observables, conditioned on the hypothesis in force. Here, the observables are the L vectors $(Z_1,.....,Z_L)$. Suspending the conditioning on H_1 and H_0 for the moment:

$$p(Z_1,.....,Z_L) = \prod_{i=1}^{L} p(Z_i/Z_{i-1},.....,Z_1) \tag{6.1}$$

$$= \int_{\underline{\delta}} \prod_{i=1}^{L} p(Z_i/Z_{i-1},.....,Z_1,\underline{\delta}) p(\underline{\delta}) d\underline{\delta}$$

where $\underline{\delta}$ is the vector of uncertain parameters, which for simplicity is assumed time-invariant here. Assuming parameter conditional independence of the vectors Z_i:

$$p(Z_i/Z_{i-1},.....,Z_1,\underline{\delta}) = p(Z_i/\underline{\delta}) \tag{6.2}$$

Substituting now (6.2) into (6.1) we get:

$$p(Z_1,\ldots\ldots,Z_L) = \int_{\underline{\delta}} \prod_{i=1}^{L} p(Z_i/\underline{\delta})p(\underline{\delta})d\underline{\delta} \tag{6.3}$$

Now, applying Bayes' rule L times to the integrand in (6.3):

$$p(Z_1,\ldots\ldots,Z_L) = \prod_{i=1}^{L} \int_{\underline{\delta}} p(Z_i/\underline{\delta})p(\underline{\delta}/Z_{i-1},\ldots\ldots,Z_1)d\underline{\delta} \tag{6.4}$$

where $p(\underline{\delta}/Z_{i-1},\ldots\ldots,Z_1)$ is an updated version of the a-priori probability density function of $\underline{\delta}$:

$$p(\underline{\delta}/Z_{i-1},\ldots\ldots,Z_1) = \frac{p(Z_{i-1},\ldots\ldots,Z_1,\underline{\delta})}{p(Z_{i-1},\ldots\ldots,Z_1)} \tag{6.5}$$

$$= \frac{p(Z_{i-1}/Z_{i-2},\ldots\ldots,Z_1,\underline{\delta})p(Z_{i-2},\ldots\ldots,Z_1,\underline{\delta})}{p(Z_{i-1},\ldots\ldots,Z_1)}$$

and assuming parameter conditional independence:

$$= \frac{p(Z_{i-1}/\underline{\delta})p(Z_{i-2},\ldots\ldots,Z_1,\underline{\delta})}{p(Z_{i-1},\ldots\ldots,Z_1)} \tag{6.6}$$

$$= \frac{p(Z_{i-1}/\underline{\delta})p(\underline{\delta}/Z_{i-2},\ldots\ldots,Z_1)p(Z_{i-2},\ldots\ldots,Z_1)}{p(Z_{i-1}/Z_{i-2},\ldots\ldots,Z_1)p(Z_{i-2},\ldots\ldots,Z_1)}$$

$$= \frac{p(Z_{i-1}/\underline{\delta})p(\underline{\delta}/Z_{i-2},\ldots\ldots,Z_1)}{p(Z_{i-1}/Z_{i-2},\ldots\ldots,Z_1)}$$

Note that the updated version of the a-priori probability density function of $\underline{\delta}$ is formed using probability density functions which are either known, or computed in the previous iteration.

Equations (6.1), (6.4) and (6.6), when conditioned on H_1 and H_0, are the design equations used to obtain the marginal distributions in the likelihood ratio

expression for L iterations:

$$\Lambda_L = \frac{p(Z_1,\ldots\ldots,Z_L/H_1)}{p(Z_1,\ldots\ldots,Z_L/H_0)} = \frac{\prod_{i=1}^{L} \int_{\delta} p(Z_i/\delta,H_1)p(\delta/Z_{i-1},\ldots\ldots,Z_1,H_1)d\delta}{\prod_{i=1}^{L} \int_{\delta} p(Z_i/\delta,H_0)p(\delta/Z_{i-1},\ldots\ldots,Z_1,H_0)d\delta} \tag{6.7}$$

Note that since we are dealing with an active sonar problem, the signal (target echo) is present only in the final iteration currently considered. The assumption is made that there is only one target in the look direction and that it resides in the current range cell. Thus the updated a-priori probability density functions under both hypotheses are identical in all iterations but the last.

6.2. Time varying uncertain parameter vector

The previous discussions limited the uncertain parameter vector to be time-invariant. In actuality, the uncertain parameter may be time-varying. In the first case we are dealing with, there is a single uncertain parameter - boundary reverberation element to element time delay, which certainly is time-varying. That results in having to find a transition equation which makes use of the problem geometry, to update $p(\delta_i/Z_{i-1},\ldots\ldots,Z_1,H_j)$ for iteration $i+1$. The likelihood ratio expression is now:

$$\Lambda_L = \frac{p(Z_1,\ldots\ldots,Z_L/H_1)}{p(Z_1,\ldots\ldots,Z_L/H_0)} = \frac{\prod_{i=1}^{L} \int_{\delta_i} p(Z_i/\delta_i,H_1)p(\delta_i/Z_{i-1},\ldots\ldots,Z_1,H_1)d\delta_i}{\prod_{i=1}^{L} \int_{\delta_i} p(Z_i/\delta_i,H_0)p(\delta_i/Z_{i-1},\ldots\ldots,Z_1,H_0)d\delta_i} \tag{6.8}$$

and the a-priori probability density function update equation is:

$$p(\delta_i/Z_{i-1},\ldots\ldots,Z_1,H_j) = \frac{p(Z_{i-1}/\delta_{i-1},H_j)p(\delta_i/Z_{i-2},\ldots\ldots,Z_1,H_j)}{p(Z_{i-1}/Z_{i-2},\ldots\ldots,Z_1,H_j)} \tag{6.9}$$

where $j = 0,1$ represents the hypothesis in force. The need for a transition equation arises since following iteration $i-1$, we have available only $p(\delta_{i-1}/Z_{i-2},.....Z_1,H_j)$, and in (6.9) we need $p(\delta_i/Z_{i-2},.....Z_1,H_j)$.

The transition equation is developed in Appendix B, based on the geometry of Figure 5.3, and the result is quoted here:

$$\delta_{i+1} = \frac{\delta_i}{1+\frac{l-c\delta_1}{l(i-1)}} \tag{6.10}$$

Making use of this transition equation, we can arrive at the desired pdf by computing the pdf of a function of a random variable:

$$p(\delta_i/Z_{i-2},.....Z_1,H_j) = \frac{p(\delta_{i-1}/Z_{i-2},.....Z_1,H_j)}{\left|\frac{d\delta_i}{d\delta_{i-1}}\right|_{\delta_{i-1}}} \tag{6.11}$$

Appendix B also develops the exact expression for the above derivative. Equations (6.8), (6.9) and (6.11) constitute the final design equations of the time sequential Bayes optimum processor with a single uncertain parameter.

We now examine the more complex case where a fixed interference source of uncertain direction is added to the scenario. Here, the uncertain parameters indeed form a two-dimensional vector:

$$\underline{\delta} = \begin{bmatrix} \delta_i \\ \delta_f \end{bmatrix} \tag{6.12}$$

where δ_i is the time-varying boundary reverberation element to element time delay, and δ_f is the time-invariant fixed interference element to element time delay. We again have:

$$\Lambda_L = \frac{p(Z_1,\ldots\ldots,Z_L/H_1)}{p(Z_1,\ldots\ldots,Z_L/H_0)} = \frac{\prod_{i=1}^{L} \int_{\underline{\delta}} p(Z_i/\underline{\delta},H_1)p(\underline{\delta}/Z_{i-1},\ldots\ldots,Z_1,H_1)d\underline{\delta}}{\prod_{i=1}^{L} \int_{\underline{\delta}} p(Z_i/\underline{\delta},H_0)p(\underline{\delta}/Z_{i-1},\ldots\ldots,Z_1,H_0)d\underline{\delta}} \tag{6.13}$$

and since δ_i and δ_F are independent random variables:

$$\Lambda_L = \frac{\prod_{i=1}^{L} \int\int_{\delta_i\delta_f} p(Z_i/\delta_i,\delta_f,H_1)p(\delta_i/Z_{i-1},\ldots\ldots,Z_1,H_1)p(\delta_i/Z_{i-1},\ldots\ldots,Z_1,H_1)d\delta_i d\delta_f}{\prod_{i=1}^{L} \int\int_{\delta_i\delta_f} p(Z_i/\delta_i,\delta_f,H_0)p(\delta_i/Z_{i-1},\ldots\ldots,Z_1,H_0)p(\delta_i/Z_{i-1},\ldots\ldots,Z_1,H_0)d\delta_i d\delta_f} \tag{6.14}$$

Obtaining the update equations of δ_i and δ_f is a simple extension of the ideas previously described and will not be repeated here. Suffice it to say that the transition equation for δ_i remains the same, while no transition equation is required for δ_f since it is time-invariant.

7. Detector evaluation and comparison - methods and tools.

7.1. Detector comparison

As described in Chapter 3, the performance of two detection schemes will be evaluated and compared. One scheme, which represents an ad-hoc approach, employs an adaptive filter to first reduce boundary interference level. It then assumes that the processed signal contains only the volume reverberation component, and treats the problem as one of signal known exactly in noise known exactly. The adaptive filter chosen to be used in the comparison is the all-zero least squares lattice filter (JCLSL). It has been shown previously (Chapter 4), that it is quite adequate for the task, and that a pole-zero adaptive filter has only a very slight advantage over it, in the scenarios used. The second scheme is the result of a more global approach which uses our knowledge of the problem's statistics to arrive at an optimum solution in the Bayesian sense. Figure 7.1 depicts the two schemes.

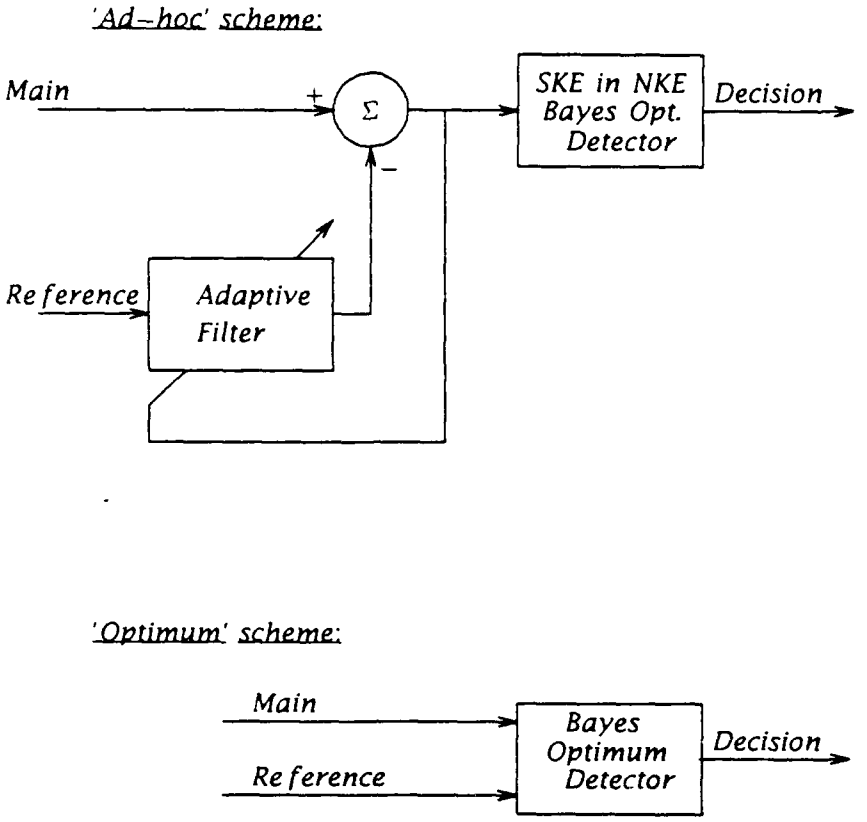

Figure 7.1 The two detection schemes

The array used in the comparison is a 4-element array, where the main beam was derived by summing all four element outputs, and the reference beam(s) was generated by subtracting two adjacent element outputs.

7.2. Adaptation parameter selection

One of the parameters defining the behavior of an adaptive structure is the adaptation coefficient α, which takes values between 0 and 1. This parameter determines the filter's "forgetting factor", or how much emphasis the filter puts on past samples. Typically, the filter's time constant (in samples) will be:

$$\tau = \frac{1}{\alpha} \tag{7.1}$$

When using an adaptive structure such as the adaptive filter used in this dissertation, the questions always arise as to how is the adaptation coefficient α selected, and for how long the adaptive filter should be permitted to run and adapt before its output is considered valid to sample. In order to resolve these questions, a run was generated, where a simulated target echo in the look direction was superimposed on an ordinary reverberation return ping. This ping was picked out of the ensemble of pings which are later used in this work to compare the different detection approaches. The ping was processed three times by the same adaptive filter with three different adaptation coefficients, namely 0.02, 0.05 , and 0.2. Then, the adaptive filter output power was plotted against main beam power, for the three different α's. Figure 7.2 details the results.

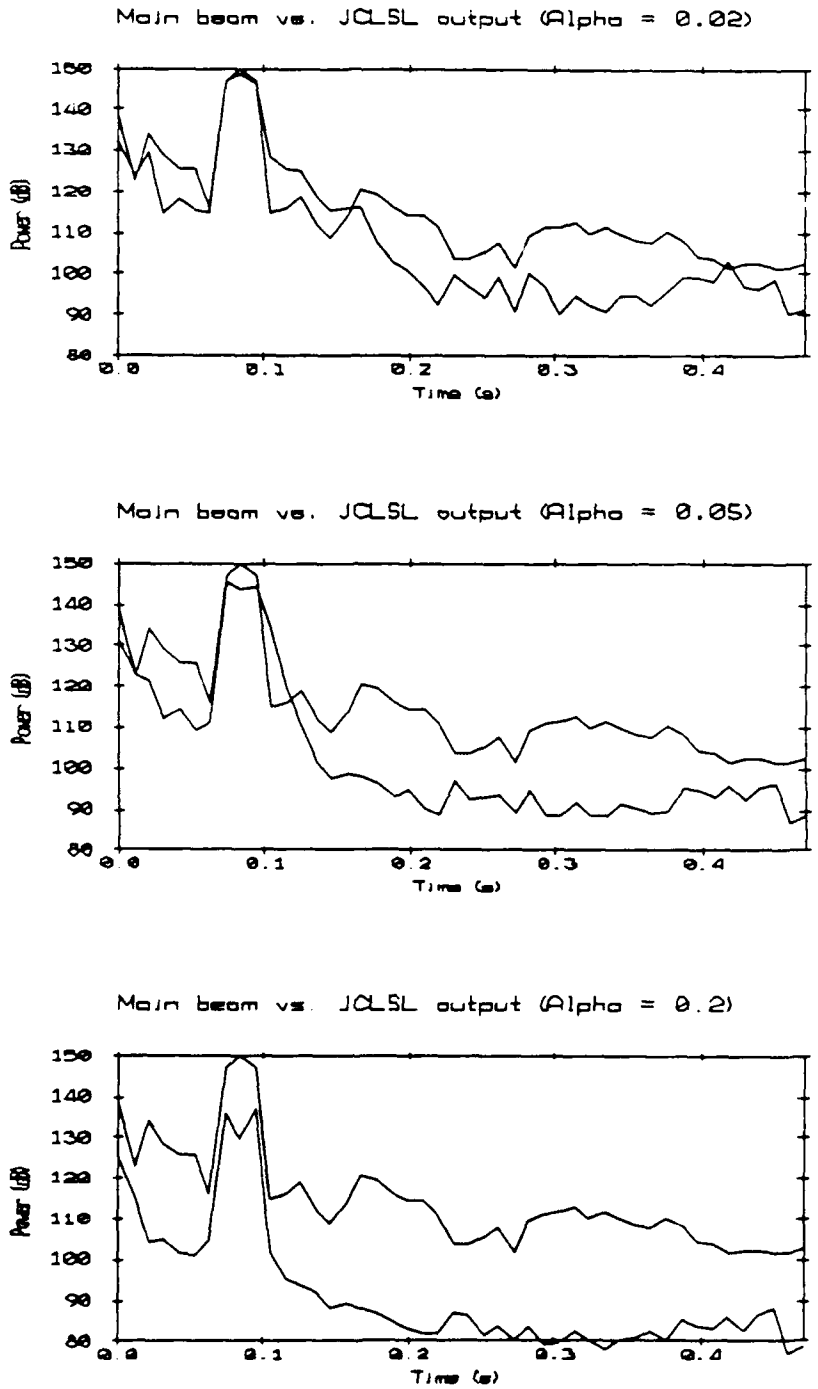

Figure 7.2 Main beam vs. adaptive filter output power.

It is clear from observing the plots, that as soon as α is chosen larger than 0.02, the filter starts canceling the target echo as well as the reverberation interference.

This is undesirable. Therefore, throughout this work α was kept at 0.02. The selection of α answers the second question as well, since an adaptive filter typically takes a few time constants to adapt. With this selection of α, the time constant τ is 50 samples. Therefore, sampling the filter's output anywhere beyond, say, 500 samples (10 time constants) is safe.

7.3. Test scenario description

The two detection approaches are tested and compared under three different interference conditions:

Case 1. Boundary interference is coming from a known direction.

Case 2. Boundary interference is coming from an uknown direction, whose probability density function is known.

Case 3. Boundary interference is coming from an uknown direction, whose probability density function is known, and there is another fixed source of interference coming from an unknown direction whose probability density function is known.

One source of uncertainty in boundary interference direction is uncertainty in the array platform's depth. Therefore, depth was chosen as the uncertain parameter, and its probability density functions were assumed known. When dealing with the fixed interferer, probability densities of direction were defined directly. In all cases of uncertainty, uniform probability density functions were assumed. The basic test scenario selected for Case 1 above is described in Figure 7.3.

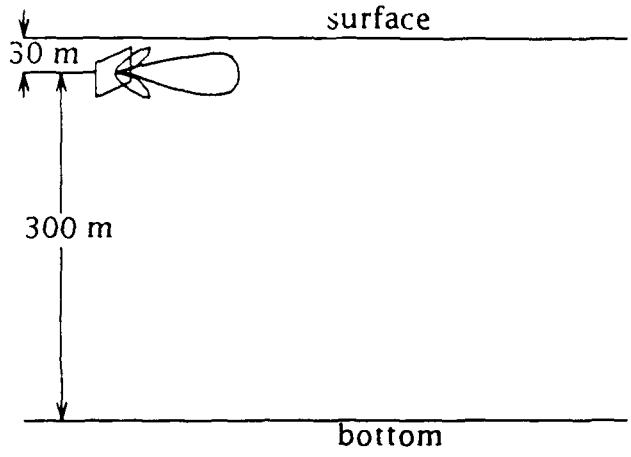

Figure 7.3 Basic test scenario (Case 1)

As can be seen from the figure, the bottom depth is purposefully given a large value, so that bottom reverberation will come in late, and only one source of boundary reverberation (surface) is dealt with.

Figures 7.4 and 7.5 describe the test scenarios for Cases 2 and 3 above.

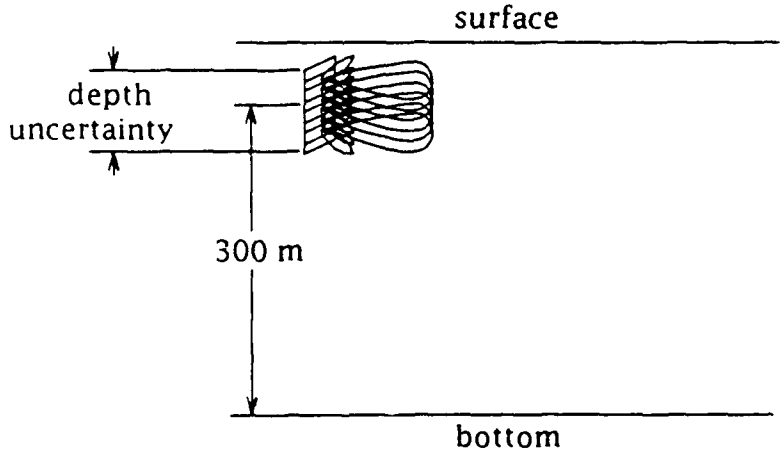

Figure 7.4 Test scenario for uncertain depth (Case 2)

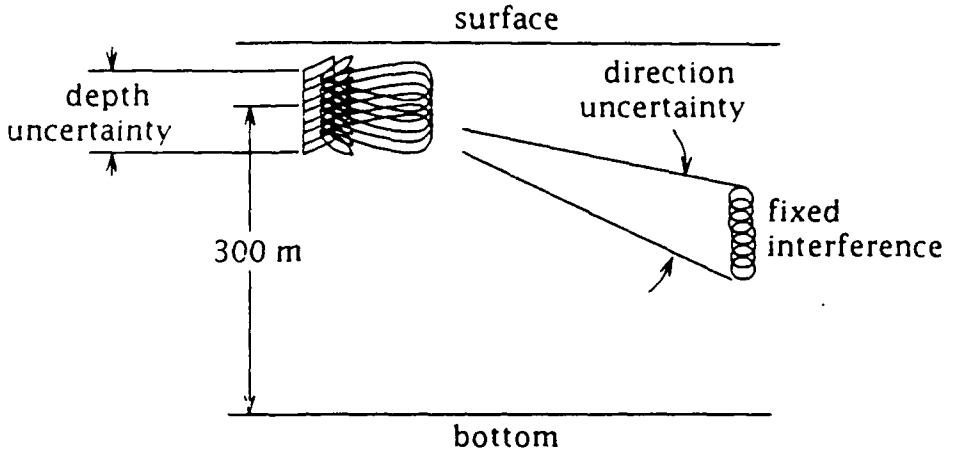

Figure 7.5 Test scenario for uncertain depth and fixed interference (Case 3)

The output of both detectors is examined approximately 0.2 sec following transmit, or at about the 800^{th} sample. This gives the adaptive filter enough time to adapt. This time corresponds to a distance to the illuminated surface patch of 150m. The maximum depth uncertainty used in this work is 54m, centered around 30m. That spans a depth between 3 and 57m. The corresponding angular span to the surface is as follows:

$$\alpha_{max} = \sin^{-1}\left(\frac{54}{150}\right) = 21.1^{\circ} \tag{7.2}$$

$$\alpha_{min} = \sin^{-1}\left(\frac{3}{150}\right) = 1.15^{\circ} \tag{7.3}$$

Similarly, the fixed interference direction uncertainty spans the range of -10° to -20°. Examining the sum and difference polar beampatterns, we see that within the above angular ranges, both are well behaved, and the main beam has no nulls.

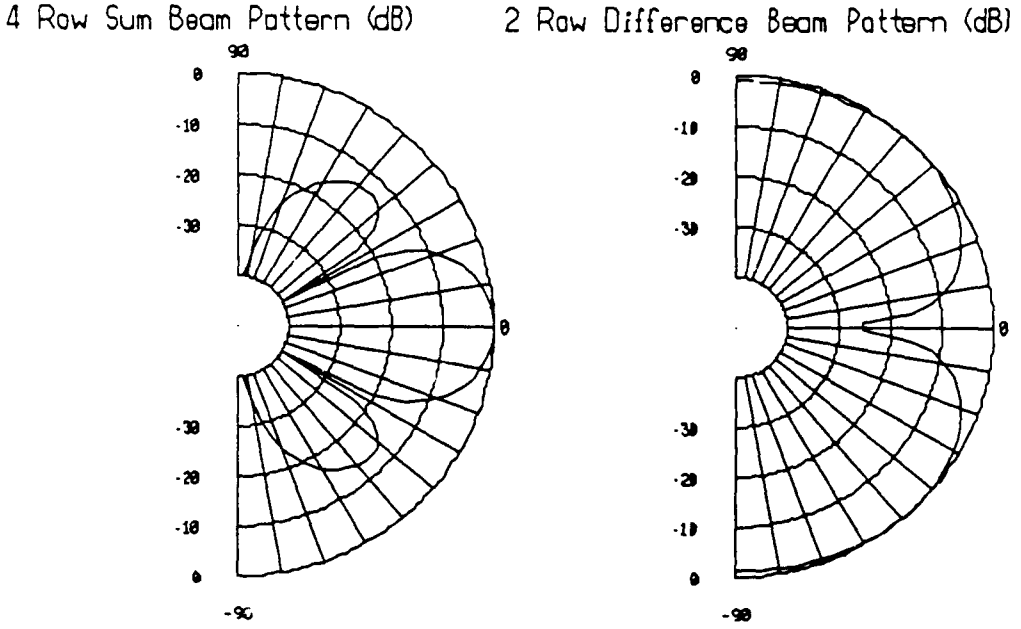

Figure 7.6 Sum and Difference polar beampatterns

7.4. ROC curves

The output produced by both detection schemes is the likelihood ratio which in turn is compared to a threshold in order to make the decision whether a target is present or not. The likelihood ratio Λ, summarizes all the information about the data for a given observation interval and therefore is significant in evaluating the detector's performance. A complete description of a detector includes the likelihood ratio Λ and the receiver operating characteristic (ROC) curves. These curves plot the detection probability versus the false alarm probability, where the threshold η serves as a parameter. The false alarm probability P_F and the detection probability P_D are:

$$P_F = \int_{\eta}^{\infty} p(\Lambda/H_0)d\Lambda \tag{7.4}$$

$$P_D = \int_{\eta}^{\infty} p(\Lambda/H_1)d\Lambda \tag{7.5}$$

Where η is the detection threshold. It has been shown[48] that:

$$p(\Lambda/H_1) = \Lambda p(\Lambda/H_0) \tag{7.6}$$

Thus P_D can be written as:

$$P_D = \int_{\eta}^{\infty} \Lambda p(\Lambda/H_0)d\Lambda \tag{7.7}$$

When the densities of Λ cannot be determined analytically, one carries out a Monte Carlo simulation of the detector under test. From the simulation results one then forms estimates $\hat{p}(\Lambda/H_1)$ and $\hat{p}(\Lambda/H_0)$ of the desired densities. These can be used to calculate P_F and P_D which constitute the ROC curve. We see that (7.47 above implies that only the density under H_0 need be obtained. This eliminates the need to simulate the signal. Note that (7.7) places an emphasis on the upper tail of $p(\Lambda/H_0)$, where typically only a few observations will lie. An equivalent expression to (7.7) is:

$$P_D = 1 - \int_{0}^{\eta} \Lambda p(\Lambda/H_0)d\Lambda \tag{7.8}$$

and it is shown in[27] that it is actually preferable to use (7.8).

As a point of reference, and an example of ROC curve generation, 100 observation intervals of white Gaussian noise, at each of 4 known variances were generated. These sequences were then passed through the optimum detector for this case (signal known exactly in noise known exactly (SKE in NKE)). The ROC curves were then computed and drawn. The signal to noise ratio (SNR) is:

$$SNR = \frac{E}{N_0} \tag{7.9}$$

where E is the signal energy, and N_0 is the noise power spectral density.

Figure 7.7 contains the ROC curves for the 4 different SNR's. These match well the ROC curves originally reported in [48] for this case:

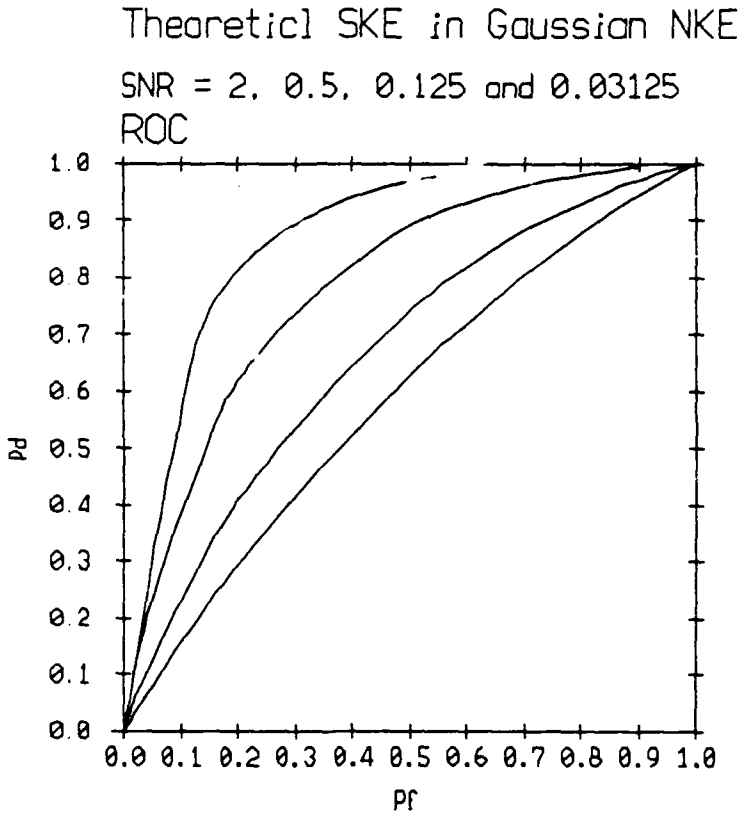

Figure 7.7 SKE in Gaussian NKE ROC curves

Two different approaches are considered for the Bayes optimum detector, namely block processing and time sequential. These were described in detail in Chapter 6, and the next two chapters are concerned with the detector comparisons subject to these approaches. We now posess the tools, and are ready to examine the detector performance evaluations and comparisons.

8. Block processing optimum detector vs. ad-hoc detector comparisons.

In this chapter, the performance of a block processing Bayes Optimum Detector (BOD) is compared to that of an ad-hoc adaptive detector. The reason the (sub-optimum) block processing approach is considered here at all is that for real-time systems, this sometimes is the only viable approach. The test scenario under which both detection approaches were tested was described in Chapter 7. The array used in the comparison is a four element array, where the main beam was composed of summing all four element outputs, and the reference beam(s) was generated by subtracting two adjacent element outputs. When the fixed interference is present, the problem's order is increased, and there is a need for another degree of freedom. Then, another reference beam is generated, and both detector schemes tested have another input available for processing.

Figure 8.1 depicts the typical range-Doppler map of a synthesized ping used in the basic test scenario where the interference direction is assumed known precisely (i.e. the sonar array is at a known depth). Here, since the sonar array is in relatively shallow water, surface reverberation is hard to distinguish from volume reverberation since they both have an almost zero Doppler shift. Figure 8.2 shows the adaptive filter's output range-Doppler map.

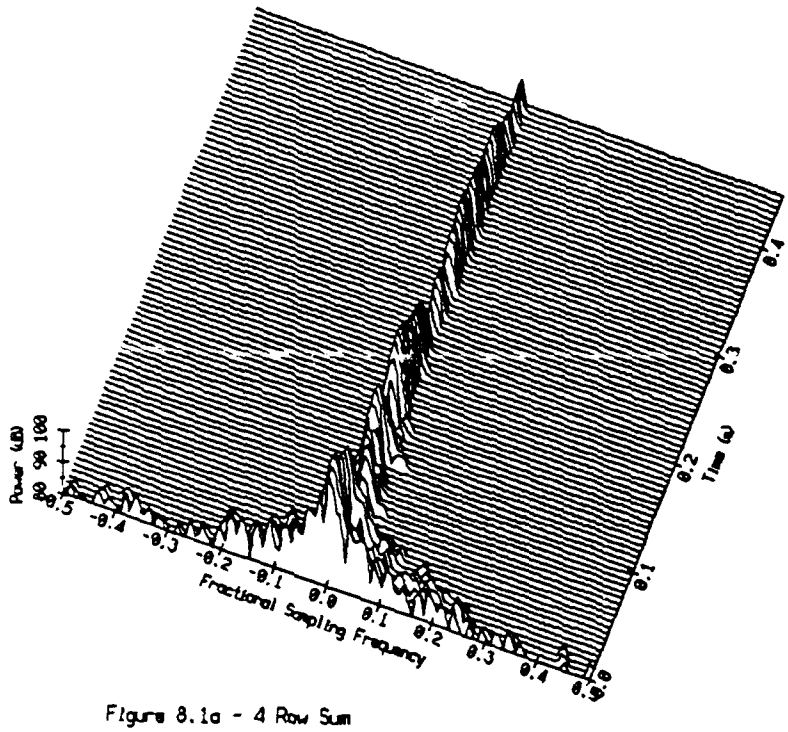

Figure 8.1a - 4 Row Sum

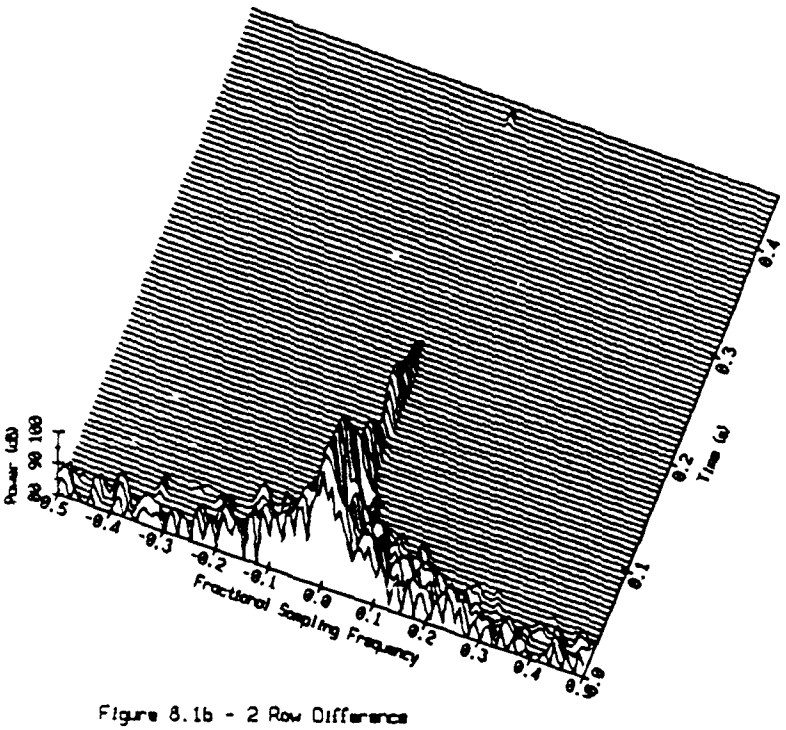

Figure 8.1b - 2 Row Difference

Figure 8.1 Main and reference beam range-Doppler maps

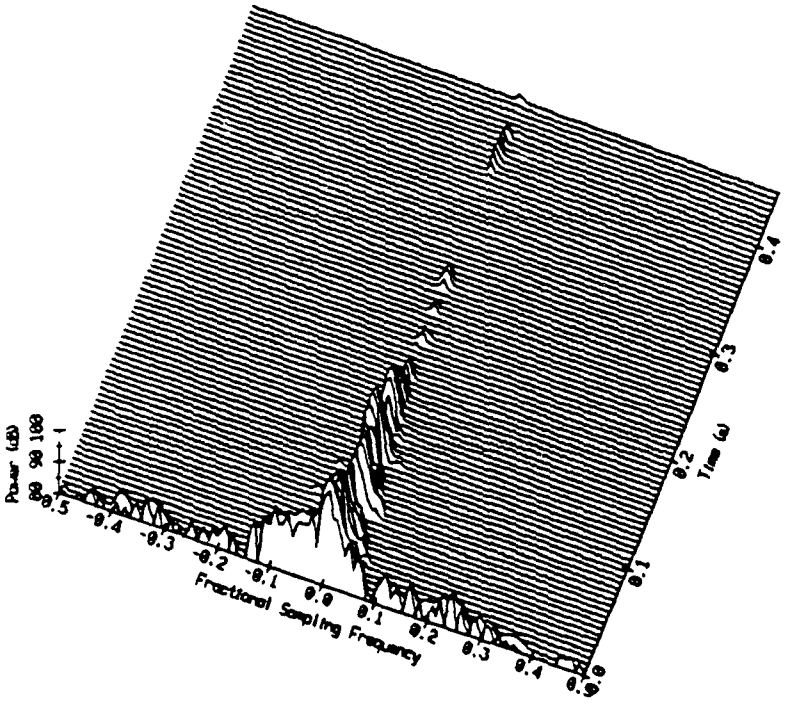

Figure 8.2 Adaptive filter output range-Doppler map.

Figure 8.3 plots main beam power, reference beam power, adaptive filter's output power and reverberation cancellation power (ratio between adaptive filter's output power and main beam power). Here, one can see how much of the surface interference is canceled by the ad-hoc detection structure's adaptive filter around 0.2 sec, where both detectors' outputs are sampled.

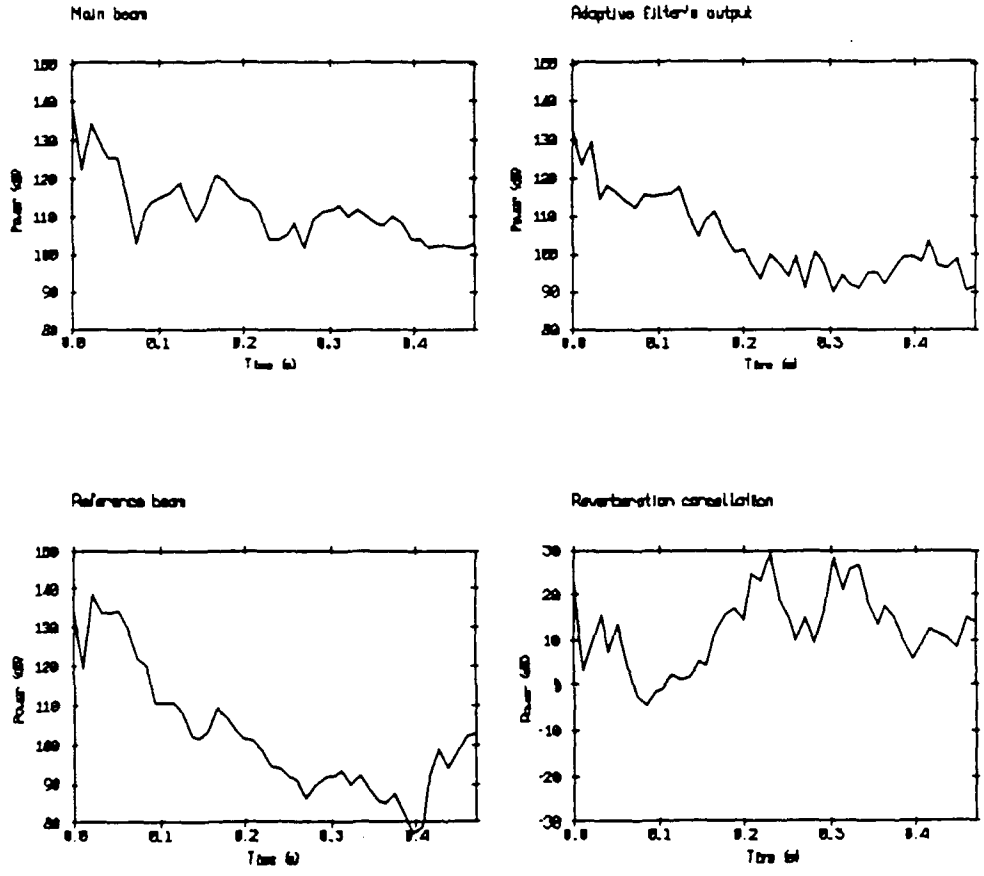

Figure 8.3 Main, reference and filter's output power.

8.1. Known depth

Each comparison between the two detection approaches is based on a Monte-Carlo simulation of 500 runs. In the first comparison made, the sonar array was placed at a known depth, and the Bayes optimum detector was given that

depth. Signal to surface interference ratio was set to 2.8. Figure 8.4 shows the ROC curves of both detectors.

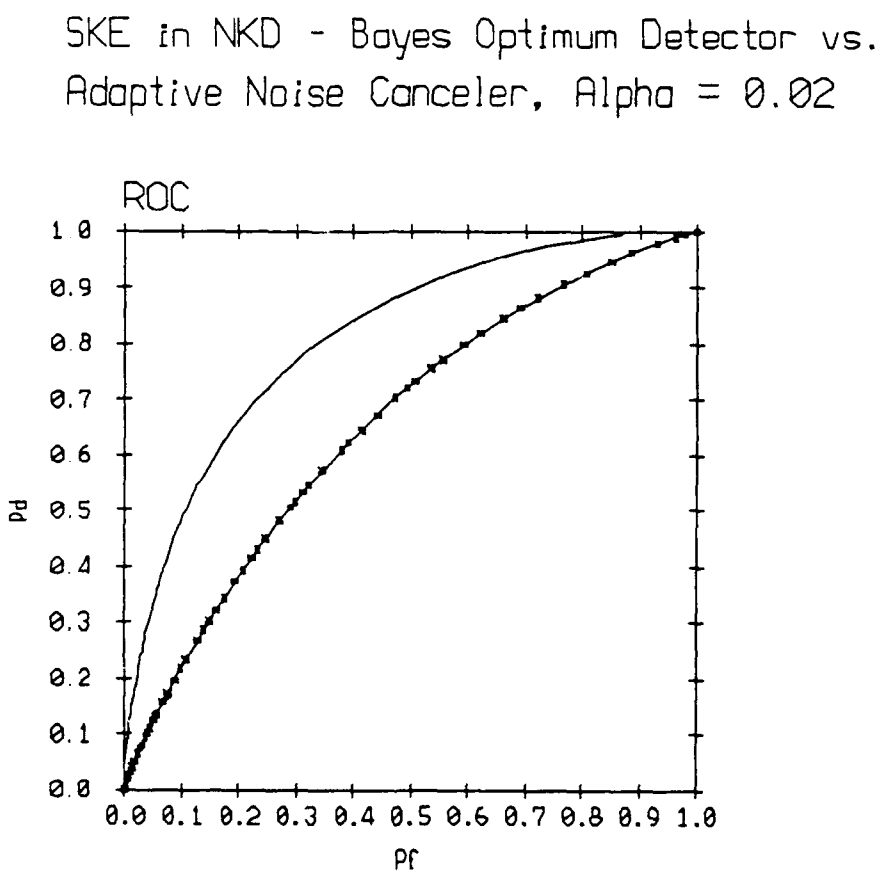

Figure 8.4 The two detectors' ROC curves (ANC is *****)

It is obvious that the Bayes Optimum detector (BOD) performs better than the ad-hoc Adaptive Noise Canceler (ANC). In fact, compare these ROC curves to the curves given in Figure 7.7 (theoretical SKE in Gaussian NKE (SKENKE)), which can serve as a reference. One sees that the BOD performs close to a SKENKE detector when SNR=0.5, while the ANC performs as a SKENKE detector when SNR=0.125. This translates into a ~6 dB performance difference.

8.2. Uncertain depth

In the next comparison, array depth is not a known quantity. What is known is its probability density function, which is assumed uniform between 16.5m and 43.5m. In this way, the average depth is kept the same as the previous comparison's depth (30m). The comparison is based again on 500 Monte-Carlo simulation runs, where the array was physically placed at various depths, commensurate with a uniform distribution. Figure 8.5 shows the ROC curves for this comparison.

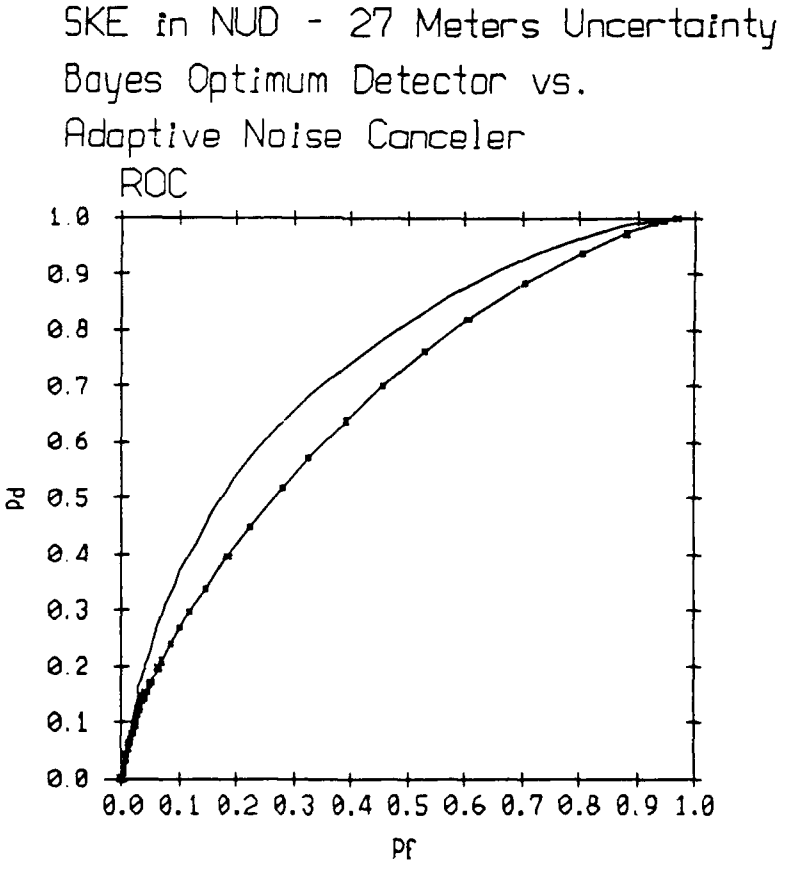

Figure 8.5 Uncertain depth (27m) ROC curves (ANC is *****)

It is clear that the ANC's performance hasn't changed, since it has the ability to adapt to the varying depth. The BOD's performance has degraded, but with this

level of uncertainty, it is still performing better than the ANC. Naturaly, we will now check what happens when the depth uncertainty is increased. Depth was given twice the uncertainty (i.e 54m), still keeping the average depth at 30m as before. Figure 8.6 plots the ROC curves for this case.

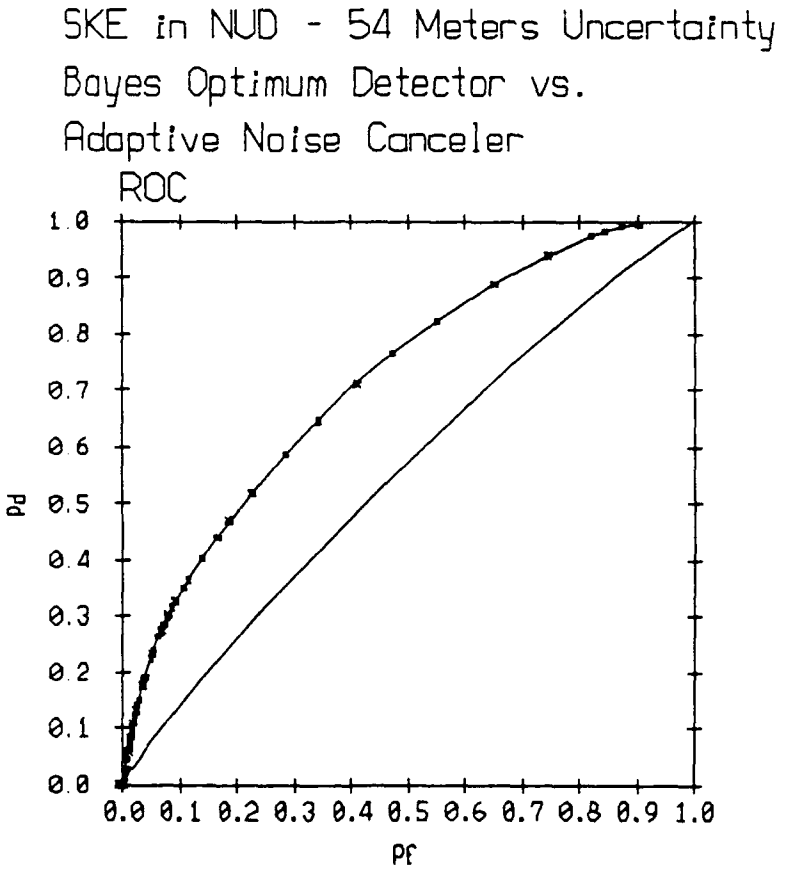

Figure 8.6 Uncertain depth (54m) ROC curves (ANC is *****)

Here, the BOD has basically fallen apart, since the interference direction uncertainty is large. The ANC, whose performance is essentially unchanged, is now performing better than the BOD, using its capability to adapt to the varying interference direction.

Another interesting point is to see what happens when the signal to noise ratio is increased. This was done for the 27m of depth uncertainty, and an SNR of

11.2. Figure 8.7 shows the comparison result.

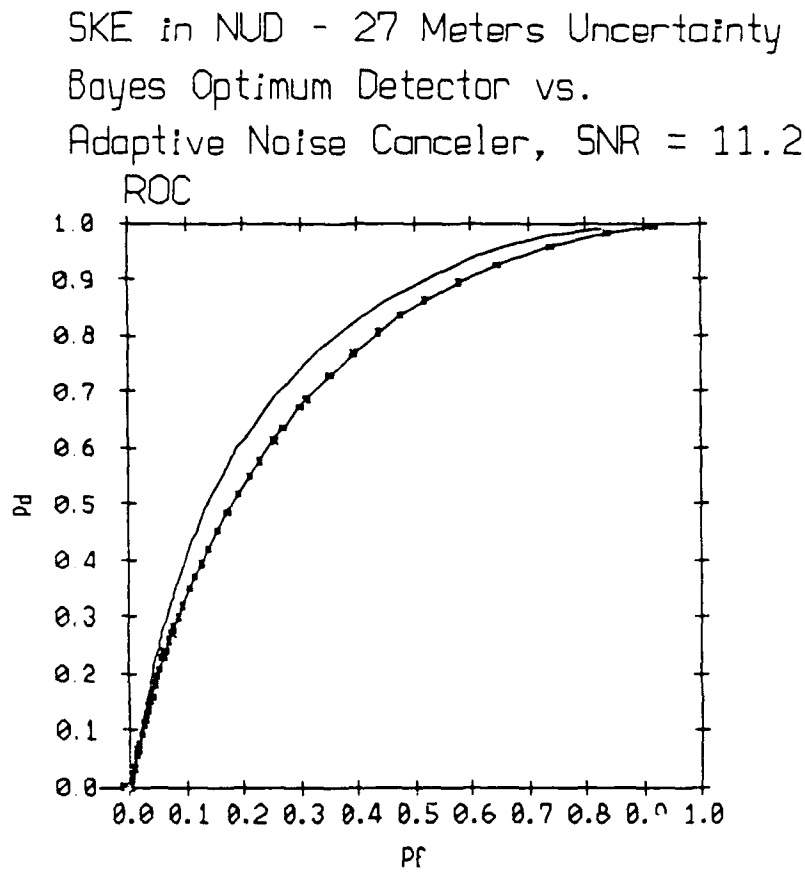

Figure 8.7 Higher SNR ROC curves (ANC is *****)

As can be seen, the performance of both detectors has improved as expected.

8.3. Uncertain depth plus a fixed interference

At this point in time, it was clear that as soon as the depth (interference direction) uncertainty exceeds some value, the ANC starts performing better than the BOD. The next step was to check what effect an extra interference source has on both detectors' performance. An interference source whose direction is uncertain, but whose direction probability density function was known, has been added into the scenario. The interference was coming from directions between

$-10°$ and $-30°$. Interference power level was made equal to the boundary interference power at the detection range. Figure 8.8 shows the results. we see that the result of the added interference is that the BOD performs poorly.

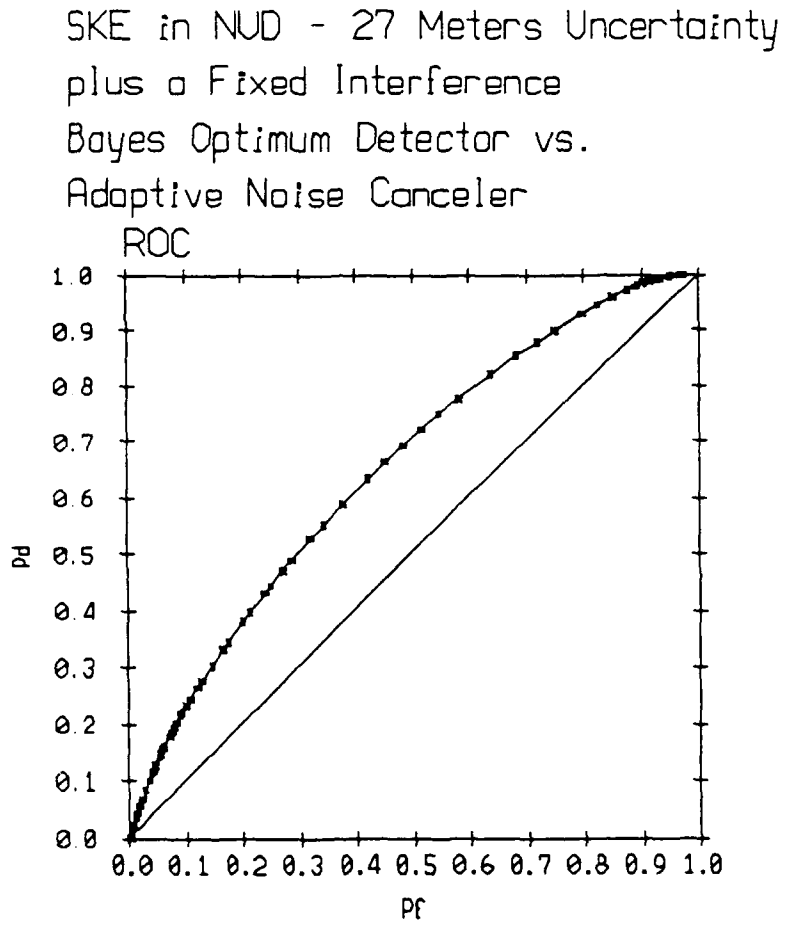

Figure 8.8 Fixed interference introduced (ANC is *****)

8.4. Conclusion

When comparing Figure 8.8 to Figure 8.5 (see Figure 8.9), we see that the ANC's performance remained essentially the same, even after the addition of the fixed interference. This demonstrates its ability to adapt to another interference source, when the adaptive filter order is given another degree of freedom. As expected, the BOD performs very poor, and the effect another interference source has on it, is akin to the effect that an increased depth uncertainty had (see Figure 8.6). Figure 8.9 combines Figures 8.5 and 8.8, to compare both detectors' performance under the same depth uncertainty (27m), with and without the fixed interference.

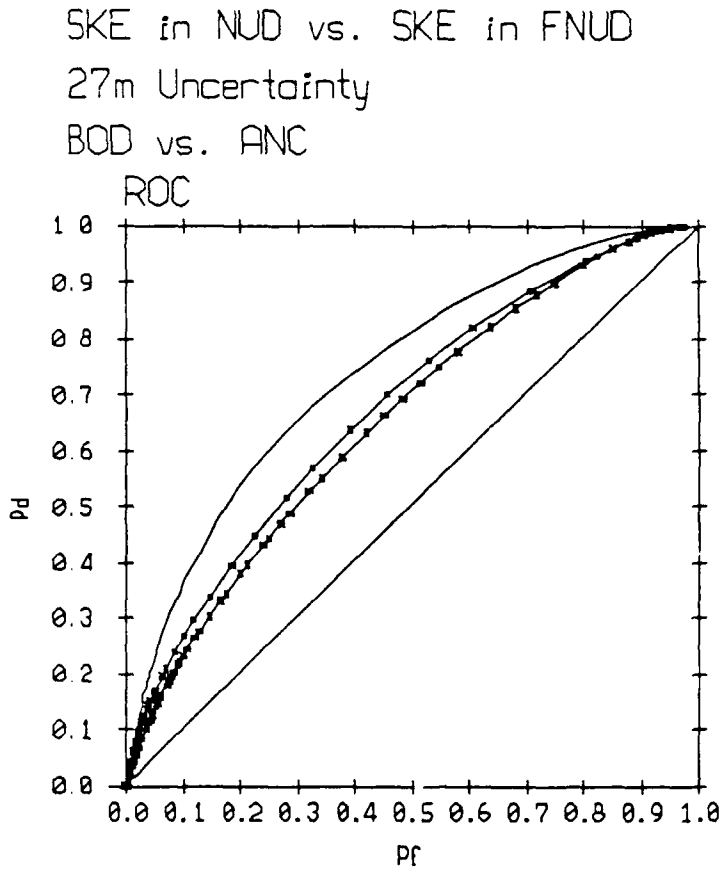

Figure 8.9 Performance with and without fixed interference (ANC is *****)

We have compared the performance of the two detection approaches, when the Bayes Detector was restricted to block processing. Since this restriction makes the detector sub-optimal, its performance has not been uniformly better than its ad-hoc counterpart. The next chapter will remedy that by using a time sequential approach for the BOD.

9. Time sequential optimum detector vs. ad-hoc detector comparisons.

In this chapter we will remove the block processing restriction from the Bayes Optimum Detector (BOD) and let it make use of all the available data. This way, the BOD becomes a truly optimum solution, and the comparison between the two detectors is more fair. This will also enable us to demonstrate the adaptive nature of the BOD. The difference between the block processing and the time sequential approaches has been detailed in Chapter 6.

9.1. Uncertain depth

The first comparison is identical to the second comparison made in Chapter 8 (SKE in NUD). Here, there is a 27m depth uncertainty, and the BOD is time sequential. Figure 9.1 shows the ROC curves for this case.

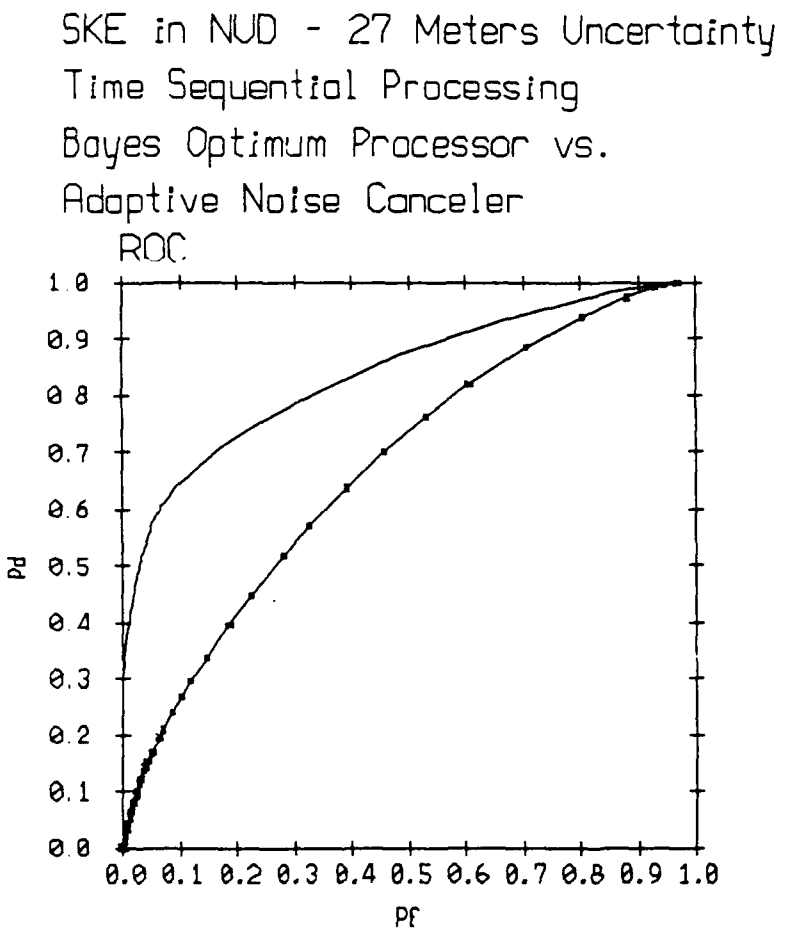

Figure 9.1 Time sequential BOD vs. ANC (ANC is *****)

Obviously, the performance difference between the BOD and the ANC has increased (compare to Figure 8.5). Now that the BOD is making use of past data to update the a-priori pdf, it performs better. As before, the next step is to increase the depth (interference direction) uncertainty, and observe the performance. The uncertanty is increased to 54m as before, and Figure 9.2 details the result.

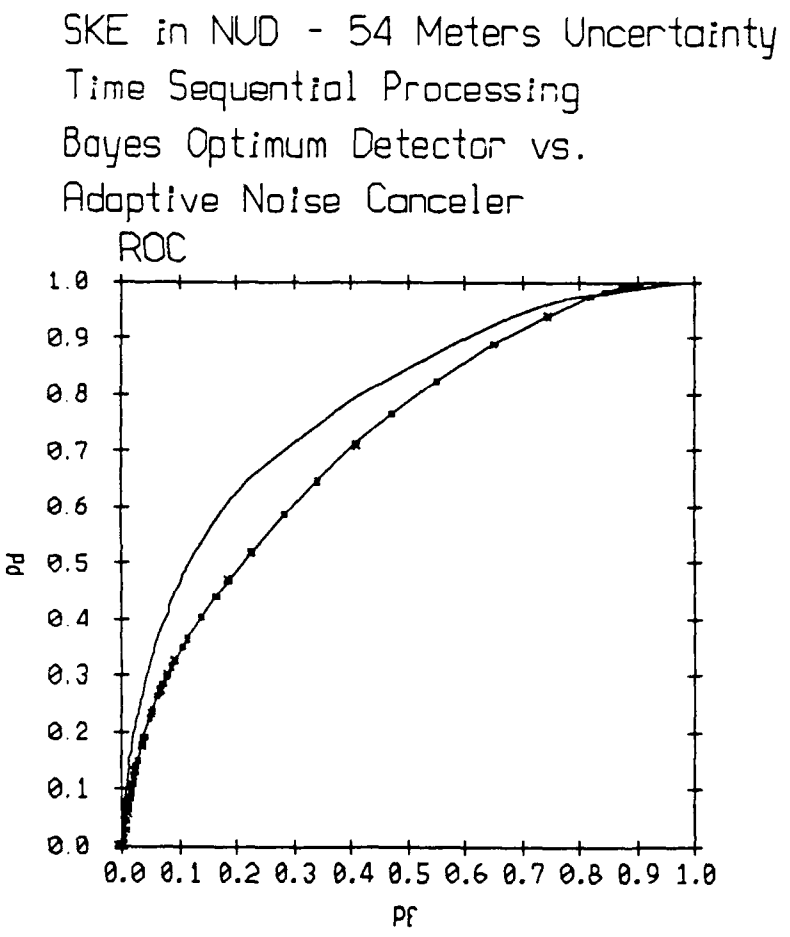

Figure 9.2 54m uncertainty ROC curves (ANC is *****)

As opposed to what happened in the same situation when the block processing approach was used, now even with the increased depth uncertainty, the BOD still performs better than the ANC, though the performance differential is reduced.

As described in Chapter 6, the time sequential detector presents an adaptive quality in that it updates the a-priori probability density functions (pdf's) of the uncertain parameters from iteration to iteration, thereby carrying important information from the past to the present. It is interesting to watch how these pdf's adapt as time progresses (see equations (6.8) and (6.9)). Figure 9.3 depicts the behaviour of the array element to element delay (AEED) pdf for the iterations

preceding the one in which detection is made. AEED is a linear function of interference direction, and was the unknown parameter used.

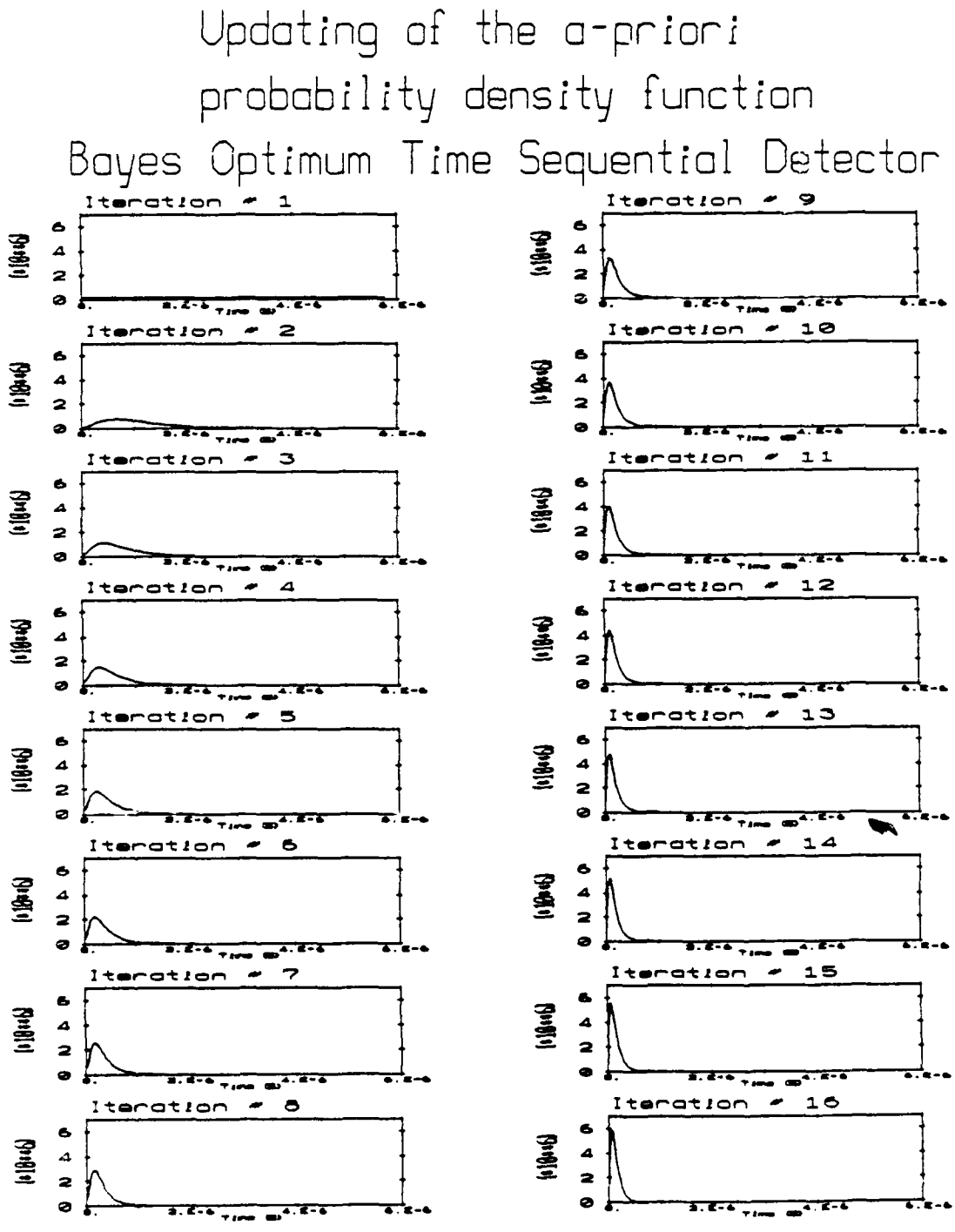

Figure 9.3 Updating pdf's.

Note how system's knowledge of the AEED improves from very diffuse (Iteration #1), to more and more precise, as time progresses. Since the surface return comes from shallower and shallower angles as the ping propagates through the water, the AEED becomes smaller and smaller, and so does its estimate.

9.2. Uncertain depth plus a fixed interference

As before, we now check what effect an extra interference source has on both detectors' performance. An interference source whose direction is uncertain, but whose direction probability density function is known has been added into the scenario. The interference is coming from directions between $-10°$ and $-30°$. Interference power level was made equal to the boundary interference power at the detection range. Figure 9.4 shows the results.

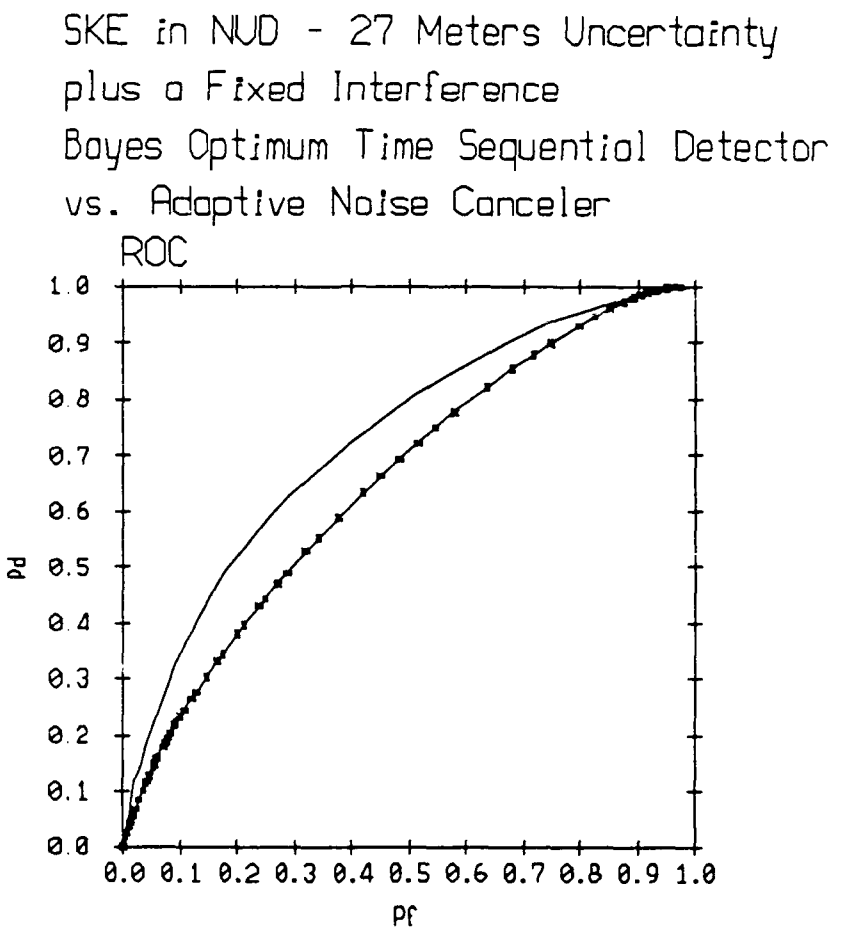

Figure 9.4 Fixed interference introduced (ANC is *****)

Here, the BOD's performance has degraded due to the presence of the fixed interference. Even though the ANC seems to be less sensitive to the presence of the fixed interference, the BOD still performs better than the ANC. This is contrasted with Figure 8.8, where the ANC performs better than the block processing BOD.

9.3. No surface interference

It is interesting to check what influence removing the surface interference from the scenario will have on both detectors' performance. Time-varying

boundary interference power and fixed interference power were purposefully kept at an equal level. It is expected, therefore, that performance will be very close to the case where only the surface interference was present. Figure 9.5 shows the results:

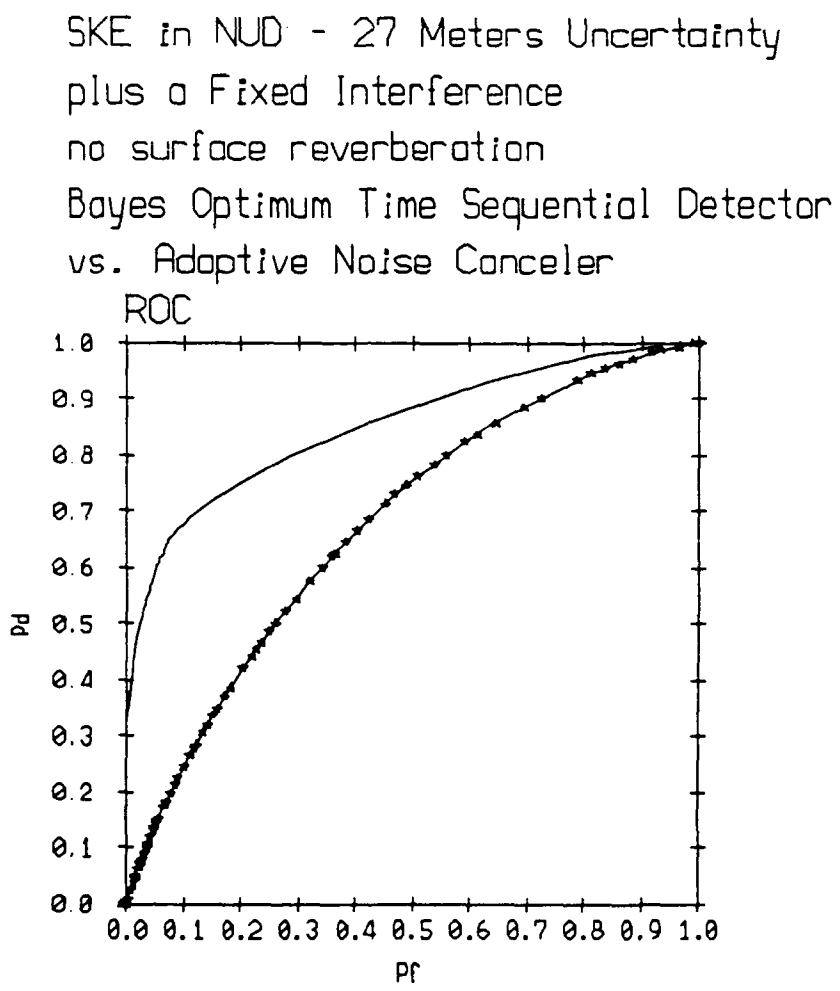

Figure 9.5 Surface interference removed (ANC is *****)

It is clear that indeed the performance is very similar to the one reported in Figure 9.1.

Lastly, Figure 9.6 shows the detector performance when depth uncertainty

is increased from 27m to 54m, and when the fixed interference is present.

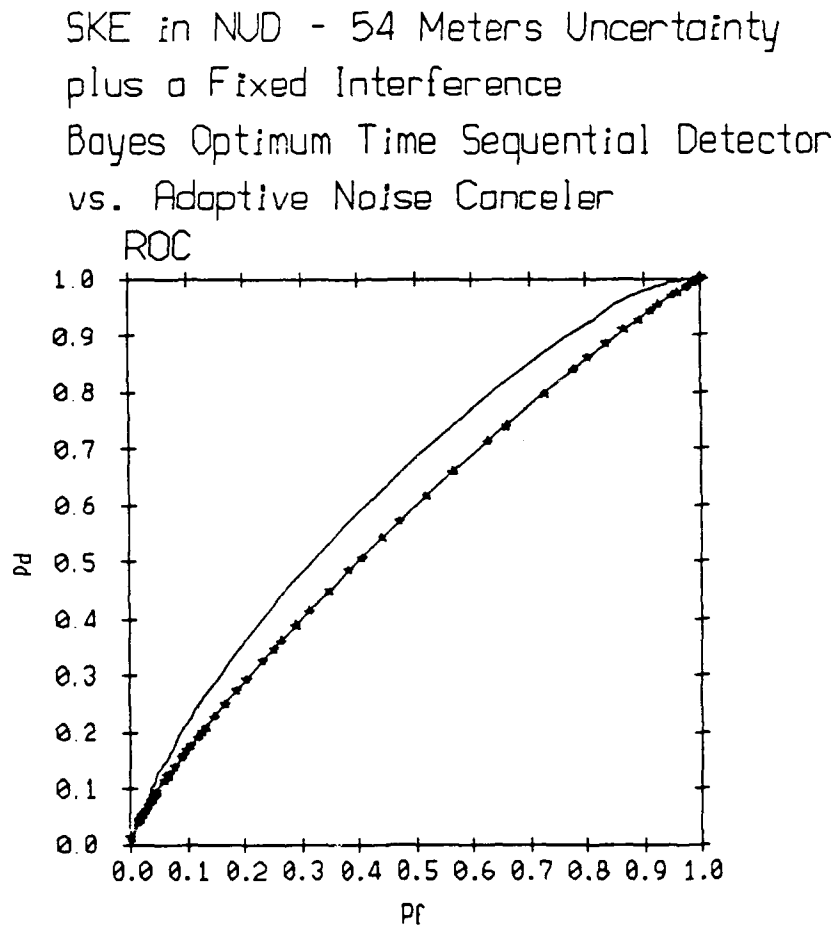

Figure 9.6 Higher depth uncertainty (ANC is *****)

The performance of both processors has degraded uniformly, while the BOD still performs best, as expected.

9.4. Conclusion

When a truly optimum approach is taken, and the Bayes optimum detector is allowed to make use of all the available data, it performs better than the ad-hoc

adaptive noise canceler. With the time-sequential approach, the BOD also posesses an adaptive quality, in updating the a-priori pdf's of the unknown parameter from iteration to iteration.

Conclusion

The active sonar problem has been carefully examined in this dissertation. Specifically, situations under which the sonar suffers from boundary interference were analyzed. Underwater acoustic reverberation, which is typically the limiting noise process for this problem, has been studied. Then, two main schemes designed to detect a desired signal buried in ocean reverberation were suggested and examined. These two schemes represent two different approaches to the problem. The first is an ad-hoc engineering approach, which uses an adaptive noise canceler in the front end, to get rid of the undesired boundary interference, and then uses a matched filter assuming now that the problem is one of known Gaussian statistics. The second approach is a more global one. It makes use of the known statistical properties of the problem to arrive at an optimal solution in the Bayesian sense.

Recognizing that close analytic expressions for system performance are often very hard to derive, an important tool has been developed. This software package is capable of synthesizing multi-element (or beam) time series outputs, taking into account transmit and receive beampatterns, the ocean environment including surface, volume and bottom scattering strengths, and the sonar platform dynamics. It sets up the normal equations for the problem, and uses the solution to create a time varying IIR filter which represents the time varying characteristics of a sonar ping propagating in the ocean. Once the filter has been derived, an ensemble of sonar pings may be collected by passing uncorrelated white noise vectors through the filter. This tool is then heavily used in assessing performance of the various detection algorithms.

Next, a multi-channel, joint process pole-zero adaptive filter is developed and its performance is compared to its all-zero counterpart. It is shown that some

cases exist where the ability to adapt poles is important.

Last, but not least, the performance of the ad-hoc detectors is compared to that of Bayes optimum detectors. It is shown that optimum detectors, when allowed to make use of all the available data, perform better than the ad-hoc adaptive detectors. Moreover, it is shown that the optimum detector possesses an adaptive learning quality, through the process of updating the a-priori probability density functions of the unknown parameters.

The work done in this dissertation can be extended in a few directions. The multi-channel joint process ARMA adaptive filter developed here can be used in various noise canceling and spectral estimation problems, and its ability to adapt poles can be exploited. The reverberation simulation tool (REVSIM) incorporates only isovelocity sound speed profiles, and the next step would be to allow a variable sound speed. Other reverberation synthesis techniques exist, and have been implemented by other researchers. It would be interesting, and beneficial for the active sonar community, to compare and evaluate the different methods against each other. The application of Bayes optimum detectors when there are uncertain parameters has been outlined and demonstrated for the active sonar problem. Two uncertain parameters concentrated on were platform depth, and direction of arrival of a fixed interference. It would be very interesting to extend the methods and ideas outlined, to other uncertain parameters such as sound velocity. Finally, the investigation of applying Bayes optimum schemes for feature estimation and extraction (e.g direction of arrival) using their adaptive learning capability, may prove beneficial.

Appendix A

The linear minimum mean square estimation problem:

The problem is presented in the following figure:

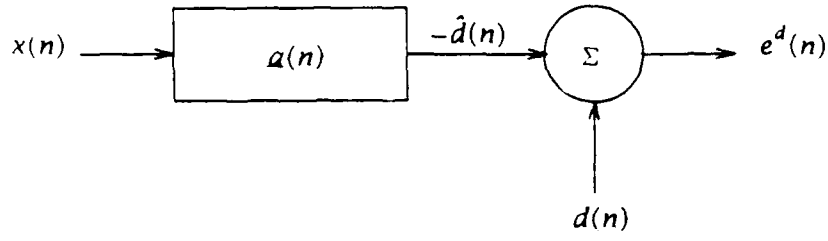

Figure A.1 - The MMSE estimation problem

$a(n)$ is a causal FIR filter of length $p+1$. The goal is to filter the stochastic time series $x(n)$ to yield an optimal estimate (in some sense) of the "desired" time series $d(n)$. The error is given by:

$$e^d(n) = d(n)+\sum_{0}^{p} a_k x(n-k) \tag{A.1}$$

or in vector notation:

$$e^d(n) = d(n)+a^T x \tag{A.2}$$

where ^{T} represents the vector transpose operator. The solution to the problem depends on the assumptions made about the input time series, and the optimality criterion chosen. The Wiener filtering approach assumes the input time series is stochastic, and seeks to minimize the mean square error:

$$\min E\left[| e^d(n) | ^2 \right] \tag{A.3}$$

where $E[\,.\,]$ is the expected value operator.

$$\begin{aligned} |\, e^d(n)\,|^2 &= |\, d(n)+\underline{a}^T\underline{x}\,|^2 \\ &= d(n)d^*(n)+d(n)\underline{a}^T\underline{x}+\underline{a}^H\underline{x}^*(n)d(n)+\underline{a}^H\underline{x}^*(n)\underline{a}^T\underline{x}(n) \end{aligned} \tag{A.4}$$

where ^{H} represents the Hermitian operator. Now, taking the expected value yields:

$$E\left[\,|\, e^d(n)\,|^2\right] \equiv E^d(\underline{a}) = \phi_{00}^d+\underline{g}^H\underline{a}+\underline{a}^H\underline{g}+\underline{a}^H[\Phi]^T\underline{a} \tag{A.5}$$

where ϕ_{00}^d is the desired signal power, $\underline{g}$ is the crosscorrelation vector between the input $x(n)$ and the desired signal $d(n)$, and $[\Phi]$ is the autocorrelation matrix of the input process $x(n)$. Minimizing $E^d(\underline{a})$ with respect to $\underline{a}$ yields:

$$0 = \underline{g}+[\Phi]^T\underline{a} \tag{A.6}$$

or

$$[\Phi]^T\underline{a} = -\underline{g} \tag{A.7}$$

which are called the *normal* equations. Solving for $\underline{a}$ we get:

$$\underline{a} = -\left[[\Phi]^T\right]^{-1}\underline{g} \tag{A.8}$$

In the case that the input time series $x(n)$ is stationary, $[\Phi]$ is of a Toeplitz form:

$$\phi_{k,j} = \phi_{j-k} \tag{A.9}$$

Here, all matrix elements along any diagonal are equal. This becomes useful when solving (A.7), avoiding the need to directly invert $[\Phi]$.

Appendix B

Transition equations for the time-varying element to element delay.

In time-sequential processing, when transitioning from one iteration to the next, an update is made on the a-priori pdf's. Since δ_i, the element to element time delay is time-varying, a transition equation is required, which determines the next iteration's time delay as a function of this iteration's delay. Consider the problem's geometry as is shown in figure B.1:

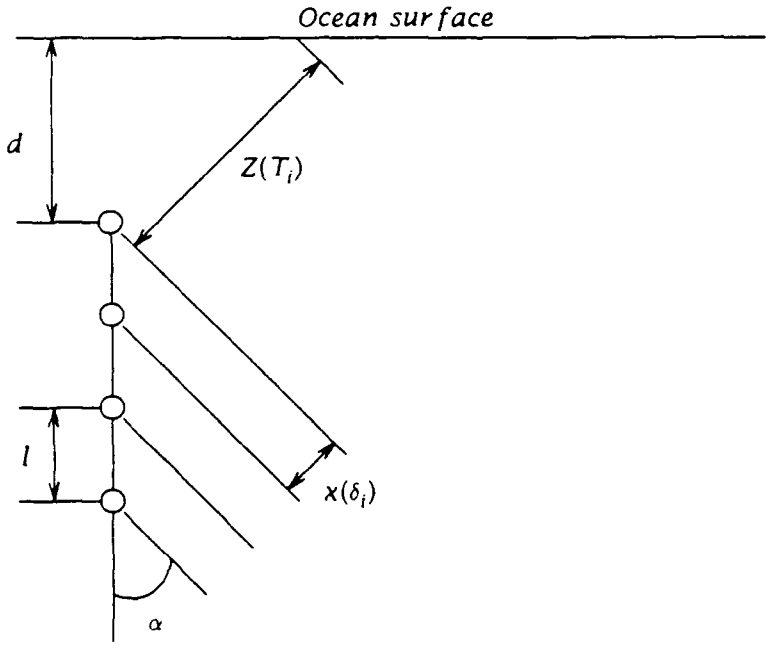

Figure B.1 - element to element time delay computation

At time T_i, the element to element delay is:

$$\delta_i(T_i) = \frac{ld}{cZ(T_i)} = \frac{ld}{c^2 T_i} = \frac{K}{T_i} \qquad \text{(B.1)}$$

where

$$K \equiv \frac{ld}{c^2}$$

At time T_{i+1}, the element to element delay is:

$$\delta_{i+1}(T_{i+1}) = \frac{K}{T_{i+1}} = \frac{K}{T_i + \Delta T} \tag{B.2}$$

where

$$T_{i+1} = T_i + \Delta T$$

Let

$$\delta_{i+1} = \delta_i + A \tag{B.3}$$

then

$$A = \delta_{i+1} - \delta_i = \frac{K}{T_i + \Delta T} - \frac{K}{T_i} = \frac{KT_i - KT_i - K\Delta T}{T_i(T_i + \Delta T)} = -\frac{K\Delta T}{T_i(T_i + \Delta T)} = -\delta_i \delta_{i+1} \frac{\Delta T}{K} \tag{B.4}$$

Substituting A back into (B.3) yields:

$$\delta_{i+1} = \delta_i - \delta_i \delta_{i+1} \frac{\Delta T}{K} \tag{B.5}$$

$$\delta_{i+1} = \frac{\delta_i}{1 + \delta_i \dfrac{\Delta T}{K}}$$

Now, since

$$T_i = \frac{d}{c} + (i-1)\Delta T$$

then (B.5) becomes:

$$\delta_{i+1} = \frac{\delta_i}{1+\frac{K}{T_i}\frac{\Delta T}{K}} = \frac{\delta_i}{1+\frac{\Delta T}{T_i}} = \frac{\delta_i}{1+\frac{\Delta T}{\frac{d}{c}+(i-1)\Delta T}} \tag{B.6}$$

Now,

$$\delta_i = \frac{ld}{c^2 T_i} = \frac{ld}{c^2\left[\frac{d}{c}+(i-1)\Delta T\right]} \tag{B.7}$$

$$d = \frac{c^2\delta_i(i-1)\Delta T}{l-c\delta_i} \quad ; \quad i>1$$

Substituting (B.7) back into (B.6) yields:

$$\delta_{i+1} = \frac{\delta_i}{1+\frac{1}{\frac{c\delta_i(i-1)}{l-c\delta_i}+(i-1)}} = \frac{\delta_i}{1+\frac{l-c\delta_i}{l(i-1)}} \quad ; \quad i>1 \tag{B.8}$$

which is the desired result used in (6.10).

Part of the update equation for the a-priori probability density function of δ_i is the derivative $\left|\frac{d\delta_{i+1}}{d\delta_i}\right|_{\delta_i}$. It may be more convenient to compute $\left|\frac{d\delta_i}{d\delta_{i+1}}\right|$ and then use:

$$\frac{d\delta_{i+1}}{d\delta_i} = \frac{1}{\frac{d\delta_i}{d\delta_{i+1}}}$$

Using (B.8) we have:

$$\delta_i = \delta_{i+1} + \frac{\delta_{i+1}}{\frac{c\delta_i(i-1)}{l-c\delta_i} + (i-1)} = \frac{il\delta_{i+1}}{l(i-1)+c\delta_{i+1}} \tag{B.9}$$

$$\frac{d\delta_i}{d\delta_{i+1}} = \frac{il(l(i-1)+c\delta_{i+1}) - cil\delta_{i+1}}{(l(i-1)+c\delta_{i+1})^2} = \frac{il^2(i-1)}{(l(i-1)+c\delta_{i+1})^2} \tag{B.10}$$

Now, inverting the derivative we get:

$$\frac{d\delta_{i+1}}{d\delta_i} = \frac{(l(i-1)+c\delta_{i+1})^2}{il^2(i-1)} \tag{B.11}$$

and finally:

$$\left| \frac{d\delta_{i+1}}{d\delta_i} \right|_{\delta_i} = \frac{\left(l(i-1) + \frac{c\delta_i}{1+\frac{l-c\delta_i}{l(i-1)}} \right)^2}{il^2(i-1)} \tag{B.12}$$

References

1. Adams, S. L. and L. W. Nolte, "Bayes optimum array detection of targets of known location," *J. Acoust. Soc. Am.*, vol. 58 No. 3, 1975.

2. Alexandrou, D., "Boundary reverberation rejection via constrained adaptive beamforming," *J. Acoust. Soc. Am.*, vol. 82(4), pp. 1274-1290, 1987.

3. Alexandrou, D. and C. de Moustier, "Adaptive Noise Canceling Applied to Sea Beam Sidelobe Interference Rejection," *IEEE J. Oceanic Engr.*, vol. OE-13 no.2, pp. 70-76, 1988.

4. Alexandrou, D., *Selective reverberation cancellation via adaptive beamforming*, Univ. Calif., San Diego, 1985. Ph.D. dissertation

5. Alexandrou, D., "Signal recovery in a reverberation-limited environment," *IEEE Journal of Oceanic Engineering*, vol. OE-12, No. 4, pp. 553-559, Oct. 1987.

6. Bayes, Thomas, "An essay toward solving a problem in the doctrine of chances," *Phil. Trans. Roy. Soc.*, vol. 53, pp. 370-418, 1763. Reprinted in Biometrika 45, 293-315 (1958)

7. Berlinsky, A., "Techniques of Modeling a Sonar Guidance System," *Proc. OCEANS*, pp. 211-216, 1982.

8. Buckley, J.P and R.J Urick, "Backscattering from the deep sea bed at small grazing angles," *Jour. Acoust. Soc. Am.*, vol. 44 No. 2, pp. 237-252, 1968.

9. Chamberlain, S. and J. Galli, "A model for numerical simulation of nonstationary sonar reverberation using linear spectral prediction," *IEEE J. Oceanic Engr.*, vol. OE-8, pp. 21-36, 1983.

10. Chapman, R.P and J.H Harris, "Surface backscattering strengths measured with explosive sound sources," *Jour. Acoust. Soc. Am.*, vol. 34, pp. 1592-1597, 1962.

11. Clay, C.S and H. Medwin, *Acoustical Oceanography*, Wiley, New York, N.Y., 1977.

12. Clay, C.S and H. Medwin, "High frequency acoustical reverberation from a rough sea surface," *Jour. Acoust. Soc. Am.*, vol. 36(11), pp. 2131-2135, 1964.

13. Cron, B.F. and W.R. Schumacher, "Theoretical and experimental study of underwater sound reverberation," *J. Acoust Soc. Am.*, vol. 33, p. 881, 1961.

14. Durbin, J., "The fitting of time-series models," *Rev. Inst. Int. Stat.*, vol. 28, pp. 233-243, 1960.

15 Faure, P., "Theoretical model of reverberation noise," *J. Acoust. Soc. Am.*, vol. 36, pp. 259-266, 1964.

16. Friedlander, B., "Lattice Filters for Adaptive Processing," *Proc. IEEE*, vol. 70(8), pp. 829-867, 1982.

17. Friedlander, B., "Lattice Methods for Spectral Estimation," *Proc. IEEE*, vol. 70(9), pp. 990-1017, 1982.

18. Garrison, G.R, S.R Murphy, and D.S Potter, "Measurement of the backscattering of underwater sound from the sea surface," *Jour. Acoust. Soc. Am.*, vol. 32, pp. 104-111, 1960.

19. Hansen, D.S., "Asymptotic Performance of a Pulse-to-Pulse Incoherent Doppler Sonar in an Oceanic Environment," *IEEE J. Oceanic Engr.*, vol. OE-10, pp. 144-158, 1985.

20. Higgins, R., J. Francis, and R. Hoy, "Implementation and validation of a model for surface reverberation," *J. Acoust. Soc. Am.*, vol. 61, pp. 449-507, 1977.

21. Hodgkiss, W.S and D. Alexandrou, "An Adaptive Algorithm for Array Processing," *IEEE Trans. Antennas and Propagation*, vol. AP-34, pp. 454-458, 1986.

22. Hodgkiss, W.S, "An Oceanic Reverberation Model," *IEEE J. Oceanic Engr.*, vol. OE-9(2), pp. 63-72, 1984.

23. Hodgkiss, W. S. and D. Alexandrou, "Sea surface reverberation rejection," *ICASSP*, vol. 33, pp. 7.1-7.4, 1984.

24. Hodgkiss, W. S. and L. W. Nolte, "Adaptive optimum array processing," *J. Acoust. Soc. Am.*, vol. 61, pp. 763-775, 1976.

25. Hodgkiss, W. S. and L. W. Nolte, "Array processor performance under directional uncertainty," *IEEE Trans. Aerosp. Electron. Sys.*, vol. AES-14, pp. 827-832, 1978.

26. Hodgkiss, W. S. and L. W. Nolte, "Optimal array processor performance tradeoffs under directional uncertainty," *IEEE Trans. Aerosp. Electron. Sys.*, vol. AES-12, pp. 605-615, 1976.

27. Hodgkiss, W. S., *The sequential Implementation of Array Processors when there is Directional Uncertainty*, Department of Electrical Engineering, School of Engineering, Duke University, 1975. Ph.D dissertation

28. Inouye, Y., "Modeling of Multichannel Time Series and Extrapolation of Matrix-Valued Autocorrelation Sequences," *IEEE Trans. Acoust., Speech, Signal Proc.,*, vol. ASSP-31, pp. 45-55, 1983.

29. Kolmogorov, A. N., "Interpolation and extrapolation of stationary random sequences," *Bull. Acad. Sci. USSR*, vol. Ser. Math 5, 1962.

30. Kotel'nikov, V. A., *The Theory of Optimum Noise Immunity*, McGraw-Hill, New York, N. Y., 1959. R. A. Silverman trans.

31. Lee, D.T.L, *Canonical ladder form realizations and fast estimation algorithms*, Stanford University, 1980. (Ph.D. Dissertation)

32. Lee, D.T.L., B. Friedlander, and M. Morf, "Recursive Ladder Algorithms for ARMA Modeling," *IEEE Trans. Automatic Control*, vol. AC-27(4), pp. 753-764, 1982.

33. Levinson, N., "The Wiener RMS (root-mean-square) error criterion in filter design and prediction," *J. Math. Phys.*, vol. 25, pp. 261-278, 1947.

34. Luby, J. and D. Lytle, "Autoregressive Modeling of Nonstationary Multibeam Sonar Reverberation," *IEEE J. Oceanic Engr.*, vol. OE-12, pp. 116-129, 1987.

35. McConneli, S.O., J.G. Lilly, and G.R. Steiner, *Modeling of high-frequency surface reverberation and ambient noise* , Applied Physics Lab, University of Washington, November 1978. Technical report APL-UW 7821

36. McConneli, S.O. and J.G. Lilly, *Surface reverberation and ambient noise measured in the open ocean and Dabob bay*, Applied Physics Lab, University of Washington, January 1978. Technical report APL-UW 7727

37. Mckinney, C.M and C.D Anderson, "Measurement of backscattering of sound from the ocean bottom," *Jour. Acoust. Soc. Am.*, vol. 36 No. 1, pp. 158-163, 1964.

38. Mellen, R.H, "Doppler Shift of Sonar Backscatter from the Surface," *J. Acoust. Soc. Am.*, vol. 36, p. 1395, 1964.

39. Middleton, D., "Statistical criteria for the detection of pulsed carriers in noise," *J. Appl. Phys.*, vol. 24, pp. 371-378, 379-391, April, 1953.

40. Middleton, D., "A statistical theory of reverberation and similar first-order scattered fields, Part I: Waveforms and the general process," *IEEE Trans. Inform. Theory*, vol. IT-13, pp. 372-392, 1967.

41. Middleton, D., "A statistical theory of reverberation and similar first-order scattered fields, Part II: Moments, spectra and special distributions ," *IEEE Trans. Inform. Theory*, vol. IT-13, pp. 393-414, 1967.

42. Middleton, D., "A statistical theory of reverberation and similar first-order scattered fields, Part III: Waveforms and fields ," *IEEE Trans. Inform. Theory*, vol. IT-18, pp. 35-67, 1972.

43. Middleton, D., "A statistical theory of reverberation and similar first-order scattered fields, Part IV: Statistical models ," *IEEE Trans. Inform. Theory*, vol. IT-18, pp. 68-90, 1972.

44. OSRD., *Reverberation Studies at 24 Kc*, Nov 23 1942. OSRD 1098, NDRC 6.1-sr30-401, Report U-7, UCDWR Div. 6-520-M2

45. Ol'shevskii, V., *Characteristics of Sea Reverberation*, 1967. translated from Russian by Consultants Bureau, a division of Plenum Publishing Corp, New York.

46. Ol'shevskii, V.V., "Probability distribution of sea reverberation levels," *Sov. Phys. Acoust.*, vol. 9, p. 378, 1964.

47. Papoulis, A., *Probability, Random Variables, and Stochastic Processes*, McGraw-Hill, New York, 1965.

48. Peterson, W. W., T. G. Birdsall, and W. C. Fox, "The theory of signal detectability," *Trans. I.R.E*, vol. PGIT-4, pp. 171-212, September 1954.

49. Princehouse, D., "REVGEN, A real-time reverberation generator," *Proc. ICASSP*, vol. 77, pp. 827-835, 1977.

50. R.P, Goddard, *REVGEN, high fidelity simulation of sonar signals*, Applied Physics Lab, University of Washington, Seattle, 1985. APL-UW 8805.

51. Rayleigh, Lord, *Theory of Sound*, The Macmillan Company, New York, 1926. first edition

52. Robinson, E., *Multichannel Time Series Analysis with Digital Computer Programs*, Holden-Day, San Francisco, 1970.

53. Swanson, David C., *All-zero and pole-zero least squares lattice filter structures for adaptive processing of complex acoustic data*, The Pennsylvania State University, 1984. (Masters Thesis)

54. Trees, H. L. Van, *Estimation and Linear Modulation Theory.*, Wiley, New York, 1971.

55. Trees, H. L. Van, *Radar-Sonar Signal Processing and Gaussian Signals in Noise*, Wiley, New York, 1971.

56. Urick, R.J and R.M Hoover, "Backscattering of sound from the sea surface; its measurement, causes and application to the prediction of reverberation levels," *Jour. Acoust. Soc. Am.*, vol. 28, pp. 1038-1042, 1956.

57. Urick, R.J and G.R Lund, "Horizontal coherence of explosive reverberation," *Jour. Acoust. Soc. Am.*, vol. 47 No. 3 (part 2), pp. 904-911, 1970.

58. Urick, R.J and G.R Lund, "Vertical coherence of explosive reverberation," *Jour. Acoust. Soc. Am.*, vol. 36 No. 11, pp. 2164-2170, Nov, 1964.

59. Urick, R.J and G.R Lund, "Vertical coherence of shallow-water reverberation," *Jour. Acoust. Soc. Am.*, vol. 47 No. 1 (part 2), pp. 342-349, 1970.

60. Urick, R. J., *Principles of Underwater Sound*, McGraw-Hill, New York, 1975.

61. Wald, A., "Contributions to the theory of statistical estimation and testing of hypotheses," *Ann. Math. Stat.*, vol. 10, pp. 299-326, 1939.

62. Walker, R., D. Crowe, and W. Mayo, "Synthetic Multichannel Time Series for Simulating Underwater Acoustic Noise," *Proc. ICASSP*, pp. 1042-1045, 1981.

63. Weydert, M., *Measurement of Acoustic Backscatter of the Deep Sea Floor Using a Deeply Towed Vehicle: A Technique to Investigate the Physical and Geological Properties of the Sea Floor and to Assess Manganese Nodule Resources*, Scripps Institution of Oceanography, University of California at San Diego, 1985. Ph.D Dissertation

64. Whalen, A. D., *Detection, Estimation of Signals in Noise*, Academic Press, New York, 1971.

65. Whittle, P., "On the fitting of multivariate autoregressions, and the approximate canonical factorization of a spectral matrix," *Biometrika*, vol. 50, pp. 129-134, 1963.

66. Widrow, B., J. R. Glover, J. M. McCool , J. Kaunitz , C. S. Williams , R. H. Hearn , J. R. Zeidler , E. Dong, Jr. , and R. C. Goodlin, "Adaptive noise canceling: principles and applications," *Proc. IEEE*, vol. 63, pp. 1692-1716, 1975.

67. Widrow, B. and M. Hoff, Jr., "Adaptive switching circuits," *IRE WESCON Conv. Rec.*, vol. 4, pp. 96-104.

68. Wiener, N., *Extrapolation, interpolation and smoothing of stationary time series with engineering applications*, Technology Press and Wiley, New York, 1949.

69. Wiggins, R. A and E. A. Robinson, "Recursive solution to the multichannel filtering problem," *J. Geophys. Res.*, vol. 70, pp. 1885-1891, 1965.

70. Woodward, P. M. and I. L. Davies, "Information theory and inverse probability in telecommunications," *Proc. I.E.E*, vol. 99(III), pp. 37-51, March 1952.

71. Woodward, P. M., *Probability and Information Theory with Applications to Radar*, McGraw-Hill Book Co., New York, N. Y., 1953. (2nd ed., 1965).